Volume 94 • Number 2 • December2023
Established in 1923 • ISSN 1945-0702

The Chemist

Journal of the American Institute of Chemists

In this Issue

Official journal of
The American Institute of Chemists, Inc.
http://www.theaic.org/pub_thechemist_journals/

The Chemist

Established in 1923, The Chemist is the official publication of The American Institute of Chemists, Inc. (AIC). The Chemist was published quarterly in magazine format up until 2006. The Chemist is currently being set up and formatted as an online journal.

Subscription: $35 per year to members, $100 per year to non-members. Single copy: $50.
The Chemist (ISSN-0009-3025) is published online by The American Institute of Chemists, Inc.

Volume 94 | Issue 2 | 2023

The Chemist

Journal of the American Institute of Chemists

The Chemist (Established in 1923)

Editorial

Alexander G. Zestos, Ph. D
American University

Nayiri M. Kaissarian, Ph.D
Montgomery College

Chemistry remains at the forefront of society's past, present, and future. We are currently living through a seemingly continuous COVID-19 pandemic in addition to other infectious diseases such as Respiratory Syncytial Virus Infection (RSV), monkeypox, and several others. The depletion of natural resources such as oil, gas, coal, fossil fuels, and others have led the race towards clean, green, sustainable, and renewable energy sources such as hydrothermal, geothermal, solar, wind, nuclear, and others. The safety, efficiency, and feasibility of these alternative sources are primarily determined by engineers and chemists alike. Chemistry is often referred to as "The Central Science" because it is at the intersection of the physical and life sciences and integrates several fields of knowledge through high impact research and relevant studies. Several subdisciplines such as electrochemistry are incredibly diverse as they encompass several fields such as sensors, catalysis, batteries, electroanalytical, and many more.

We are proud to announce that Prof. Robert Savinell from the Department of Chemical Engineering at Case Western Reserve University and Prof. Kara Bren from the Department of Chemistry at the University of Rochester have been named our Chemical Pioneer awardees for the year 2023 at the AIC Annual meeting in May of 2023. Their contributions to The Chemist are currently planned to be included in a subsequent issue.

In this issue of The Chemist published by the American Institute of Chemists (AIC), we explore several research topics relevant to all forms of chemistry. We begin this issue with a contribution from Dr. Thad Le-Vasicek, who details the development of catalysts immobilized to magnetic nanoparticles. The study ultimately shows that increasing the recovery of the magnetic nanoparticles decreases the loss of recycled enzyme activity illustrating the importance of optimizing particle recovery to increase the retained activity of recycled catalysts, which has been shown to be a crucial parameter for the industrial use of enzymes to magnetic nanoparticles.

We further present research from Dr. Atolani's laboratory that depicts an eco-friendly formulation and characterization of cosmetics prepared from seed oils. The study shows that seed oils from several underutilized plants can be used for industrial and medicinal purposes such as green cosmetics formulation for the regulation of skin pigmentation. Another contribution from the Atolani laboratory focuses on the isolation and characterization of novel bioactives from Vernonia amygdalina, a tropical shrub that has been known to have health-promoting properties. Hassan et al. also analyzed other plant extracts as they studied the quantitative chemical analysis and biological effectiveness on germination and the growth of Maize seeds. They analyzed many chemical compounds extracted from fig, eucalyptus, and mulberries such as proteins, carbohydrates, phenols, flavonoids, and several other compounds as well.

In the fields of polymer and physical chemistry, Yousef Alqaheem contributed a review on testing methods for permeability and selectivity of polymeric membranes. The paper provided precise guidelines for evaluating membrane permeability and porosity for energy-saving gas separations and several commercial applications. Continuing in the fields of membranes, Tawari and Brika developed a statistical analysis for developing cellulose acetate (CA) Hollow-fine-fiber membranes. This work had great applications for brackish water desalination with improved salt retention and flux. Lastly, Busari et al. detail synthesis, characterization, and docking studies of zinc and copper complexes of 4-methylbenzoic acid and 2-methylimidazole. These metal-derived complexes could be considered promising candidates for combatting pathogenic infections.

We sincerely hope that you enjoy reading this issue and wish you a safe and prosperous New Year.

With best wishes,

Alexander G. Zestos and Nayiri M. Kaissarian
Co-Editors of The Chemist

The Chemist
Journal of the American Institute of Chemists

Catalysts Immobilized to Magnetic Nanoparticles: Assessment of Particle and Activity Loss During Recycling

Angela, Corbin D. Snavely, Blakely M. Adair-Hudson, and Thaddeus W. Vasicek†

Department of Chemistry, The Citadel, Charleston, SC 29409
†Corresponding author (E-mail: tlevasic@citadel.edu)

Abstract: The immobilization of enzymes to magnetic nanoparticles facilitates the recovery and reuse of the enzyme, which mitigates the financial burden of enzyme use. Particles are typically modified to enhance enzyme immobilization. However, the modification of magnetic nanoparticles alters the magnetic properties of the particles which may diminish the particle recovery and therefore decrease the efficiency of magnetically recycled catalysts. In this work, magnetic nanoparticles were synthesized and modified with varying amounts of an aminosilane. β-Glucosidase, an enzyme relevant for bioethanol production, was immobilized on the particles. The enzyme immobilized particles were subjected to a recycling experiment, where the activity and particle loss during recycling were quantified. The particle loss was ~2% × cycle^{-1} and was not dependent upon the extent of aminosilane modification. The activity loss × cycle^{-1} was ~3% and did not depend on the extent of aminosilane modification but was proportional to the particle loss. The results from this study suggest that increasing the recovery of the magnetic nanoparticles will decrease the loss of recycled enzyme activity.

Key Words: Cellulases, immobilized enzymes, activity loss, magnetic nanoparticles, functional group density

1. Introduction

Enzymes possess many desirable traits as catalysts in the industrial sector. Enzymes have high selectivity, operate in relatively benign solutions, and require low energy input [1]. However, enzymes can account for ~48% of the value of the product [2], which may hinder the use of enzymes in specific sectors. The financial burden of enzyme use is mitigated when the enzymes are recovered and reused for multiple production cycles. Immobilizing enzymes to solid supports enable for the recovery and reuse of the enzymes, thereby reducing their financial impact [3,4].

Nanoparticles (NPs) are routinely used as supports for enzyme immobilization, because they do not suffer from appreciable mass transport limitations, they can be readily modified to facilitate immobilization and they have a high surface area, enabling the immobilization of an abundance of enzyme [1]. Magnetic nanoparticles (MNPs) have the additional benefit of being readily separated from bulk solution by the application of an external magnetic field. This ease of MNP recovery has led to their use in several studies as supports for enzyme immobilization [5-7].

MNPs are modified with agents to introduce functional groups that promote enzyme immobilization. Amines are routinely introduced to MNP surfaces, as the amine can be activated to covalently bind enzymes [8]. Amines can be introduced to the MNP surface by the condensation of 3-aminopropyl triethoxysilane (APTES). The amine density on the MNP is correlated with the APTES concentration used during the modification step, which is pivotal in controlling the enzyme density on the MNP. It is therefore desirable to have MNPs with a high APTES density for the immobilization of large quantities of enzyme.

The financial impact of inactivated enzymes can be minimized when the enzymes maintain high activity throughout subsequent catalytic cycles. Immobilized enzymes will denature during use, which reduces the activity when reused. MNPs with high APTES densities are able to form multiple interactions with the immobilized enzyme and stabilize the enzyme conformation, which hinders inactivation [9,10]. A challenge with APTES modification of MNPs, is that nonmagnetic modifications lower the MNP magnetic susceptibility [11-14] and may reduce the MNP recovery. Incomplete MNP recovery lowers the quantity of catalyst for subsequent production cycles, as immobilized enzyme is lost along with unrecovered MNP. This loss of catalyst would lead to lower subsequent production yields, from reduced catalytic activity when reused.

To the authors' knowledge, there are no reports that simultaneously explore how MNP recovery and recovered enzyme activity are affected by the extent of APTES modification. In this work, the MNP loss and activity loss were studied as a function of APTES modification extent. Specifically, MNPs were modified with different densities of APTES and then β-glucosidase (BGL) was immobilized to the APTES modified MNPs. BGL is an industrially relevant enzyme utilized for the production of bioethanol from cellulose [15]. To assess how the extent of BGL immobilization affects activity and particle recovery, the quantity of BGL used for immobilization was varied to create particles with a low or high BGL loading. The BGL immobilized MNPs were subjected to a recycling experiment where the loss of MNPs and the activity during recycling was studied. Neither the MNP nor activity loss during recycling correlated with the extent of APTES modification. The results of this study indicate that the loss in immobilized BGL activity is primarily caused by incomplete MNP recovery.

2. Experimental Methods

Materials

Water with an electrical resistance of 18 MΩ was used for all experiments. Iron (III) chloride hexahydrate ($FeCl_3·6H_2O$) and glutaraldehyde (50%) were purchased from Sigma-Aldrich (St. Louis, MO, USA). Iron (II) chloride tetrahydrate ($FeCl_2·4H_2O$), 4-nitrophenyl-β-D-glucopyranoside (*p*NPG), and 3-aminopropyltriethoxysilane (APTES) were purchased from Acros Organics (Geel, Belgium). BGL from almonds, used as received, was purchased from GoldBio (St Louis, MO, USA). Copper (II) sulfate pentahydrate ($CuSO_4·5H_2O$), sodium acetate, sodium carbonate, sodium bicarbonate, sodium monohydrogen phosphate, sodium dihydrogen phosphate, ammonium hydroxide (29%), trace-metal grade hydrochloric acid and nitric acid and tetraethyl orthosilicate (TEOS) were purchased from Fisher Scientific (Pittsburgh, PA, USA). Sodium bicinchoninate (BCA), hexylamine, and 4-nitrophenol were purchased from Tokyo Chemical Industry (Portland, OR, USA). The Fe standard was purchased from Spex CertiPrep (Metuchen, NJ, USA).

Preparation and Modification of Iron Oxide Nanoparticles

MNPs were synthesized by the co-precipitation of a 2:1 mole ratio of Fe^{3+} and Fe^{2+} in an aqueous alkaline solution and modified with TEOS, followed by APTES as previously described [16]. In brief, a 47 mL aqueous solution of Fe^{3+} and Fe^{2+} was heated to 80 °C and degassed with N_2 for 30 min. To the iron solution, 2.2 mL of ammonium hydroxide was added dropwise at a rate of 0.5 mL/min and left to stir at 80 °C under N_2 atmosphere for 1 hr. The black precipitate was collected by magnetic decantation, washed twice with degassed H_2O and three times with ethanol.

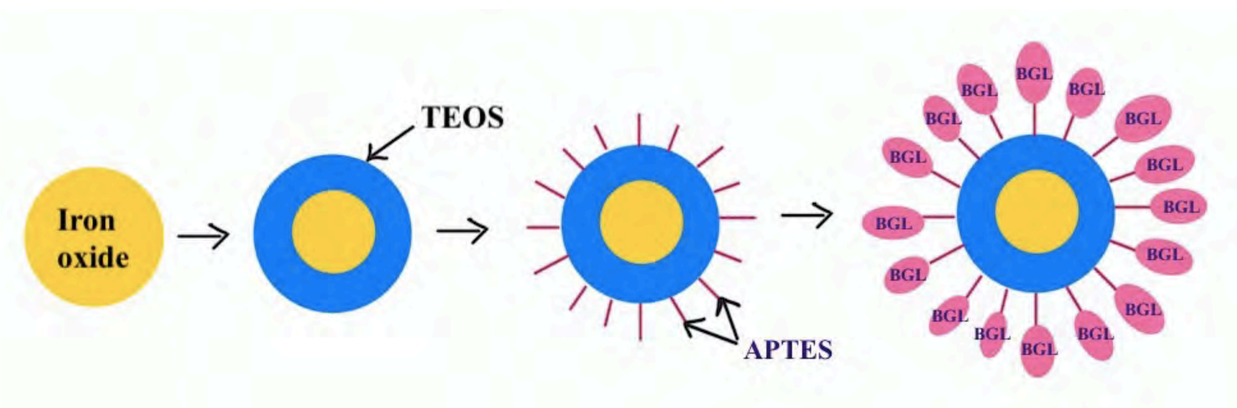

Figure 1. Modification of MNPs. MNPs were initially coated with TEOS, then subsequently modified with varying extents of APTES. Lastly, BGL was immobilized to the APTES modified MNPs.

The prepared MNPs were then modified with TEOS and APTES as displayed in Figure 1. For TEOS modification, 1 mL of the washed MNPs was added to 7.8 mL ethanol, and 0.3 mL of TEOS. The hydrolysis was initiated by the rapid addition of 0.9 mL of 29% ammonium hydroxide and left to react at 350 RPM for 15 hours. The TEOS modified MNPs (MNP-TEOS) were washed three times with ethanol and reconstituted in 15, 30 or 300 mM APTES, hereafter referred to as MNP-TEOS-APTES-15, MNP-TEOS-APTES-30, or MNP-TEOS-APTES-300, respectively. The MNP-TEOS-APTES mixtures were placed on a shaker set at 350 rpm, at room temperature, and allowed to react overnight. The MNP-TEOS-APTES particles were then washed three times in ethanol and dried overnight in a vacuum oven at 60 °C and analyzed using an iS20 ATR-FTIR (Thermo Fisher, Waltham, MA, USA). The MNP-TEOS-APTES were then reacted with glutaraldehyde, which served as a covalent linker between the terminal amine on APTES and primary amines in BGL. A 1 mg/mL MNP solution containing 10 mM phosphate, and 20 mM glutaraldehyde pH 7.4 was created. The solution was placed on a shaker at 350 RPM for 2 hr. After two hours, the MNPs were washed three times into 10 mM acetate pH 5.0 solution containing 0.1 or 1 mg/mL BGL to create particles with a low or high BGL loading, respectively. The BGL-modified MNPs (MNP-TEOS-APTES-BGL) were washed with 10 mM acetate pH 5.0 three times to remove unbound biomolecules. The quantity of immobilized BGL was determined indirectly by mass balance according to equation 1.

$$Immobilization\ Percent = \frac{C_i V_i - C_s V_s}{C_i V_i} \times 100 \tag{1}$$

where C_i is the initial concentration of the BGL solution, V_i is the initial volume of solution, C_s is the concentration of the supernatant and V_s is the volume of the supernatant.

Activity Assay and MNP Loss

The BGL activity was quantified using *p*NPG as a model substrate, measuring the 4-nitrophenol produced after 15 min at 37 °C. The MNP-TEOS-APTES-BGLs were gently mixed and diluted to 0.16 mg/mL in 10 mM acetate pH 5.0 to a volume of 750 µL. The kinetic assay was initiated by the addition of 250 µL of 5 mM *p*NPG in 10 mM acetate pH 5.0 to the samples, which were then placed on a shaker at 350 RPM at 37 °C. After 15 min, the MNP-TEOS-APTES-BGLs were magnetically separated for 2 min; the supernatant was removed and split into two aliquots. The 2-minute magnetic separation time was chosen as all the particles were visually observed to be collected within ~20 seconds. One aliquot was added to 200 mM sodium carbonate at a 2:1 volume ratio, and the concentration of 4-nitrophenol determined by measuring the absorbance at 400 nm. The second aliquot was placed in a vacuum oven at 60 °C until dry for analysis by ICP-OES.

Additional cycles of the kinetic assay were performed using the previously used MNP-TEOS-APTES-BGLs. A scheme for the recycling of MNP-TEOS-APTES-BGLs for repeated cycles is shown in Figure 2.

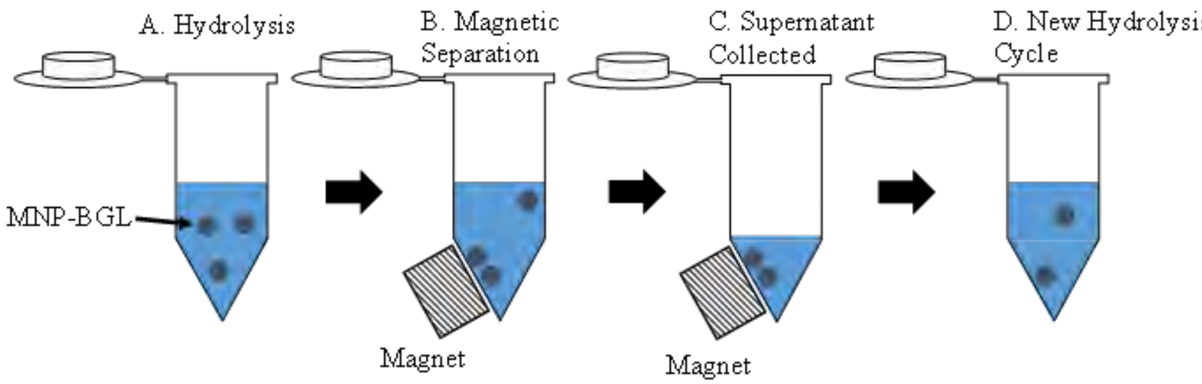

Figure 2. MNP-TEOS-APTES-BGL Recycling Scheme. A) MNP-TEOS-APTES-BGL hydrolyzing cellulose. B) MNP-TEOS-APTES-BGL magnetically separated from bulk. C) Supernatant collected to quantify MNP-TEOS-APTES-BGL loss and BGL activity. D) MNP-TEOS-APTES-BGL washed, fresh substrate added to begin new hydrolysis cycle.

The additional cycles were initiated by washing the MNPs once with 10 mM acetate and adding *p*NPG substrate. The enzyme activity for subsequent cycles was normalized to the activity of the first cycle, and the difference in activity percent for each cycle calculated to determine the activity loss percent.

The quantity of Fe loss during magnetic separation was determined by ICP-OES and assumed to be indicative of MNP-TEOS-APTES-BGLs not recovered during magnetic separation. The dried supernatants were digested in trace metal grade nitric acid at 60 °C for 4 hours. The digested samples were then diluted in 2% nitric acid and analyzed by an Agilent 700 ICP-OES.

3. Results and Discussion

MNP Synthesis and Modification

The magnetic nanoparticles were synthesized by the co-precipitation of Fe^{3+}/Fe^{2+} at a 2:1 mole ratio by the addition of NH_4OH. The synthesis yielded a black precipitate that was readily separated from bulk solution by a handheld neodymium permanent magnet. The handheld neodymium magnet with a 151 pound pull down force was used for the collection of MNPs throughout this study. The synthesized product was modified with TEOS and subsequently APTES. The FTIR spectra for the MNP-TEOS and MNP-TEOS-APTES particles are shown in Figure 3.

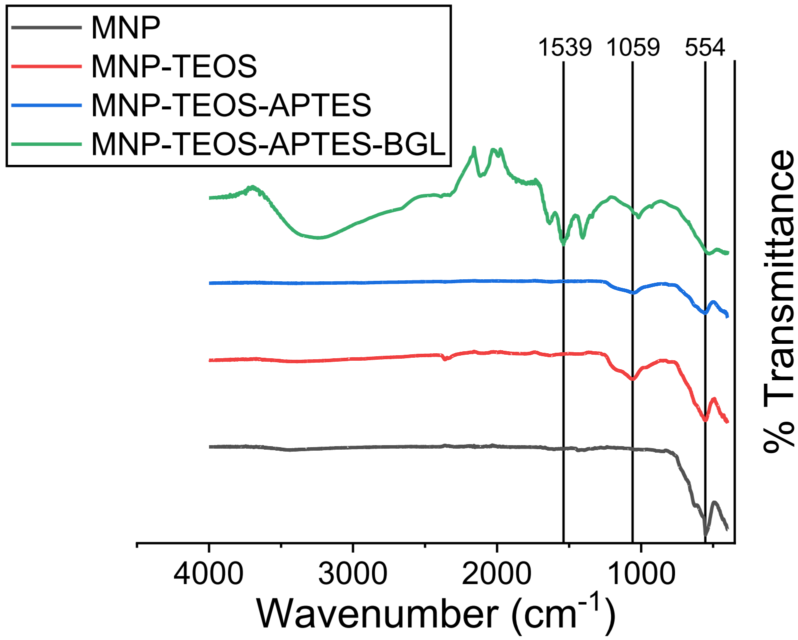

Figure 3. FTIR of MNP (black), MNP-TEOS (red), MNP-TEOS-APTES (blue) and MNP-TEOS-APTES-BGL (green). The spectra are offset for clarity. The peaks at 554, 1059 and 1539 cm^{-1} correspond to the Fe-O from the MNP, the silica from TEOS and the amide bond from BGL, respectively.

The MNPs possessed a peak at 554 cm^{-1}, which is characteristic of the Fe-O bond, and another asymmetric peak at 1059 cm^{-1}, which is indicative of the Si-Fe-Si [17,18]. The MNP-TEOS-APTES particles displayed the same peaks at 554 and 1059 cm^{-1}, however we did not observe a peak corresponding to the terminal amine in APTES at 1530 cm^{-1}. The intensity of the amine peak is proportional to the APTES density on the MNP-TEOS-APTES, and the APTES densities obtained in this study were not significant enough to contribute a prominent FTIR peak. The BGL immobilized particles had a prominent peak at 1539 cm^{-1} which was assigned to the peptide bond from BGL [19].

BGL Immobilization

The MNP-TEOS-APTES particles were reacted with glutaraldehyde and subsequently with BGL. Glutaraldehyde acts as a linker forming covalent bonds between the terminal amine in APTES and a primary amine in BGL [8]. The BGL immobilization percent ranged from 32 to 77% and was greater for particles with a low BGL loading when a 0.1 mg/mL BGL concentration was used for immobilization, as shown in Figure 4.

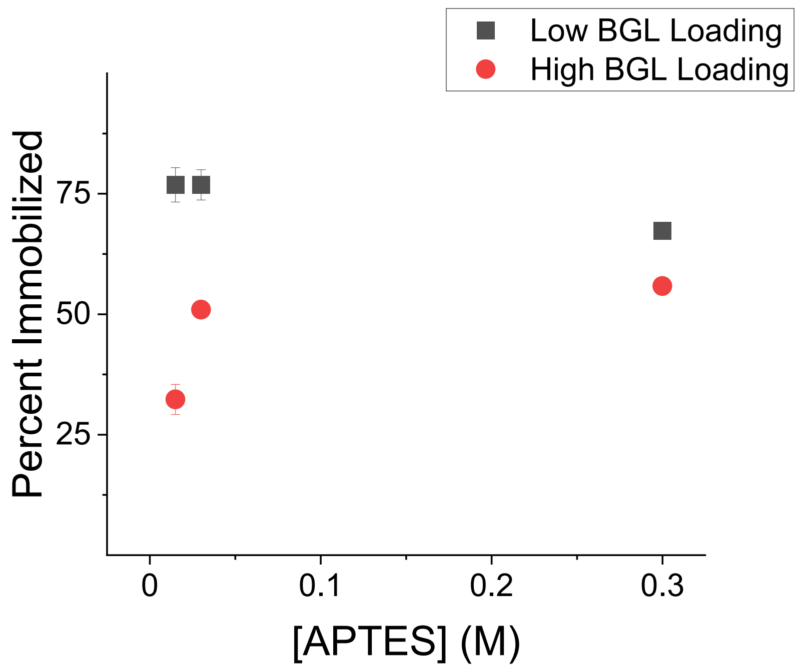

Figure 4. Percent BGL Immobilized on MNP-TEOS-APTES. The [APTES] refers to the [APTES] used for MNP modification. The BGL loading refers to the [BGL] used for immobilization; the low and high loading refer to either a 0.1 or 1 mg/mL BGL solution.

The decrease in immobilization efficiency at the high loading is interpreted initial BGL which attaches to the particle first, sterically hinders subsequent immobilization of adjacent binding sites.

While the presence of APTES was not observed in the IR spectra, the differing BGL immobilization yields between the different APTES concentrations at the high loading suggest that the APTES was present on the MNP-TEOS-APTES particles. Previous work has identified that the APTES concentration used for MNP-TEOS modification is proportional to the APTES density on the MNP-TEOS-APTES particles [16]. While the APTES density on the MNP-TEOS-APTES was not determined in this work, the correlation between the APTES concentration and BGL immobilization yield suggests that the different MNPs have differing APTES densities. At the high loading, MNP-TEOS-APTES-30 and MNP-TEOS-APTES-300 had similar BGL immobilization yields, 51 and 56%, which suggests the particle surface is approaching saturation with BGL.

BGL Activity and MNP Loss

Immobilizing BGL to the MNP-TEOS-APTES permits the capture and reuse of the enzyme. Recovery and reuse of enzymes is practical when immobilization to the particle is efficient, the enzyme maintains activity for subsequent catalytic cycles, and when an abundance of enzyme is immobilized to the MNP. To promote BGL immobilization, the MNP-TEOSs are routinely modified with APTES. However, the APTES modification of MNP-TEOSs lowers the magnetic susceptibility of the MNP, which may lessen the recovery of the MNP-TEOS-APTES between catalytic cycles. Incomplete recovery of MNP-TEOS-APTES-BGL would reduce the quantity of BGL for subsequent catalytic cycles and be observed as a reduction in activity for future cycles. To assess how the extents of APTES modification altered MNP-TEOS-APTES-BGL recovery, the MNP-TEOS-APTES-BGLs were subjected to a recycling study. The MNP-TEOS-APTES-BGLs were subjected to five catalytic cycles. Between each cycle, the MNP-TEOS-APTES-BGLs were magnetically separated and the supernatants collected. The supernatants were analyzed by ICP-OES to quantify the Fe concentration. The Fe in the supernatants was assumed to be unrecovered particles lost during washing between catalytic cycles.

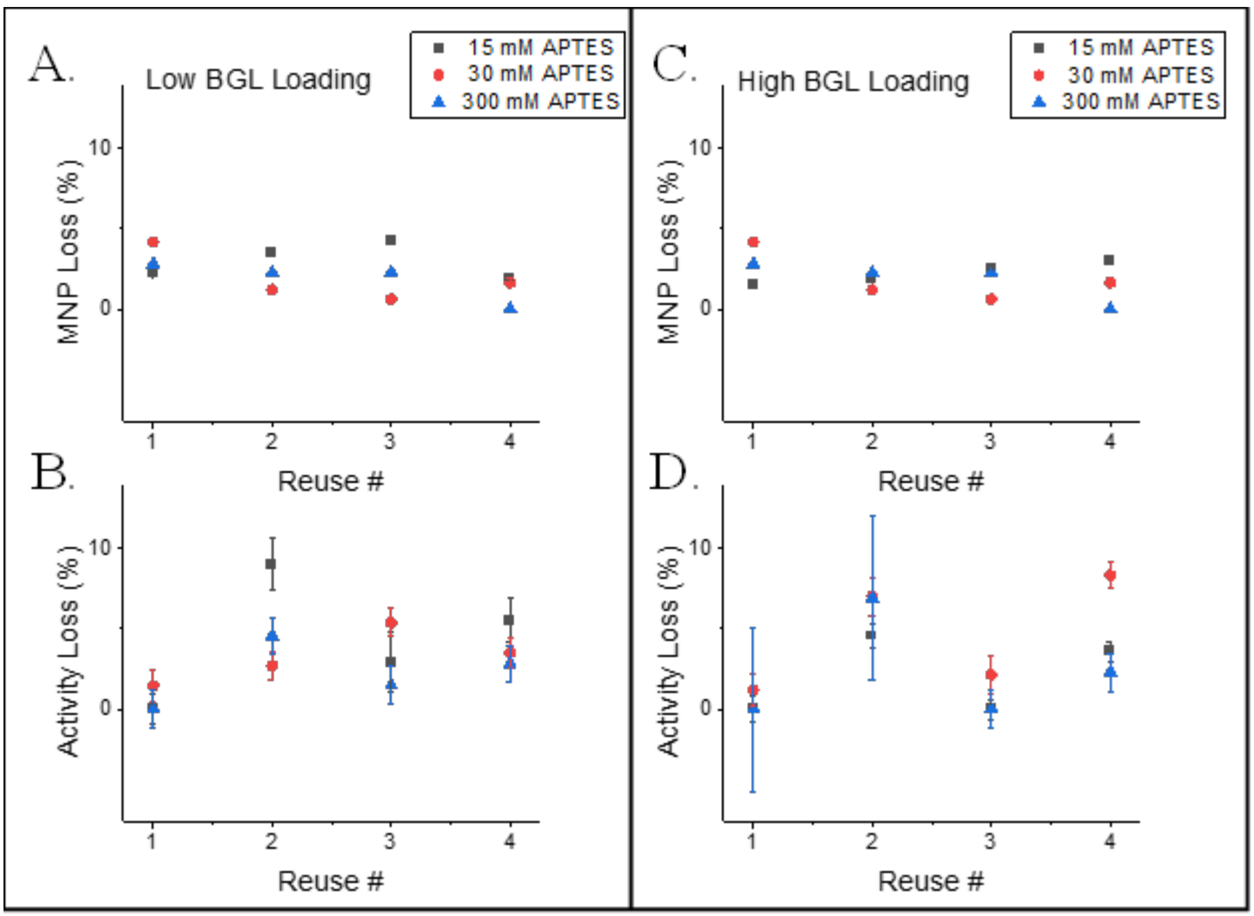

Figure 5. Particle and Activity Loss During Reuse for Particles with a Low BGL Loading (A and B) or a High BGL Loading (C and D). The [APTES] refers to the [APTES] used for MNP modification. BGL activity was measured following a 15 min hydrolysis step at 37 °C in 10 mM acetate buffer pH 5.0.

The particle loss and activity loss per cycle are shown in Figure 5, while the average particle and activity loss are shown in Figure 6.

The average particle loss for each cycle was ~2% relative to the initial Fe concentration. Neither the extent of APTES modification nor the BGL loading had a significant effect on the particle loss × cycle^{-1} as identified by two-way ANOVAs at the 95% confidence interval. These results were surprising as MNP modification is known to decrease the magnetic susceptibility [12], with the extent of MNP modification correlating to the decrease in magnetization [20]. However, the obtained APTES densities in this work for MNP-TEOS-APTES-15, MNP-TEOS-APTES-30 and MNP-TEOS-APTES-300 may be too similar to cause observable differences in magnetic susceptibility.

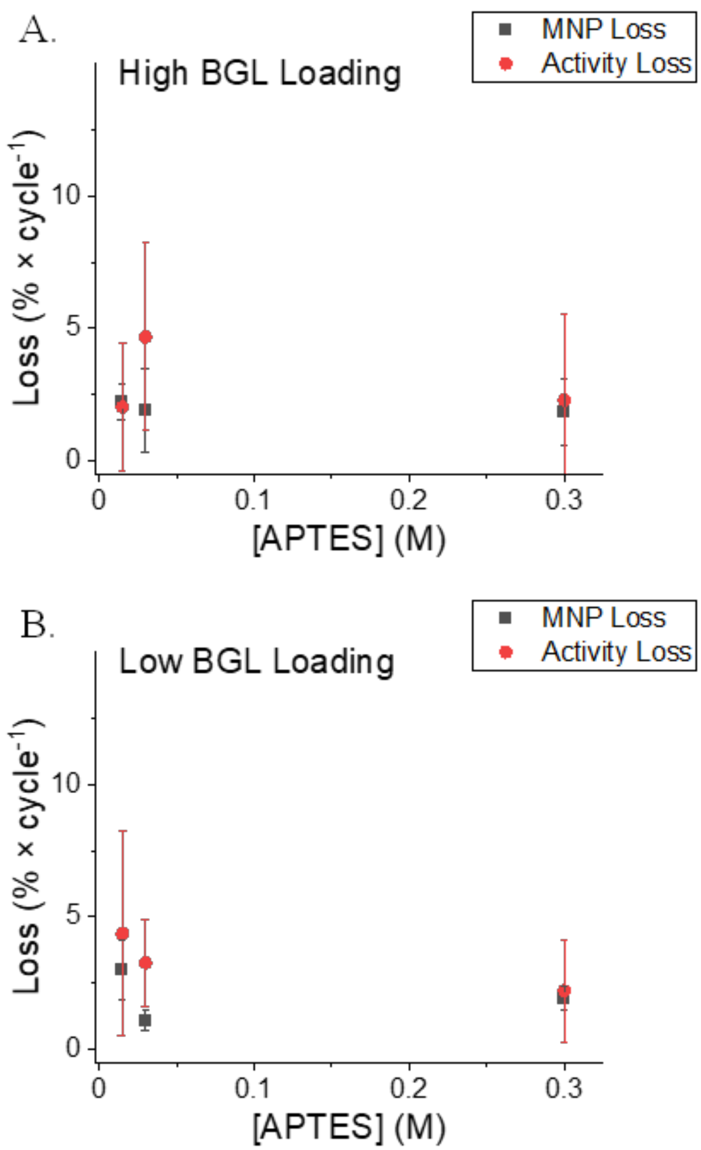

Figure 6. Average Particle Loss (black square) and Average Activity Loss (red circle) During Recycling for High BGL Loading (A) and Low BGL Loading (B).
The [APTES] refers to the [APTES] used for MNP modification. BGL activity was measured following a 15 min hydrolysis step at 37 °C in 10 mM acetate buffer pH 5.0. Avg ± 1 SD.

The immobilized BGL activity decreases upon use due to incomplete particle recovery and enzyme denaturation. The average activity decrease between catalytic cycles ranged from ~0 to 8% per cycle as shown in Figure 6. Neither the extent of APTES modification nor the BGL loading had a significant effect on the activity loss as observed by a two-way ANOVA at the 95% confidence interval. The activity loss per cycle obtained in this study agree with previously reported values of BGL activity loss ranging from ~4 to 6% per cycle [21].

An additional goal of this work was to explore how MNP-TEOS-APTES-BGL loss correlated with activity loss during recycling. The two reasons for activity loss during recycling are loss of the particles and enzyme denaturation. We therefore assumed that the total activity loss during recycling was the sum of the enzyme which denatured and the MNPs which were unrecovered. We analyzed the activity loss and particle loss data using an ANOVA which found no significant difference between the particle and activity loss × cycle^{-1} at the 95% confidence interval. This result suggests that that the loss of particles during magnetic separation is the prime contributor to activity loss during recycling, as unrecovered MNP-TEOS-APTES-BGL cannot participate in subsequent in the hydrolysis of substrate.

The cause(s) of low particle recovery observed in this study could not be elucidated with the present data. However, it is possible that magnetic susceptibility of the MNP-TEOS-APTES-BGLs decreased during use. The particles used in this study were comprised of magnetite, Fe_3O_4. The magnetic susceptibility of magnetite decreases exponentially as the mole ratio of Fe^{3+}:Fe^{2+} deviates from a 2:1 ratio [22], creating a challenge in aqueous applications of MNPs as Fe^{2+} rapidly oxidizes to Fe^{3+} in water [23]. It is possible that oxidation of Fe^{2+} in the particles lowered their recovery during the recycling experiment. Future experiments should quantify the Fe^{3+}/Fe^{2+} ratio in the recovered MNP-TEOS-APTES-BGLs and in the supernatants to identify if Fe oxidation is the cause of MNP-TEOS-APTES-BGL loss.

4. Conclusions

The immobilization of enzymes to MNPs enables the recovery and reuse of BGL. The low protein loading had the highest immobilization efficiency; therefore, immobilization should be performed at the low loading to reduce the financial cost of immobilized BGL. The activity of the recovered enzyme is diminished as the enzyme denatures and due to incomplete recovery MNP. However, low particle recovery is the main determinant in activity loss between catalytic cycles. Further, particle recovery is not affected by the extent of APTES modification nor the protein loading. These results suggest that particle recovery must be optimized to increase the retained activity of recycled catalysts, a pivotal parameter for the industrial use of enzymes immobilized to MNPs.

5. Acknowledgment

Funded by The Citadel Foundation and The Near Center for Climate Studies.

6. References

1. Liese A, Hilterhaus L. Evaluation of immobilized enzymes for industrial applications. *Chem. Soc. Rev.*, 2013, 42(15), 6236-6249. https://doi.org/10.1039/C3CS35511J.
2. Liu G, Zhang J, Bao J. Cost evaluation of cellulase enzyme for industrial-scale cellulosic ethanol production based on rigorous Aspen Plus Modeling. *Bioprocess Biosyst. Eng.*, 2016, 39(1), 133-140. https://doi.org/10.1007/s00449-015-1497-1.
3. Razzaghi M, Homaei A, Vianello F, Azad T, Sharma T, Nadda AK, Stevanato R, Bilal M, Iqbal HMN. Industrial applications of immobilized nano-biocatalysts. *Bioprocess Biosyst. Eng.*, 2022, 45(2), 237-256. https://doi.org/10.1007/s00449-021-02647-y.
4. DiCosimo R, McAuliffe J, Poulose AJ, Bohlmann G. Industrial use of immobilized enzymes. *Chem. Soc. Rev.*, 2013, 42(15), 6437-6474. https://doi.org/10.1039/C3CS35506C.
5. Khoshnevisan K, Poorakbar E, Baharifar H, Barkhi M. Recent advances of cellulase immobilization onto magnetic nanoparticles: An update review. *Magnetochemistry*, 2019, 5(2). https://doi.org/10.3390/magnetochemistry5020036.
6. Melo RLF, Sales MB, de Castro Bizerra V, de Sousa Junior PG, Cavalcante ALG, Freire TM, Neto FS, Bilal M, Jesionowski T, Soares JM, Fechine PBA, Dos Santos JCS. Recent applications and future prospects of magnetic biocatalysts. *Int. J. Biol. Macromol.*, 2023, 253 (Pt 3), 126709. https://doi.org/10.1016/j.ijbiomac.2023.126709.
7. Khoshnevisan K, Vakhshiteh F, Barkhi M, Baharifar H, Poor-Akbar E, Zari N, Stamatis H, Bordbar A-K. Immobilization of cellulase enzyme onto magnetic nanoparticles: Applications and recent advances. *Mol. Catal.*, 2017, 442, 66-73. https://doi.org/10.1016/j.mcat.2017.09.006.
8. Vandenberg E, Elwing H, Askendal A, Lundström I. Protein immobilization of 3-aminopropyl triethoxy silaneglutaraldehyde surfaces: Characterization by detergent washing. *J. Colloid Interface Sci.*, 1991, 143(2), 327-335. https://doi.org/10.1016/0021-9797(91)90266-B.
9. Bilal M, Asgher M, Cheng H, Yan Y, Iqbal HMN. Multi-point enzyme immobilization, surface chemistry, and novel platforms: A paradigm shift in biocatalyst design. *Crit. Rev. Biotechnol.*, 2019, 39(2), 202-219.

https://doi.org/10.1080/07388551.2018.1531822.
10. Adriano WS, Filho EHC, Silva JA, Gonçalves LRB. Optimization of penicillin G acylase multipoint immobilization on to glutaraldehyde-chitosan beads. *Biotechnol. Appl. Biochem.*, 2005, 41(3), 201-207. https://doi.org/10.1042/BA20040061
11. Banaei M, Salami-Kalajahi MA. Grafting to approach to synthesize low cytotoxic poly(aminoamide)-dendrimer-grafted Fe_3O_4 magnetic nanoparticles. *Adv. Polym. Technol.*, 2018, 37(3), 943-948. https://doi.org/10.1002/adv.21741.
12. Ghazanfari MR, Kashefi M, Shams SF, Jaafari MR. Perspective of Fe_3O_4 nanoparticles role in biomedical applications. *Biochem. Res. Int.*, 2016, 2016, 7840161. https://doi.org/10.1155/2016/7840161.
13. Dhavale RP, Waifalkar PP, Sharma A, Dhavale RP, Sahoo SC, Kollu P, Chougale AD, Zahn DRT, Salvan G, Patil PS, Patil PB. Monolayer grafting of aminosilane on magnetic nanoparticles: An efficient approach for targeted drug delivery system. *J. Colloid Interface Sci.*, 2018, 529, 415-425. https://doi.org/10.1016/j.jcis.2018.06.006.
14. Yuan Y, Rende D, Altan CL, Bucak S, Ozisik R, Borca-Tasciuc D-A. Effect of surface modification on magnetization of iron oxide nanoparticle colloids. *Langmuir ACS J. Surf. Colloids*, 2012, 28(36), 13051-13059. https://doi.org/10.1021/la3022479.
15. Singh G, Verma AK, Kumar V. Catalytic properties, functional attributes and industrial applications of β-glucosidases. *3 Biotech*, 2016, 6(1), 3. https://doi.org/10.1007/s13205-015-0328-z.
16. Vasicek TW, Guillermo S, Swofford DR, Durchman J, Jenkins SV. β-Glucosidase immobilized on magnetic nanoparticles: Controlling biomolecule footprint and particle functional group density to navigate the activity-stability tradeoff. *ACS Appl. Bio Mater.*, 2022, 5(11), 5347-5355. https://doi.org/10.1021/acsabm.2c00735.
17. Ma M, Zhang Y, Yu W, Shen H, Zhang H, Gu N. Preparation and characterization of magnetite nanoparticles coated by amino silane. *Colloids Surf., A*, 2003, 212(2), 219-226. https://doi.org/10.1016/S0927-7757(02)00305-9.
18. Shahbazi R, Babazadeh M, Afzali E. Surface modification of silica-coated on the magnetic nanoparticles with covalently immobilized between imidazolium cation and silane groups for potential application as a green catalyst. *MOJ Bioorg. Org. Chem.*, 2018, 2. https://doi.org/10.15406/mojboc.2018.02.00048.
19. Barth A. Infrared spectroscopy of proteins. *Biochim. Biophys. Acta, Bioenerg.*, 2007, 1767(9), 1073-1101. https://doi.org/10.1016/j.bbabio.2007.06.004.
20. Digigow RG, Dechézelles J-F, Dietsch H, Geissbühler I, Vanhecke D, Geers C, Hirt AM, Rothen-Rutishauser B, Petri-Fink A. Preparation and characterization of functional silica hybrid magnetic nanoparticles. *J. Magn. Magn. Mater.*, 2014, 362, 72-79.

https://doi.org/10.1016/j.jmmm.2014.03.026.

21. Park HJ, Driscoll AJ, Johnson PA. The development and evaluation of β-glucosidase immobilized magnetic nanoparticles as recoverable biocatalysts. *Biochem. Eng. J.*, 2018, 133, 66-73. https://doi.org/10.1016/j.bej.2018.01.017.
22. Schwaminger SP, Bauer D, Fraga-García P, Wagner FE, Berensmeier S. Oxidation of magnetite nanoparticles: Impact on surface and crystal properties. *CrystEngComm*, 2017, 19(2), 246-255. https://doi.org/10.1039/C6CE02421A.
23. Demangeat E, Pédrot M, Dia A, Bouhnik-le-Coz M, Grasset F, Hanna K, Kamagate M, Cabello-Hurtado F. Colloidal and chemical stabilities of iron oxide nanoparticles in aqueous solutions: The interplay of structural, chemical and environmental drivers. *Environ. Sci.: Nano*, 2018, 5(4), 992-1001. https://doi.org/10.1039/C7EN01159H.

The Chemist
Journal of the American Institute of Chemists

Eco-Friendly Formulation, Characterizations, Bioactivity Studies and *in silico* Evaluation of Cosmetic prepared from the Seed Oils of *Carica papaya*, *Dacryodes edulis* and *Raphia hookeri*

***Stephen Olubunmi Oguntoye, Oluebube Love Ezennaya, Olaniyi Kamil Yusuff, *Olubunmi Atolani**

Department of Chemistry, University of Ilorin, Ilorin, Nigeria
**Corresponding author (E-mail: stevorol@unilorin.edu.ng; atolani.o@unilorin.edu.ng)*

Abstract: A quarter of a century ago, there was a renewed interest in the application of natural products in cosmetic formulations as a result of increased toxicities and side effects associated with synthetic/orthodox body care products. In the present study, oils obtained via Soxhlet/cold extraction from different underexplored tropical seeds, include: *Carica papaya*, *Dacryodes edulis* and *Raphia hookeri*, were investigated and characterised for their potential sustainable application in skin care formulations. The three oils obtained from the seed samples were also analysed for their fatty acids composition by capillary gas chromatography-mass spectrometry (GC-MS) following trans-esterification using acid-catalysed hydrolysis. Several *in vitro* biological activities, include: antibacterial, antifungal, and antityrosinase, were determined using standard procedure. The seed oils from *C. papaya*, *D. edulis,* and *R. hookeri* afforded a yield of 19.89, 8.27 and 0.04%, respectively. The major fatty acids composition of the seed oils from *C. papaya* were docosanoic (15.36%), elaidic (51.83%), linoleic (17.47%) and stearic (11.22%) acids while *D. edulis* had palmitic (13.98%), linoleic (50.08%), dihomo-γ-linolenic (15.53%) and oleic acids (10.16%). Palmitic acid (33.88%), elaidic (28.74%), palmitoleic acid (18.98%) and stearic acids (8.57%) were the most prominent in *R. hookeri*. The antimicrobial activity of the oils investigated at 30 μg/mL revealed that *C. papaya* significantly inhibited the growth of *Saccharomyces cerevisiae*, while *D. edulis* inhibited the growth of *Staphylococcus aureus*, *Rhizopus stolonifera*, *Penicillium citrinum*, *Saccharomyces cerevisiae* and *Aspergillus niger*. *R. hookeri* inhibited the growth of *Salmonella typhi, Rhizopus stolonifera, Penicillium citrinum* and *Saccharomyces cerevisiae*. Likewise, *C. papaya* had an antityrosinase activity with an IC_{50} value of 0.26 μg/mL, while *D. edulis* and *R. hookeri* had an IC_{50} value of 4.52 and 0.83 μg/mL, respectively. The formulated cream products from the seed oils of *C. papaya* and *D. edulis* exhibited dose response activities on the microorganisms and the tyrosinase enzyme. The *in silico* analysis also re-affirms that the oil components had significant interactions with the tyrosinase enzyme by exhibiting strong affinity via numerous van der Waals forces comparable to the standard, kojic acid. This study has revealed that oils from the seeds of the underutilised plants; *C. papaya*, *D. edulis,* and *R. hookeri*, can be further exploited for medicinal and industrial purposes, particularly in the green cosmetic formulation sector for the regulation of skin pigmentation. However, more studies in animal models would be required to validate the bioactivity and toxicity.

Key Words: Lipid, fatty acid, antimicrobial, *in silico*, tyrosinase, binding affinity

1. Introduction

There is an increasing global demand for the adoption of green chemistry for products and product development due to its benign properties. Green Chemistry, also known as Sustainable Chemistry, which involves the creation of chemical products and processes that minimize or eliminate the use of hazardous substances has received global attention in the last few decades. The concept has had a significant impact on businesses, education, the environment, and the general consumer world. The concept is both profitable and beneficial to human health and the environment [1]. Hence, the application of green chemistry in the preparation and manufacture of skin care products forms the fulcrum of recent developments in the cosmetic world [2]. The concept has been promoted recently in the cosmetic sectors for the preparation and production of products that are safe for humans and the environment. Seed oil plays an important role in the production of green cosmetics [2,3]. Among tropical seeds that have been underexplored and underutilised are *Carica papaya*, *Dacryodes edulis,* and *Raphia hookeri.*

Carica papaya of the family Caricacea is a globally renowned plant that produces fleshly edible pulp with high quality vitamins. It contains seeds that are round and dark brown in nature. Like the fruit, the seed is also very rich in nutrients with excellent medicinal properties that can be used to manage a variety of ailments. The leaves, seeds, latex, and fruit of the plant have all been shown to possess significant medicinal value [4]. Despite its medicinal potential, the seed and the seed oil are grossly discarded, under-valued, or ignored. *D. edulis* of the family *Burseraceae* is an endemic tropical African plant. The fruit and seed are used as food, fodder, and medicine to cure earache, fever, and headache [5]. *D. edulis* seeds have been investigated as a source of high-quality oil [6]. *R. hookeri* (Raphia palm) of the family *Arecaceae* is a rare tropical tree with characteristic oblong edible pulp but an extremely hard nut when matured and dried [7]. On account of its rare nature, there is a dearth of information on the studies on the plant. Hence, this research aimed to characterize three underexplored tropical seeds (*C. papaya*, *D. edulis,* and *R. hookeri*) and explore their oil for bioactive, eco-friendly, safe cosmetic formulations using the principle of green chemistry.

2. Materials and Method

Chemicals, solvents, and other reagents used were of analytical grade. Where applicable, the solvent was re-distilled before use. L-tyrosine was a product of Sigma-Aldrich, USA, while the microplate spectro-photometer was a Spectra Count, Packard, USA. For centrifugation, a Bench centrifuge Model 800D was used.

Plant Material and Preparation

Matured *C. papaya* seeds were obtained within the Ilorin metropolis in Kwara State, while *D. edulis* seeds were obtained from Owerri in Imo State and *R. hookeri* from Umuchu, Anambra State, Nigeria. The seeds were identified and authenticated at the herb-arium unit of the Plant Biology Department, University of Ilorin, Ilorin, Nigeria. The seeds were dried at ambient temperature, de-shelled, pulverized, and then kept in a cool dark place for further work.

Extraction of Oils from the Seeds

The pulverized seed material was extracted in Soxhlet extractor for 6 hr, as well as cold n-hexane, for three days. The extracts obtained were concentrated *in vacuo* using the rotary evaporator and the resulting oils were air-dried, stored a in glass vial and kept in a cool dry place for further work. The yield was determined using the expression below:

$$\%\ \text{Oil yield} = \frac{\text{Weight of the oil}}{\text{Weight of seeds}} \times 100 \qquad (1)$$

Physicochemical Analysis of the Extracted Seed Oils

The physicochemical properties of the oils determine their quality and hence, what the seed oils are suitable for. These properties of the oils, which include acid value, iodine value, saponification value, peroxide value, ester value, density, specific gravity, and pH, were determined using standard procedures with slight modifications where applicable [8 – 11].

Determination of Acid Value

Each of the oils (1 g) was weighed into a flask with 25 mL of diethyl ether and 25 mL of methanol. Three drops of phenolphthalein indicator were added. The mixture was warmed in a water bath for 5 minutes and titrated against 0.1 M KOH with constant shaking until the pink colour appeared that indicated the end point [10 – 14]. The acid value of the oil was evaluated using the equation:

$$\text{Acid value} = \frac{56.1 \times V \times N}{W} \quad (2)$$

where, W = Weight of oil (in grams)
V = Volume of the standard alcoholic potassium hydroxide solution required to neutralize the sample
N = Normality of the solution

Determination of Iodine Value

Each of the oils (1 g) was weighed into a 250 mL conical flask and the oil was dissolved in 25 mL carbon tetrachloride. Twenty - five mL Wijis solution was added and the mixture allowed to stand in the dark for one hour. The liberated iodine was titrated against 0.1 M sodium thiosulphate using starch indicator [10 – 12, 14] The iodine value was determined using the expression:

$$\text{Iodine value} = \frac{12.69\ (B-A)}{W} \quad (3)$$

where, W = Weight of oil (in grams)
B = Volume of standard sodium thiosulfate solution for blank (in mL)
A = Volume of standard sodium thiosulfate solution required for the sample
N = Normality

Determination of Specific Gravity

A clean and dried measuring cylinder (10 mL) was weighed and recorded as W_o. Each oil (1 mL) was measured into the cylinder, weighed and recorded as W_1. Distilled water (1 mL) was measured into the cylinder and the weight was recorded as W_2 [12 – 14]. The specific gravity was calculated using the expression:

$$\text{Specific gravity} = \frac{W1 - W0}{W2 - W0} \quad (4)$$

where, W_o = Weight (in grams) of empty measuring cylinder
W_1 = Weight (in grams) of measuring cylinder with oil
W_2 = Weight (in grams) of measuring cylinder with water

Determination of Density

A clean and dried measuring cylinder (10 mL) was weighed and recorded as W_o. Each oil (1 mL) was measured into the cylinder, weighed and recorded as W_1 [12 – 14]. Thereafter, the density was determined by using the formula:

$$\text{Density} = \frac{\text{Weight of the oil (W1} - W0)}{Volume\ of\ the\ oil} \tag{5}$$

where, W_o = Weight (in grams) of empty measuring cylinder

W_1 = Weight (in grams) of measuring cylinder with oil

Determination of Peroxide Value

Each of the oils (0.5 g) was weighed into a flask containing 1 g of potassium iodide and 13 mL glacial acetic acid; 7 mL chloroform was added to it. The conical flask was placed in a water bath for 1 minute, after which 20 mL of 5% potassium iodide mixture and 25 mL of water were added. The mixture was titrated against 0.002 M sodium thiosulphate to attain a colourless solution using a starch indicator. Blank titration was carried out [10 – 14]. The peroxide value was calculated from the expression [15]:

$$\text{Peroxide value} = \frac{S \times \text{N X } 100}{W} \tag{6}$$

where, W = Weight (in grams) of the oil

N = Normality of $Na_2S_2O_3$

S = Volume (in mL) of $Na_2S_2O_3$

Determination of Saponification value

Each of the oils (0.5 g) was weighed into a flask containing 25 mL of methanolic KOH and mixed together. The mixture was warmed in a water bath for 5 min and 3 drops of phenolphthalein were added while the contents were titrated against 0.5 M HCl until the pink colour disappeared. The discolouration indicated the end point. A blank titration was performed by omitting the oil (b mL). The saponification value was calculated using the expression [2 – 15]:

$$\text{Saponification value} = \frac{56.1 \times \text{M X (b} - a)}{W} \tag{7}$$

where, W = Weight (in grams) of the oil

M = Molarity of HCl

56.1 = Molecular weight of KOH

Determination of Ester Value

The Ester value was estimated as the difference between the saponification value and the acid value [10 – 14].

Determination of pH

The pH meter was used to determine the level of acidity or basicity of the oil and the formulated cream products.

Determination of Transesterification

The oil (2g) was weighed and transferred to a beaker containing 10 mL of 0.2 M methanolic HCl. The mixture was refluxed for 1 hour, poured into a separating funnel and extracted with hexane. The mixture was shaken and allowed to settle down for the two layers to separate. The oil layer was collected, concentrated, and air-dried; the oil obtained was kept in glass vials for GC-MS analyses [2].

Gas Chromatography-Mass Spectrometric (GC-MS) Analysis of the Oils

To determine the fatty acid profile from the seeds of *C. papaya*, *D. edulis* and *R. hookeri*, 1.0 µL of the trans-esterified oil was injected in a non-overlap mode to a Gas Chromatography-Mass Spectrometry GC–MS QP 2010SE Ultra Shimadzu Japan with a FI and selective mass detector 5973 RTx. The GC was equipped with a HP-5MS column with a size of 30 m by 0.25 mm and 0.25 µm film thickness set to pressure flow control mode at 100.0 kPa. The heater and interface were operated at 100 and 300 °C, respectively, while the injection temperature was set at 250 °C. Total flow and column flow were 58.7 and 1.79 mL/min, respectively, as linear velocity was 35.2 cm/sec. Elution was done isothermally using a split ratio of 30:1 at an equilibration time of 3.0 minutes and a purge flow of 3.0 mL/min. The MS parameters included electron impact ionization with electron energy of 70 eV, and mass range of *m*/*z* 50–550, using the selective ion monitoring (SIM) mode. The scan was operated for few 25.5 minutes and chemical constituents were identified primarily by comparing the fragmentation pattern of each spectrum with reference compounds in the NIST library.

UV-Visible Spectroscopic Analysis

The UV-Visible analysis of the seed oils was carried out using a VWR UV-6300PC Double Beam Spectrophotometer using n-hexane as the dissolving solvent. The concentration of the stock solution was 30 µg/mL.

Antimicrobial Assay

The antibacterial and antifungal assays with the minimum inhibitory concentrations were evaluated using standard protocol by determining the zone of inhibition of the oil and cream products [16]. Briefly, for the antibacterial evaluation, the test samples (30 μg/mL each) were prepared and 1 mL each was added to 9 mL of sterile molten Muller Hinton agar (MHA) and potato dextrose agar (PDA), respectively, at 40 °C. The medium was poured into sterile petri dishes and allowed to dry before streaking for 18 hours for selected isolates. The petri dishes were incubated at 37 °C for 24 hours for bacteria growth, while the PDA plates were incubated at ambient temperature, and fungi growth was examined after 72 hours. All the plates were examined for the presence or absence of microbial growth. The minimum inhibition concentration (MIC) was taken as the least concentration that prevents bacterial and fungal growth, respectively.

Determination of Antityrosinase Activity

The tyrosinase inhibition activity potential was carried out following standard protocol [17]. Aliquots (10 μL) of a solution composed of 125 μmL^{-1} of mushroom tyrosinase (Sigma-Aldrich, USA) were added to 96-well microplates, and then 70 μL of pH 6.8 phosphate buffer solution and 60 μL of the oils (350 $\mu g\ mL^{-1}$ in n-hexane) were also added. For the positive control, 60 μL of kojic acid (17.5 μgmL^{-1} in n-hexane) was used instead of the seed oil, and for the negative control, 60 μL of n-hexane was used. To the resultant mixture, 70 μL of L-tyrosine (Sigma-Aldrich, USA) was added at a concentration of 0.3 $mgmL^{-1}$ in distilled water. The absorbance of the microplate wells was read using a microplate spectro-photometer (Spectra Count, Packard, USA) at 510 nm (T_0). Then, the microplates were incubated at 30 ± 1°C for 60 min and the absorbance was measured again (T_1). An additional incubation period of 60 min at 30 ± 1°C was done and, after this period, a new spectrophotometric reading was taken (T_2). The inhibitory percentage at the two time points (T_1 and T_2) was obtained according to the formula:

$$IA\ (\%) = [((C-T_0) - (S- T_0)) / (C- T_0)] \times 100 \tag{8}$$

where IA% = Inhibitory activity

C = Negative control absorbance at 510 nm

S = Sample or positive control absorbance at 510 nm (absorbance at time T_1 or T_2 minus the absorbance at time T_0).

Membrane Stabilization Assay

The membrane stabilization activity of the oils and creams was evaluated on bovine red blood cells exposed to both heat and hypotonic induced lyses using standard procedure [18, 19]. Briefly, fresh bovine blood samples were collected into an anticoagulant [containing dextrose (2%), sodium citrate (0.8%), citric acid (0.05%) and sodium chloride (0.42%)]. Blood samples were centrifuged at 3000 rpm on a Bench centrifuge Model 800D for 10 min at room temperature. The supernatants (plasma and leucocytes) were carefully removed while the packed red blood cell was washed in fresh normal saline (0.85% w/v NaCl). The process of washing and centrifugation was repeated five times until the supernatants were clear.

The membrane stabilizing activity assay was carried out using 2% (v/v) bovine erythrocyte suspension while indomethacin was used as the standard drug. The assay mixtures consisted of 2 ml of hyposaline (0.25% w/v) sodium chloride, 1.0 ml of 0.15 M sodium phosphate buffer, pH 7.4, 0.5 ml of 2% (v/v) bovine erythrocyte suspension, 0.0 - 1.0 ml of drugs (standard, extracts/fractions) and final reaction mixtures were made up to 4.5 ml with isosaline. Drugs were omitted in the blood control, while the drug control did not contain the erythrocyte suspension. The reaction mixtures were incubated at 56°C for 30 min on a water bath, followed by centrifugation at 5000 rpm in a Gallenkamp Bench Centrifuge for 10 min at room temperature. While the blood control represents 100% lysis or zero percent stability [18], the absorbance of the released haemoglobin was read at 560 nm. The percentage membrane stability was estimated using the expression:

$$\%\, Membrane\ stabilization = \frac{100-(Abs\ of\ test\ drug - Abs\ of\ drug\ control)}{Abs\ of\ blood\ control} \times 100 \quad (9)$$

Thin Layer Chromatographic (TLC) Analysis

The thin-layer chromatography of the oils was carried out using a pre-coated TLC plate to determine the complexity of components in the extracted oils. The oils were spotted in a TLC plate and developed in an n-hexane and ethyl acetate solvent mixture (3:1 for *C. papaya* and *D. edulis*; while 9:1 for *R. hookeri*). The chromatoplate was viewed under the UV lamp at 254 and 366 nm, respectively.

Computational Analysis

Molecular docking was adopted as a computational technique used to study the interaction of molecules in the binding sites of target proteins. The goal of ligand-protein docking is to understand the interaction of a ligand with a protein of known three-dimensional structure. Molecular docking calculations are a common assay used to determine the biological activity of molecules *in silico*. With docking methods, large numbers of molecules are screened at a relatively lower cost than in laboratory experiments. The technique is a key tool in structural molecular biology and computer-assisted drug design [20]. Molecular docking technique was used to investigate the *in vitro* inhibition effects of *C. papaya, D. edulis,* and *R. hookeri* seed oil on tyrosinase enzyme with ID 5M8L. Kojic acid was used as standard. A PDF file was created, the binding site defined and the docking performed following the procedure outlined by Trott and Johnson, 2010 [20].

Cream Formulation

All materials, which include beeswax and oils from different seeds of *C. papaya* and *D. edulis*, were used for the formulation. Beeswax (1 g) was weighed into a 250 mL beaker and melted in a warm water bath. Seed oils (2 g) were added to the beaker and heated for 3 minutes. The mixture was transferred immediately to a container for cooling and solidification. This procedure was repeated while varying the amount of oil and beeswax as indicated (Table 1).

Table 1. Cream Formulation

Formulation	**Beeswax** (g)	**Oil** (g)
A	1.0	0.0
B	0.8	0.2
C	0.6	0.4
D	0.4	0.6
E	0.2	0.8
F	0.0	1.0

Data Analysis

All experiments were performed in replicate except otherwise indicated and the results were presented as mean of the values. For the bioassay, the concentration causing 50% inhibition (IC_{50}) was estimated from a dose-response curve.

3. Results and Discussion

Percentage Yield of the Seed Oils

The percentage yield of oils from the seeds of *C. papaya*, *D. edulis* and *R. hookeri* extracted using n-hexane provided 19.89, 8.27 and 0.04%. The considerable percentage yield of oil from *C. papaya* showed that it can be exploited for industrial use. *D. edulis* can also be harnessed while *R. hookeri* gave a low yield, which might be difficult to be used for any industrial application.

The thin-layer chromatographic results revealed that only oil from the seed of *C. papaya* shows one distinct component under the UV lamp at 254 nm with R_f value of 0.33. While *D. edulis* and *R. hookeri* gave three to five components with different R_f values.

Physicochemical Analysis of Different Seed Oils

The physicochemical properties of oils from the seeds of *C. papaya* and *D. edulis* are as shown (Table 2). Oil from the seeds of *R. hookeri* was not sufficient for physicochemical analysis because of very low percentage yield.

Table 2. Physicochemical Properties of Oils from the Seeds of *C. papaya*, *D. edulis* and *R. hookeri*

Parameter	*C. papaya*	*D. edulis*	*R. hookeri*
Colour	Light brown	Cream	Light yellow
Smell	Pleasant	Slightly Chocking	Pleasant
State at ambient temperature	Liquid	Semi-solid	Semi-solid
% Oil trans-esterified	90	90	-
pH value	5.4	5.1	
Specific gravity	0.91	0.83	
Density (g/cm^3)	1.0	1.0	
Saponification value (mgKOH/g)	157.08	112.2	
Acid value (mgKOH/g)	3.36	16.83	
Ester value (mgKOH/g)	153.71	95.37	
% Neutral fatty matter	164.29	107.14	
% Total fatty matter	28.575	28.57	
Peroxide value ($meqKg^{-1}$)	5.2	10	
Iodine value (Wijs)	101.53	136.42	

The acid value of oils from the seeds of *C. papaya* and *D. edulis* were 3.36±0.08 and 16.83±0.00 mg KOH/g, respectively. According to Burla *et al.,* 2018 [22], the acidity of oil suitable for edible purposes should not exceed 4 mg KOH/g. Thus, the oil from the seeds of *C. papaya* would be suitable for consumption while the oil from the seeds of *D. edulis* will not. The saponification value of oils from the seeds of *C. papaya* and *D. edulis* were relatively low in comparison to those of almond nut (163.39±15.80) and palm kernel seed oil (191.97±3.16 mg KOH/g mg KOH/g). This result indicated that the seed oil contains high molecular weight fatty acids since the saponification values have been reported to be inversely related to the average molecular weight of fatty acids in oil fractions [23]. The saponification value of *C. papaya* seed oil is 157.08 mg KOH/g, while that of *D. edulis* seed oil is 112.2 mg KOH/g.

Iodine value is used to measure the degree of unsaturation of the oil. It is useful in studying oxidative rancidity of oils since the higher the unsaturation, the greater the possibility of the oil to go rancid [22]. Oils from the seeds of *C. papaya* and *D. edulis* tested had high iodine values (101.53 and 136.42 Wijs, respectively) and are therefore not suitable as non-drying oil. The peroxide value of oils from the seeds of *C. papaya* and *D. edulis* obtained were 5.2±0.13 and 10 mEq/kg, respectively. These values were not considered high since crude vegetable oil consists of 10 mEq/kg of peroxide value [22]. The pH value of seed oils from *C. papaya* and *D. edulis* (5.4 and 5.1, respectively) were slightly low thereby affirming the acidic nature partly due to acid values. Specific gravity is an important property always considered in oils which serves as feedstock for biodiesel. Denser oils have higher specific gravity. The specific gravity affects the oil properties, particularly the flow and the volatility [22]. The specific gravity of oils from the seeds of *C. papaya* and *D. edulis* obtained were 0.91 and 0.83, respectively.

Antimicrobial Assay Result

The antimicrobial inhibition potential of the oils and formulations are as depicted (Table 3).

From the data obtained (Table 3), at 30 µg/mL, *C. papaya* seed oil had little inhibitory effect on the selected bacteria but inhibited *Saccharomyces cerevisiae* (a fungus) and *Candida albicans* (a yeast). The formulated creams from *C. papaya* possess dose response antibacterial activity against *Pseudomonas aeruginosa*, *Streptococcus faecalis*, *Escherichia coli*, *Staphylococcus aureus* and *Salmonella typhi.* They also possess dose response antifungal activity on *Candida albicans*, *Rhizopus stolonifera*, *Penicillium citrinum*, *Saccharomyces cerevisiae* and *Aspergillus niger.*

Table 3. Antibacterial Activity of the Formulations (30 µg/mL) from *C. papaya*

Test Organism	**Zone of Inhibition** (mm)					
Bacteria	**A**	**B**	**C**	**D**	**E**	**F**
Pseudomonas aeruginosa	23	35	10	-	-	-
Streptococcus faecalis	20	18	10	5	-	-
Escherichia coli	13	25	18	15	-	-
Staphylococcus aureus	18	16	10	18	-	-
Salmonella typhi	30	5	5	-	-	-

Table 4. Antifungal Activity of Different Cream Formulation (30 µg/mL) Screened by Disc Diffusion

Test Organisms	**Zone of Inhibition** (mm)					
Fungi	**A**	**B**	**C**	**D**	**E**	**F**
Candida albicans	15	5	-	-	-	-
Rhizopus stolonifera	-	-	-	-	-	-
Penicillium citrinum	-	-	-	-	18	
Saccharomyces cerevisiae	15	-	-	-	-	5
Aspergillus niger	10	15	18	10	-	-

Likewise, at 30 µg/mL, *D. edulis* seed oil (Table 5) inhibited *Staphylococcus aureus* (a bacterium), *Rhizopus stolonifera*, *Penicillium citrinum*, *Saccharomyces cerevisiae* and *Aspergillus niger* (fungi). The formulated creams from *D. edulis* possess dose response antibacterial activity against *Pseudomonas aeruginosa*, *Streptococcus faecalis*, *Escherichia coli*, *Staphylococcus aureus* and *Salmonella typhi.* They also possess dose response antifungal activity on *Candida albicans*, *Rhizopus stolonifera*, *Penicillium citrinum*, *Saccharomyces cerevisiae* and *Aspergillus niger*.

Table 5. Antibacterial Activity of Different Cream Formulation (30 µg/mL) from *D. edulis*

Test Organism	**Zone of Inhibition** (mm)					
Bacteria	**A**	**B**	**C**	**D**	**E**	**F**
Pseudomonas aeruginosa	23	25	13	-	-	-
Streptococcus faecalis	20	16	10	22	-	-
Escherichia coli	13	10	-	-	5	-
Staphylococcus aureus	18	13	5	15	-	5
Salmonella typhi	30	18	5	18	-	-

Table 6. Antifungal Activity of Different Cream Formulations (30 µg/mL)

Test Organism	**Zone of Inhibition** (mm)					
Fungi	**A**	**B**	**C**	**D**	**E**	**F**
Candida albicans	15	23	-	15	-	-
Rhizopus stolonifera	-	-	-	25	25	30
Penicillium citrinum	-	-	-	12	16	20
Saccharomyces cerevisiae	15	5	7	5	-	6
Aspergillus niger	10	20	15	-	-	25

At 30 µg/mL, *R. hookeri* inhibited (Table 7) the growth of *Salmonella typhi* (a bacterium), *Rhizopus stolonifera*, *Penicillium citrinum* and *Saccharomyces cerevisiae* (fungi). The low yield of oil from *Raphia hookeri* impaired cream formulations.

Table 7. Antibacterial and Antifungal Activities of *R. hookeri* Seed Oil

Test Organism	Zone of Inhibition (mm)
Bacteria	
Pseudomonas aeruginosa	-
Streptococcus faecalis	-
Escherichia coli	-
Staphylococcus aureus	-
Salmonella typhi	16
Fungi	
Candida albicans	-
Rhizopus stolonifera	23
Penicillium citrinum	20
Saccharomyces cerevisiae	14
Aspergillus niger	-

Key: (-) No clear zones of inhibition

Table 8. Antibacterial Inhibitory Effects of Standard Drugs Used as Positive Control

Bacteria	S	NB	CH	CPX	E	LEV	CN	APX	RD	AMX
Pseudomonas aeruginosa	-	-	-	22	19	20	20	10	18	-
Streptococcus faecalis	-	-	-	20	20	18	15	-	-	-
Escherichia coli	25	-	-	-	17	18	20	-	-	-
Staphylococcus aureus	-	-	-	19	20	21	20	-	-	-
Salmonella typhi	-	-	-	23	-	22	23	-	15	-

Table 9. Antifungal Inhibitory Effects of Some Standard Drugs Used as Positive Control

Fungi	S	NB	CH	CPX	E	LEV	CN	APX	RD	AMX
Candida albicans	-	-	-	-	-	-	15	-	15	-
Rhizopus stolonifera	-	-	-	20	-	20	15	-	14	-
Penicillium citrinum	-	-	-	-	-	-	25	-	18	-
Saccharomyces cerevisiae	-	-	-	19	-	25	13	-	17	-
Aspergillus niger	-	-	-	15	-	23	15	-	10	-

Legend: S – Streptomycin; NB – Norfloxacin; CH – Chloramphenicol; CPX – Ciproflox; E – Erythromycin; LEV – Levofloxacin; CN - Gentamycin; APX – Ampiclox; RD – Rifampicin; AMX – Amoxil; CEP – Ceporex; OFX – Tarivid; NA – Nalidixic acid; PEF – Reflacin; AU – Augmentin; CPX – Ciproflox; SXT – Septrin

Key: Resistant (R) ≤ 13; Intermediate (I): 14-17; Sensitive (S): 18 and above

GC-MS Results of the Seed Oils

The trans-esterified seed oils subjected to GC-MS analysis revealed the lipid profile of the oils (Table 10-12). While the major fatty acids contained in *C. papaya* were docosanoic (15.36%), elaidic (51.83%), linoleic (17.47%) and stearic (11.22%) acids, *D. edulis* had linoleic (50.08%), palmitic (13.98%), dihomo-γ-linolenic (15.53%) and oleic (10.16%) acids as the major fatty acids. *R. hookeri* had palmitic (33.88%), elaidic (28.74%), palmitoleic (18.98%) and stearic (8.57%) acids as major component.

Table 10. Fatty Acid Composition of *C. papaya* Seed Oil

S/N	Compound	Retention Time	Molecular Formula	% Composition
1.	Myristic acid	14.39	$C_{14}H_{28}O_2$	0.18
2.	Palmitoleic acid	16.86	$C_{16}H_{30}O_2$	0.42
3.	Docosanoic acid	17.64	$C_{22}H_{44}O_2$	15.36
4.	8,11,14-Docosatrienoic acid	17.65	$C_{22}H_{38}O_2$	0.60
5.	Triacontanoic acid	18.47	$C_{30}H_{60}O_2$	0.22
6.	Linoleic acid	19.29	$C_{18}H_{32}O_2$	17.47
7.	Elaidic acid	19.61	$C_{18}H_{34}O_2$	51.83
8.	Stearic acid	19.80	$C_{18}H_{36}O_2$	11.22
9.	Cis-11-Eicosenoic acid	21.90	$C_{20}H_{38}O_2$	1.14
10.	Cerotic acid	22.26	$C_{26}H_{52}O_2$	1.22
11.	Heneicosanoic acid	27.20	$C_{21}H_{42}O_2$	0.31

Table 11. Fatty Acid Composition of *D. edulis* Seed Oil

S/N	Compound	Retention Time	Molecular Formula	% Composition
1.	8,11,14-Docosatrienoic acid	16.86	$C_{22}H_{38}O_2$	0.65
2.	Palmitic acid	17.16	$C_{16}H_{32}O_2$	13.98
3.	Linoleic acid	17.64	$C_{18}H_{32}O_2$	50.08
4.	Oleic acid	19.36	$C_{18}H_{34}O_2$	10.16
5.	Petroselinic acid	19.43	$C_{18}H_{34}O_2$	2.91
6.	Triacontanoic acid	19.69	$C_{30}H_{60}O_2$	6.67
7.	Dihomo-γ-linolenic acid	28.43	$C_{20}H_{34}O_2$	15.54

Table 12. Fatty Acid Composition of *R. hookeri* Seed Oil

S/N	Compound	Retention Time	Molecular Formula	% Composition
1.	Myristic acid	14.39	$C_{14}H_{28}O_2$	1.94
2.	Palmitoleic acid	16.87	$C_{16}H_{30}O_2$	18.98
3.	Palmitic acid	17.19	$C_{16}H_{32}O_2$	33.88
4.	Dihomo-γ-linolenic acid	17.68	$C_{20}H_{34}O_2$	0.88
5.	Linoleic acid	18.05	$C_{18}H_{32}O_2$	6.99
6.	Elaidic acid	19.39	$C_{18}H_{34}O_2$	28.74
7.	Stearic acid	19.71	$C_{18}H_{36}O_2$	8.57

Results of Antityrosinase Activity

The result of the antityrosinase evaluation of the oil samples at different concentrations are as depicted (Table 13).

Table 13. Antityrosinase Activity of the Oil Samples

Conc. (μg/mL)	***C. papaya***	***D. edulis***	***R. hookeri***	**Kojic acid**
200	1.25	6.5	1.05	16.44
400	3.92	7.5	1.37	24.62
600	5.77	8.62	2.75	32.62
800	6.62	10.75	3.87	47.56
1000	8.75	13.27	5.62	86.75
IC_{50} (μg/mL)	0.27	4.52	0.83	702.55

While all the seed oils exhibited dose-response activities, the antityrosinase assay showed that *D. edulis* had higher activity than *C. papaya* and *R. hookeri* seed oils. *R. hookeri* seed oils exhibited the lowest activities among all. It is reported that although the antityrosinase activity of the standard, kojic acid was high, it depletes the melanin on the skin and thereby exposes the skin to harmful radiation. From the results, the seed oils have potential to serve as good substitute as applicable in cosmetic production.

From the results above, it is seen that *R. hookeri* had the lowest IC_{50} (0.832 μg/mL) when compared to the standard kojic acid (702.55 μg/mL). Hence, *R. hookeri* oil is not a good tyrosinase inhibitor. The IC_{50} values of *C. papaya* and *D. edulis* had moderate activities (0.2667 and 4.52 μg/mL, respectively).

Antityrosinase Activity of Formulated Cream Products

Human tyrosinase is a copper-containing enzyme in the body that plays a crucial role in the synthesis of the melanin pigment [24, 25]. Tyrosinase is the initiating and rate-limiting enzyme in the synthesis of melanin and is therefore the prime target for anti-melanogenic compounds in cosmetic products. Because of this property of the enzyme, it has physiological roles in the incidence and development of melanoma, a type of skin cancer [26]. Skin disorders such as vitiligo, malignant melanoma, and freckles can all be caused by abnormal tyrosinase expression. Many studies have reported that tyrosinase inhibitors have antioxidant, antibacterial, and antifungal properties, all of which are essential in the treatment of skin diseases [27]. For example, kojic acid, a hyperpigmentation product that binds with the tyrosinase in the skin, inhibits the production of melanin that is needed by the skin and body.

The antityrosinase activity of formulated cream products from *C. papaya* and *D. edulis* seed oils was evaluated using a standard protocol. The results obtained are as indicated (Tables 14 and 15). The result indicated that cream products from *D. edulis* generally had higher antityrosinase activity than that from *C. papaya* for corresponding formulations, except for product A which had a similar activity trend in both.

It was also noted that both the formulated cream products from *C. papaya* and *D. edulis* seed oils exhibited the highest membrane stabilities in comparison to *R. hookeri* seed oils.

Table 14. Antityrosinase Activity of Formulated Cream Products from *C. papaya*

Conc (µg/mL)	**A**	**B**	**C**	**D**	**E**	**F**
200	3.75	6.25	2.37	2.25	4.25	1.25
400	6.50	7.62	3.30	3.50	5.50	3.92
600	7.37	9.12	3.75	7.50	8.12	5.77
800	8.50	11.5	6.50	9.62	10.87	6.62
1000	9.75	12.5	12.50	13.62	14.12	8.75

Table 15. Antityrosinase Activity of Formulated Cream Products from *D. edulis*

Conc (µg/mL)	**A**	**B**	**C**	**D**	**E**	**F**
200	3.75	8.75	8.75	6.62	6.50	6.50
400	6.50	4.75	14.25	14.12	8.50	7.50
600	7.37	9.12	15.62	16.50	12.27	8.62
800	8.50	12.72	23.37	18.50	16.62	10.75
1000	9.75	14.47	26.37	23.75	24.00	13.27

Computational Analysis

In this study, the molecular docking technique was used to investigate the *in vitro* inhibition effects of *C. papaya*, *D. edulis* and *R. hookeri* seed oil on tyrosinase enzyme with ID 5M8L using kojic acid as standard. Compounds that possess antityrosinase properties are used to reduce hyper-pigmentation, reduce spots and induce skin whitening. Conversely, compounds that activate tyrosinase also enhance the synthesis of melanin and ultimately the darkening of the skin. Studies showed that the tyrosinase enzyme contributes to neurodegeneration mechanisms associated with Parkinson's disease and, hence, tyrosinase inhibiting compounds have been studied as a possible therapy for this type of disease.

Some synthetic compounds have been used as antityrosinase drugs to inhibit the enzyme. Kojic acid is one of such compounds. However, the synthetic compounds have adverse effects on both the human skin and the environment. Research has found that kojic acid causes cancer in humans. The search for safe natural alternatives to harmful synthetic compounds has become imperative. Hence, oils from underutilized seeds such as *C. papaya* and *D. edulis* may play an important role.

The components identified in *C. papaya* and *D. edulis* bound effectively to the tyrosinase on the same target site that kojic acid binds to (Tables 16 and 17). The interactions of the fatty acids with the protein were primarily van der waals (Figure 1).

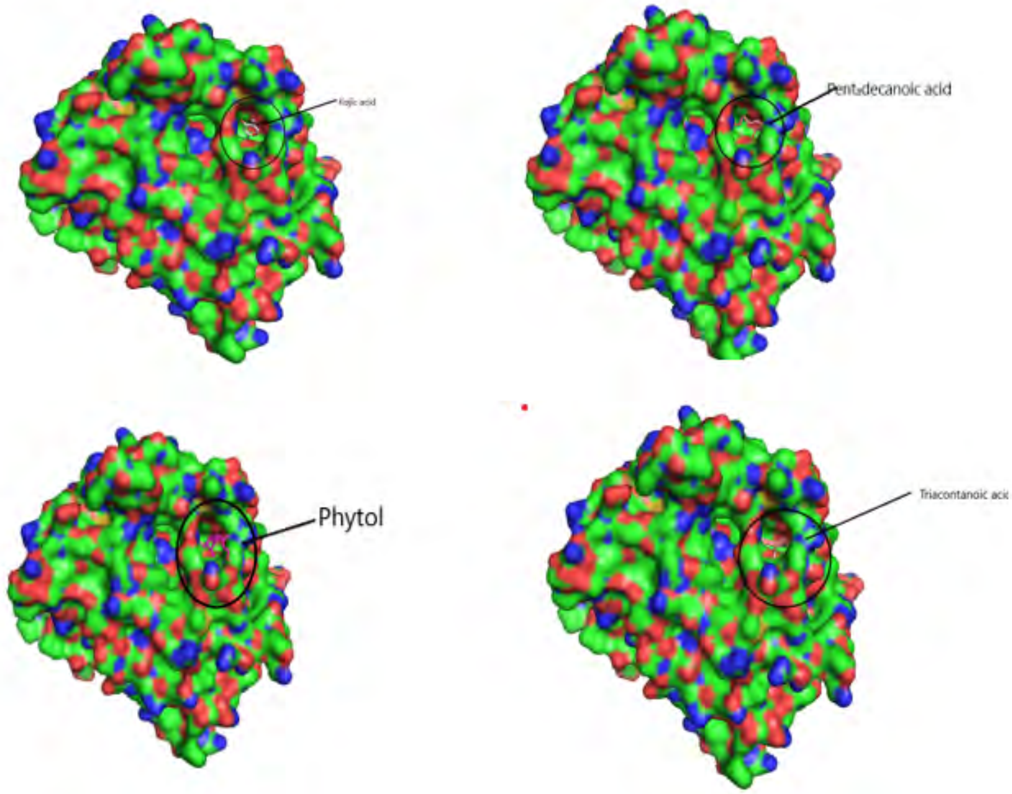

Figure 1. Molecular Interaction of *C. papaya* Seed Oil Component with Target Protein

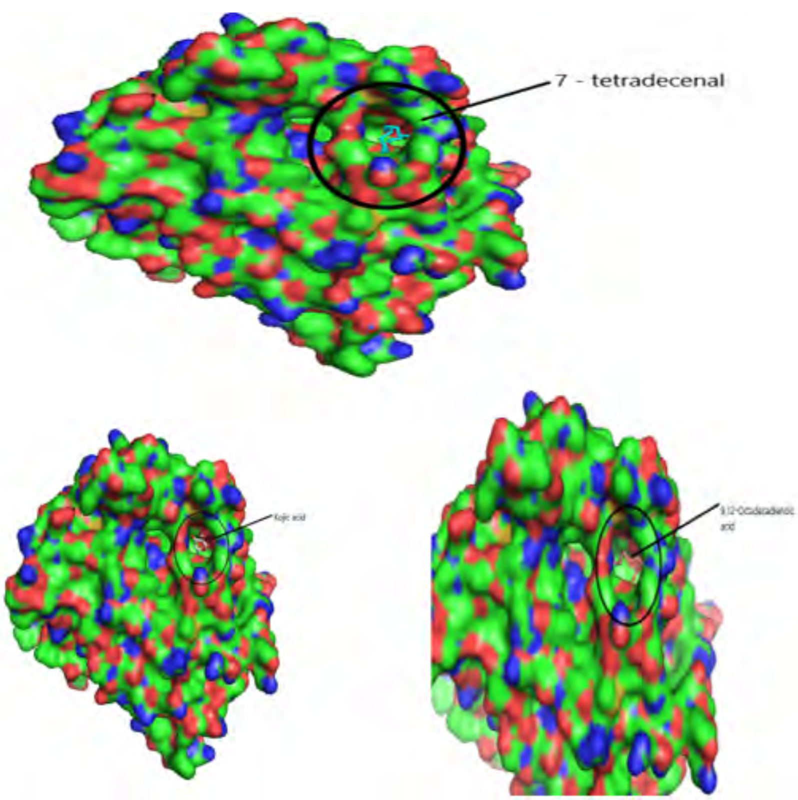

Figure 2. Molecular Interaction of *D. edulis* Seed Oil Components with Target Protein

Using computational techniques, there was structural evidences for the identical binding mode of the oil components and kojic acid in the active site of the human tyrosinase. The molecular docking of the oil components on tyrosinase showed the structural evidence for the identical binding mode of the oil components and kojic acid in the active site of the human tyrosinase. Hence, *C. papaya and D. edulis* seed oils may be further evaluated as potential alternatives to the implicated kojic acid.

Table 16. *In silico* Tyrosinase Inhibition/Binding Potential of *C. papaya* Components

S/N	**Compounds**	**Binding Affinity** (Kcal/Mol)	**Residues within Bonding Distance**	**Interaction Type**
1	8,11,14-Docosatrienoic acid	-7.7	ILE128	Van der Waals Interaction
			LYS233	Van der Waals Interaction
			LEU224	Van der Waals Interaction
			TYR226	Van der Waals Interaction
			PRO115	Van der Waals Interaction
			VAL126	Van der Waals Interaction
			PRO242	Van der Waals Interaction
			GLN236	Van der Waals Interaction
2	9-Octadecenoic acid	-6.7	GLU237	Van der Waals Interaction
			ARG118	Van der Waals Interaction
			PRO242	Van der Waals Interaction
			GLN236	Van der Waals Interaction
3	Docosanoic acid	-6.9	PRO115	Van der Waals Interaction
			VAL126	Van der Waals Interaction
			ILE128	Van der Waals Interaction
			LEU229	Van der Waals Interaction
			LYS233	Van der Waals Interaction
			GLN236	Van der Waals Interaction
			ARG330	Van der Waals Interaction
			TYR226	Van der Waals Interaction
			LEU229	Van der Waals Interaction
4	Heneicosanoic acid	-7.2	TRP117	Van der Waals Interaction
			VAL126	Van der Waals Interaction
			ILE128	Van der Waals Interaction
			PRO115	Van der Waals Interaction
			ARG114	Van der Waals Interaction
			LEU229G	Van der Waals Interaction
			LN236	Van der Waals Interaction
			LYS233	Hydrogen bonding
			ARG230	Van der Waals Interaction
			TYR226	Van der Waals Interaction

5	Hexadecanoic acid	-6.1	GLN236	Van der Waals Interaction
			ARG118	Van der Waals Interaction
			GLU232	Van der Waals Interaction
			PRO115	Van der Waals Interaction
			LYS233	Van der Waals Interaction
			THR112	Van der Waals Interaction
			CYS113	Van der Waals Interaction
			ARG230	Van der Waals Interaction
6	Triacontanoic acid	-7.2	PRO242	Van der Waals Interaction
			GLN236	Van der Waals Interaction
			ILE128	Van der Waals Interaction
			VAL126	Van der Waals Interaction
			VAL126	Van der Waals Interaction
			PRO115	Van der Waals Interaction
			TYR22G	Van der Waals Interaction
			ARG114	Van der Waals Interaction
			TYR226	Van der Waals Interaction
			LEU229	Van der Waals Interaction
7	Tridecanoic acid	-4.4	PRO242	Van der Waals Interaction
			PRO115	Van der Waals Interaction
			GLU237	Van der Waals Interaction
			LYS233	Van der Waals Interaction
			LEU229	Van der Waals Interaction
			GLN236	Van der Waals Interaction
8	Cis-11-Eicosenoic acid	-7.3	LEU229	Van der Waals Interaction
			LYS233	Hydrogen bonding
			GLN236	Van der Waals Interaction
			ARG114	Van der Waals Interaction
			PRO115	Van der Waals Interaction
			VAL126	Van der Waals Interaction
			ILE128	Van der Waals Interaction

Table 17. *In silico* Tyrosinase Inhibition/Binding Potential of *D. edulis* Components

S/N	**Compounds**	**Binding Affinity** (Kcal/Mol)	**Residues Within Bonding Distance**	**Interaction Type**
1	6-Octadecenoic acid	-3.5	THR112	Van der Waals Interaction
			GLY119	Van der Waals Interaction
			ARG118	Van der Waals Interaction
			GLU237	Van der Waals Interaction
			PRO242	Van der Waals Interaction
2	8,11,14-Docosatrienoic acid	-7.7	ILE128	Van der Waals Interaction
			LYS233	Van der Waals Interaction

			LEU224	Van der Waals Interaction
			TYR226	Van der Waals Interaction
			PRO115	Van der Waals Interaction
			VAL126	Van der Waals Interaction
			PRO242	Van der Waals Interaction
			GLN236	Van der Waals Interaction
3	9-Octadecenoic acid	-6.7	GLU237	Van der Waals Interaction
			ARG118	Van der Waals Interaction
			PRO242	Van der Waals Interaction
			GLN236	Van der Waals Interaction
4	Hexadecanoic acid	-6.1	GLN236	Van der Waals Interaction
			ARG118	Van der Waals Interaction
			GLU232	Van der Waals Interaction
			PRO115	Van der Waals Interaction
			LYS233	Van der Waals Interaction
			THR112	Van der Waals Interaction
			CYS113	Van der Waals Interaction
			ARG230	Van der Waals Interaction
5	8,11,14-Eicosatrienoic acid	-6.8	TYR226	Van der Waals Interaction
			ILE128	Van der Waals Interaction
			PRO115	Van der Waals Interaction
			PRO242	Van der Waals Interaction
			GLN236	Van der Waals Interaction
			GLU237	Van der Waals Interaction
			ARG230	Van der Waals Interaction
			GLN240	Van der Waals Interaction
			GLU237	Van der Waals Interaction
			GLN236	Van der Waals Interaction
6	9,12,15-Octadecatrienoic acid	-6.6	VAL447	Van der Waals Interaction
			PRO445	Van der Waals Interaction
			TYR226	Van der Waals Interaction
			LEU229	Van der Waals Interaction
			LYS233	Van der Waals Interaction
			GLN236	Van der Waals Interaction
			PRO115	Van der Waals Interaction
			LYS233	Van der Waals Interaction
			GLY107	Van der Waals Interaction
			CYS101	Hydrogen bonding
			CYS99	Van der Waals Interaction
7	9,12-Octadecadienoic acid	-6.4	TYR226	Van der Waals Interaction
			GNL236	Hydrogen bonding
			SER106	Van der Waals Interaction
			LEU229	Van der Waals Interaction
			ILE128	Van der Waals Interaction
			PRO115	Van der Waals Interaction
			LYS233	Van der Waals Interaction

Kojic Acid	-5.7	ARG230	Van der Waals Interaction
		VAL126	Van der Waals Interaction
		GLU232	Van der Waals Interaction
		LYS233	Hydrogen bonding
		GLN236	Hydrogen bonding
		LEU229	Van der Waals Interaction

4. Conclusion

In this study, oils were obtained via Soxhlet and cold extraction from underexplored tropical seeds, which include *C. papaya, D. edulis* and *R. hookeri*. The oil yield obtained from the *C. papaya, D. edulis* and *R. hookeri* seed were 19.89, 8.27 and 0.04%, respectively. Using an acid-catalysed trans-esterification reaction, the FAMEs of the seed oils were obtained for lipid profiling. The antimicrobial activity of the oils investigated at 30 µg/mL revealed that *C. papaya* significantly inhibited the growth of *Saccharomyces cerevisiae* and *Candida albicans,* while *D. edulis* inhibited the growth of *Staphylococcus aureus*, *Rhizopus stolonifera*, *Penicillium citrinum*, *Saccharomyces cerevisiae,* and *Aspergillus niger*. *R. hookeri* inhibited the growth of *Salmonella typhi*, *Rhizopus stolonifera*, *Penicillium citrinum,* and *Saccharomyces cerevisiae*.

The antityrosinase assay of the oils revealed that seeds of *C. papaya* had an IC_{50} value of 0.26 µg/mL, while *D. edulis* and *R. hookeri* had an IC_{50} value of 4.52 and 0.83 µg/mL, respectively. The formulated cream products from the seed oils of *C. papaya* and *D. edulis* exhibited dose response activities on the microorganisms and the tyrosinase enzyme. Likewise, the *in silico* analysis also suggested that the oil components had significant interactions with the tyrosinase enzyme by exhibiting strong affinity via numerous van der waals forces comparable to the standard, kojic acid. The oil may play a remarkable role in the cosmetics or formulations that regulate skin pigmentation.

This study has revealed that oils from the seeds of the underexplored plants; *C. papaya*, *D. edulis* and *R. hookeri* can be further exploited for medicinal and industrial purposes. However, more validation via detailed *in vivo* studies would be required.

5. Acknowledgments

The authors acknowledge the support of the Tertiary Education Trust Fund (TETFund) with reference number: UIL/CREDIT/IBRF2014/03 for funding the research. Also, appreciation goes to the CREDIT unit, University of Ilorin for the approval of the research and their cooperation.

6. Competing Interest

The authors declare no competing interests.

7. References

1. Anastas P, Eghbali N. Green chemistry: Principles and practice. *J. R. Soc. Chem.*, 2010, 39, 301-312. DOI: 10.1039/B918763B.
2. Atolani O, Olabiyi ET, Issa AA, Azeez HT, Onoja EG, Ibrahim SO, Zubair MF, Oguntoye OS, Olatunji GA. Green synthesis and characterisation of natural antiseptic soaps from the oils of underutilized tropical seeds. *Sustainable Chem. Pharm.*, 2016, 4, 32-39.
3. Zubair MF, Atolani O, Ibrahim SO, Oguntoye OS, Abdulrahim HA, Oyegoke RA, Olatunji GA. Chemical and biological evaluations of potent antiseptic cosmetic products obtained from *Momordica charantia* seed oil. *Sustainable Chem. Pharm.*, 2018, 9, 35-41.
4. Yogiraj V, Goyal PK, Chauhan CS, Goyal A, Vyas B. Carica papaya Linn.: An overview. *Int. J. Herb. Med.*, 2014, 2(5), 01-08.
5. Ajayi IA, Adesanwo O. Comparative Study of the mineral element and fatty acid composition of *Dacryodes edulis* pulp and seed. *World J. Agric. Sci.*, 2009, 5(3), 279-283.
6. Arisa NU, Lazarus A. Production and refining of *Dacryodes edulis* "native pear" seeds oil. *Afr. J. Biotechnol.*, 2008, 7(9), 1684-5315.
7. Ogbuagu MN. Vitamins, phytochemicals and toxic elements in the pulp and seed of Raphia palm fruit (*Raphia hookeri*). *Fruits*, 2008, 63(5), 297-302. DOI https://doi.org/10.1051/fruits:2008025
8. Atolani O, Areh ET, Oguntoye OS, Zubair MF, Fabiyi OA, Oyegoke RA, Tarigha, DE, Adamu N, Adeyemi OS, Kambizi L, Olatunji GA. Chemical composition, antioxidant, anti-lipooxygenase, antimicrobial, anti-parasite and cytotoxicity of *Polyalthia longifolia* seed oil. *Med. Chem. Res.*, 2019, 28(4), 515-527.
9. Atolani O, Adamu N, Oguntoye OS, Zubair MF, Fabiyi OA, Oyegoke RA, Adeyemi OS, Areh ET, Tarigha DE, Kambizi L, Olatunji GA. Chemical characterization, antioxi-dant, cytotoxicity, Anti-*Toxoplasma gondii* and antimicrobial potentials of the *Citrus sinensis* seed oil for sustainable cosmeceutical produc-tion. *Heliyon*, 2020, 6, e03399.
10. Gerpen JV. Biodiesel processing and production. *Fuel Process. Technol.*, 2005, 86(10), 1097-1107.
11. Ibeto CN, Okoye COB, Ofoefule AU. Comparative study of the physicochemical characterization of some oils as potential feedstock for biodiesel production. *Int. Scholarly Res. Network*, 2012, 12, 1-5.
12. Pearson D in The Chemical Analysis of Food, 7th edition, Church Living-stone, Longman Group Limited, Edinburgh, New York, 1991, 493-494.

13. Abdulhamid A, Sani I, Fekal IM. Physicochemical analysis of Soxhlet extracted oils from selected Nigerian seeds. *Int. J. Biol. Biomol. Agric. Food Biotechnol. Eng.*, 2014, 8(11), 1122-1124.
14. Kayode ES. Extraction and physicochemical characterization of the oil extract from the seed of umbrella tree (*Terminlia mentalis*). *Int. J. Sci. Eng. Res.*, 2015, 6(10), 144-147.
15. Tsado DB, Ndamitso MM, Ajai AI. Determination of physicochemical properties and fatty acid profile of oil extract of *Blighiasapida* fruit from selected areas in Niger state, Nigeria. *Niger. J. Chem. Res.*, 2018, 23(1), 21-34.
16. Akinpelu DA, Kolawole DO. Phytochemistry and antimicrobial activity of leaf extract of *Piliostigma thonningii* (Schum). *Sci. Focus*, 2004, 7, 64-70.
17. Macrini DJ, Suffredini IB, Varella AD. Extracts from Amazonian plants have inhibitory activity against tyrosinase: An in vitro evaluation. *Braz. J. Pharm. Sci.*, 2009, 45, 4.
18. Oyedapo OO, Sab FC, Olagunju JA. Bioactivity of fresh leaves of *Lantana camara*. *Biomed. Lett.*, 1999, 59, 175-183.
19. Oyedapo OO, Akinpelu BA, Akinwunmi KF, Adeyinka MO, Sipeolu FO. Red blood cell membrane stabilizing potentials of extracts of *Lantana camara* and its fractions. *Int. J. Plant Physiol. Biochem.*, 2010, 2(4), 46-51.
20. Morris GM, Marguerita LW. Molecular modelling of proteins. *Springer Link*, 2008, 443, 365-382.
21. Trott O, Olson AJ. AutoDock Vina: Improving the speed and accuracy of docking with a new scoring function, efficient optimization, and multi-threading. *J. Comput. Chem.*, 2010, 31(2), 455-461.
22. Burla S, VS, Malati P, Nancy A, Grace R, Swetha AM, Vivek S. Studies on physicochemical properties & proximate analysis of *Carica papaya* seed. *J. Pharmacogn. Phytochem.*, 2018, 7(6), 1514-1519.
23. Abayeh OJ, Aina EA, Okuonghae CO. Oil content and oil quality characteristics of some Nigerian oil seeds. *J. Pure Appl. Sci.*, 1998, 1, 17-23.
24. Ba S, Kumar VV. Recent developments in the use of tyrosinase and laccase in environmental applications. *Crit. Rev. Biotechnol.*, 2017, 37(8), 19-32.
25. Kondo T, Hearing VJ. Update on the regulation of mammalian melanocyte function and skin pigmentation. *Expert Rev. Dermatol.*, 2014, 6(1), 97-108.
26. Koh HK, Geller AC, Miller DR. Prevention and early detection strategies for melanoma and skin cancer: Current status. *Arch. Dermatol.*, 1996, 132(4), 436-442.
27. Sonia S, Kumari LJH, Ruckmani K, Sivakumar M. Antimicrobial and antioxidant potentials of biosynthesized colloidal zinc oxide nanoparticles for a fortified cold cream formulation: A potent nano cosmeceutical application. *Mater. Sci. Eng., A*, 2017, 79, 581-589.

The Chemist
Journal of the American Institute of Chemists

Isolation, Characterization and *in vitro* Alpha-amylase Inhibition Potential of Novel Bioactives from *Vernonia amygdalina*

***Olubunmi Atolani[1,2], Adedamola Elizabeth Ayeni[2], Mohammed Abubakar Usman[2], Jamiu Opeyemi Adejumo[2], Olamilekan Joseph Ibukun[3], Adeola T. Kola-Mustapha[1,4], Ngaitad S. Njinga[1,5], Luqman A. Quadri[1,6], Emmanuel O. Ajani [1,7], Tajudeen O. Amusa[1,8], Moji T. Bakare-Odunola[1,5], Adenike T. Oladiji[1,6], Learnmore Kambizi[1,9]**

[1]*African Centre for Herbal Research, Ilorin (ACHRI), University of Ilorin, Nigeria*
[2]*Department of Chemistry, University of Ilorin, Ilorin, Nigeria*
[3]*Department of Chemical Sciences, Indian Institute of Science Education and Research Kolkata, Mohanpur, 741246, West Bengal, India*
[4]*Department of Pharmaceutics and Industrial Pharmacy, University of Ilorin, Ilorin, Nigeria*
[5]*Department of Pharmaceutical and Medicinal Chemistry, University of Ilorin, Ilorin, Nigeria*
[6]*Department of Biochemistry, University of Ilorin, Ilorin, Nigeria*
[7]*Phytomedicine Toxicology and Drug Development Laboratory, Department of Biochemistry, Kwara State University, Malete, Nigeria*
[8]*Department of Forest Resources Management, University of Ilorin, Ilorin, Nigeria*
[9]*Department of Horticulture, Cape Peninsula University of Technology, South Africa*

**Corresponding author (E-mail: atolani.o@unilorin.edu.ng)*

Abstract: *Vernonia amygdalina* of the family *Asteraceae*, a multi-medicinal tropical shrub renowned for its nutritional and health-promoting abilities, particularly in diabetes, was investigated. The methanol extract from the root was subjected to gradient solvent elution in gravity silica gel column chromatography, and the bioactive compounds obtained were further purified using methanol and acetone. Four compounds which include two steroidal saponins; vernoamyoside C, vernoniamyoside D, a flavonoid glycoside; luteolin-7-o-glucoside and a new compound, vernilorinoside, a lactone glycoside, were isolated and characterised using infrared, ^{1}H, and ^{13}C nuclear magnetic resonance spectroscopies. The *in vitro* anti-diabetic potential of the extracts and isolated compounds were examined using 3,5-dinitrosalicylic acid (DNSA) and glucose oxidase alpha-amylase inhibitory assays using acarbose as a standard drug. All compounds exhibited significant activities with the n-hexane extract exhibiting the highest α-amylase inhibitory activity (IC_{50} 143.2 ± 5.823 µg/mL) comparable to the standard, acarbose (IC_{50} 46.22 ± 2.226 µg/mL). *Vernonia amygdalina* has been shown to possess significant alpha-amylase inhibitory activity, thereby lending credence to the folkloric uses of the plant in the sustainable management of Type 2 *Diabetes mellitus*.

Key Words: Vernonioside, vernoniamyoside, vernoamyoside, luteolin-7-o-glucuronide, NMR spectroscopy

1. Introduction

Diabetes mellitus refers to a cluster of metabolic disorders characterised by a spike blood sugar or glucose (hyperglycaemia) affixed with a defect in insulin secretion, action, or both as well as aberrations in the intermediary metabolism of carbohydrates, proteins, and lipids [1-3]. In some cases, symptoms are absent or not severe, and afterward hyperglycaemia, which is enough to cause pathological and functional changes may emanate for a protracted period before the diagnosis is made [4]. The effects of diabetes embody long-term damage, dys-function, and failure of different organs. It is often related to subsequent symptoms such as blurring of vision, excessive thirst (poly-dipsia), excessive feeding (polyphagia), excessive urination (polyuria), and weight loss [5]. Consequently, ketoacidosis report-edly develops as a result of complications resulting in stupor, coma, and in absence of effective treatment could result in death [6]. While two types of *Diabetes mellitus* are generally known, the predominant Type 2 is often managed using expensive conventional hypoglycaemic drugs, which include gliben-clamide and metformin [5,6].

The disease is a menace which plagues people of all races and has a higher co-morbidity in regions where Western medicine is inaccessible or unaffordable. As a result of the unaffordability and side effects of current mainstream drugs, which include exacerbated renal and hepatocellular injury and disorder, diarrhoea, lactic acidosis, among others, several indigenous medicinal plants have been evaluated as a potential remedy for minimising these incidences or effects [2-5]. Medicinal plants have been reported to possess different pharmacological mechanisms in combating diabetes [4,7]. However, in modulating postprandial hyperglycaemia, reducing the rate of conversion of carbohydrates into glucose by inhibiting α-amylase, a carbohydrate hydrolysing enzyme, plays a vital role in the treatment, particularly in Type 2 diabetes [7-10]. *Vernonia amyg-dalina* of the family *Asteraceae* is one of the important medicinal plants used in the treatment of diabetes in folkloric medicine that has been proven to possess strong anti-inflammatory, antimalarial, antibacterial, antioxidant, and anticancer properties, amidst other scientifically proven pharma-cological activities [11-15]. It is often referred to as bitter leaf on account of its bitter taste. It is a perennial shrub of an average height from 2-5 m, widely grown and consumed as a nutritional vegetable in Africa and Asia [16-18]. The plant has a rough bark with dense black straits, and elliptic leaves that are about 6 mm long. The leaves are green and have a characteristic odour with a bitter taste, which is due to the presence of phytocompounds such as alkaloids, saponins, glycosides, and tannins [11,16]. $\Delta^{7,\ 9(11)}$ stigmastane-type steroid glycosides, such as vernonioside A1, vernonioside A2, vernonioside A3, vernonioside A4, vernonioside B1 and vernonioside B2, have been identified as the main constituents in the plant [19].

In this study, the bioactive principles in *V. amygdalina* root were isolated, characterised and subjected to *in vitro* alpha-amylase inhibition evaluation using 3,5-dinitrosalicylic acid alpha-amylase inhibitory assay. The isolated and characterised four compounds exhibited interesting *in vitro* alpha-amylase inhibition potential, worthy of further exploration.

2. Materials and Methods

General

^{1}H and ^{13}C NMR spectra (400 MHz) were recorded on a JEOL 400 MHZ spectrometer operating at 400 (^{1}H-NMR) and 100 (^{13}C NMR) MHz at 298 K in DMSO-*d6*. Chemical shifts were reported in δ (ppm) values. The IR spectra were obtained on a Shimadzu 8400s spectrometer.

Chemicals and Regents

Pre-coated silica gel 60 F_{254} for thin-layer chromatography (TLC) and silica gel (60-200 mesh) for column chromatography (CC) were obtained from LOBA Chemie PVT, India. Alpha-amylase (A3306), glucose assay kit (glucose oxidase/peroxidase kit), soluble potato starch (33615), sodium phosphate monobasic (71496), dinitrosalicylic acid (609-99-4), acarbose and sodium phosphate dibasic (71640) were analytical standard. All solvents were analytical grades and redistilled before use where necessary.

Plant Material

Vernonia amygdalina root material were collected from the plantation of African Centre for Herbal Research Ilorin (ACHRI) University of Ilorin, Ilorin, Nigeria, and identified at the herbarium of the Department of Plant Biology, Faculty of Life Sciences, University of Ilorin, Ilorin, Nigeria where voucher specimen number UILH/001/972/2021 was assigned. The plant materials were air-dried, pulverized, and temporarily stored in a cool environment before further work.

Extraction and Isolation

The pulverized *V. amygdalina* (1.333 kg root) materials were subjected to successive sequential cold extraction starting with n-hexane, followed by ethyl acetate, then methanol, and finally water in a stoppered container for five days each. The extracts were concentrated at reduced temperature using a vacuum rotary evaporator and water bath as appropriate. The methanol crude root extract (12 g) obtained was subjected to elution on silica gel-packed column chromatography and eluted with solvents of increasing polarities using various solvents combinations comprising of hexane, ethyl acetate, methanol, and water to obtain eighty fractions. The fractions were examined on TLC and fractions with similar profiles were pooled together to afford seventeen combined fractions (A to O, S1, and S2). Fraction H (5 g) was rechromatographed on a silica gel packed column chromatography eluted with solvents of increasing polarities using solvents comprising of ethyl acetate, methanol, and water to obtain 50 sub-fractions (100 mL each) which were pooled together using TLC to obtain thirteen sub-fractions (Ha1-5, Hb-Hg, H_4, and H_5). Fraction H_4 was further purified by washing with methanol, then freeze-dried to yield compound 1, vernoamyoside C. Fractions J, K, S2 were purified by washing with acetone to yield compounds 2, vernoniamyoside D, 3, luteolin-7-o-glucoside and 4, vernilorinoside, respectively. Purified isolated compounds were subjected to proton ^{1}H nuclear magnetic resonance (NMR) and carbon ^{13}C NMR, and Fourier-transform infrared spectroscopy (FTIR). The spectra obtained were used for the structural elucidation and characterization of the isolated compounds.

DNSA Alpha-amylase Inhibitory Assay

This assay was carried out using a standard procedure [20], based on measuring the oxidizing capacity of reducing sugars in a reaction with DNSA (3,5-dinitrosalicylic acid). A total of 250 µL of extract of varied concentration ranging from 50 to 400 $\mu g\ mL^{-1}$ was placed in a tube and 250 µL of pancreatic α-amylase solution (0.5 $mg\ mL^{-1}$) in 0.02 M sodium phosphate buffer (pH 6.9) was added. The mixture was incubated at 25°C for 10 mins, after which 250 µL of starch solution (1 %) in 0.02 M sodium phosphate buffer (pH 6.9) was added. This reaction mixture was again incubated at 25°C for 10 minutes. The reaction was finally quenched by 500 µL of 96 mM 3,5-dinitrosalicylic acid (DNSA) reagent, and further incubated in boiling water for 5 minutes and then cooled to room temperature. The content of each test tube was diluted with 5 mL distilled water and the absorbance was taken at 540 nm on a spectrophotometer. The absorbance of control was also measured as the assay was carried out in triplicate. The results were expressed as percentage inhibition of α-amylase activity using the following equation.

$$Percentage\ inhibition = \left[\frac{A\ of\ control - A\ of\ sample}{A\ of\ control}\right] x100 \quad (1)$$

3. Statistical Analysis

Data collected in replicate were analysed using GraphPad Prism 9.2.0 software. Results were expressed as mean ±SEM (Standard error of mean). Data were compared using Anova one way and $P<0.05$ was considered to indicate a statistically significant difference.

4. Results

Characterization and Structural Elucidation of Bioactive Compounds

The chromatographic elution afforded four compounds (Fig. 1).

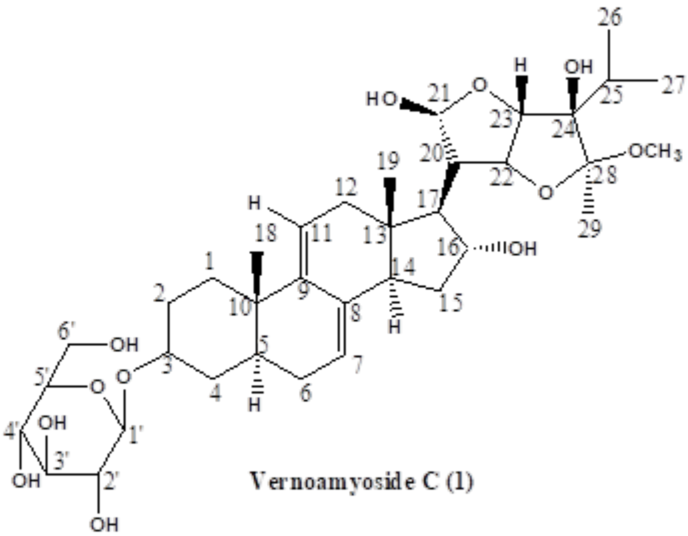

Vernoamyoside C (1)

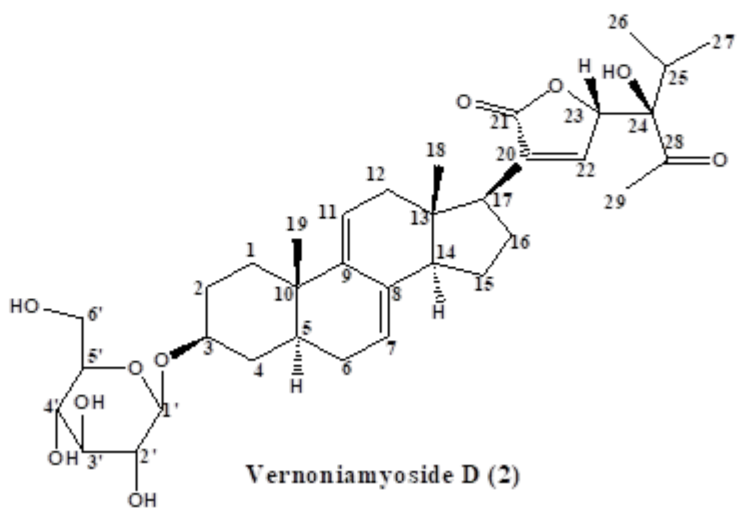

Vernoniamyoside D (2)

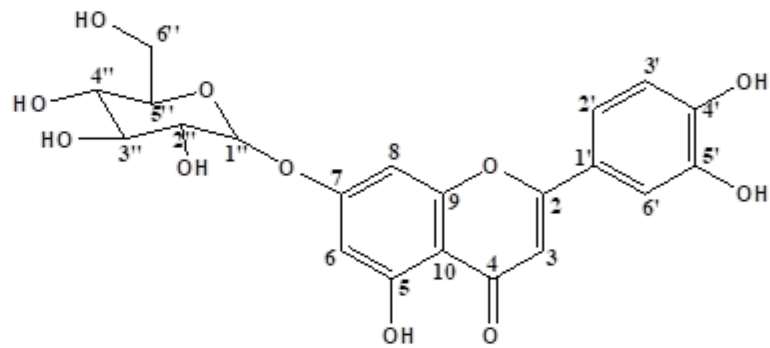

Luteolin-7-O-β-glucoside (3)

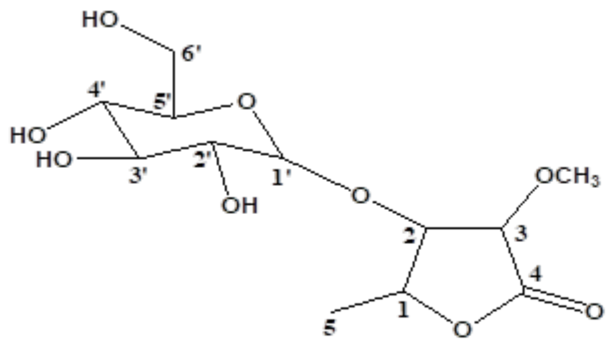

Compound (4)

Figure 1. Structures of Compounds 1-4

The NMR characterisations are as depicted (Table 1).

Compound 1: Vernoamyoside C was eluted with methanol-water (9:1) as a yellow powder. IR (KBr)ν_{max}(cm^{-1}): 3404 (O-H stretch), 2934/2876 (sp^3-CH stretch), 1632/1605, 1514 (C=C stretch), 1447 (CH_2 bend), 1377 (CH_3 bend), 1258/1163 (ester C(O)-C stretch), 1082/1051 (alcohol C-O stretch). The ^{1}H and ^{13}C NMR data (Table 1) indicated a methoxyl group at δ_H 3.13 that showed the peak from H-16 (δ_H 3.89) to Me-18(δ_H 0.42) and H-20 (δ_H 2.17) suggested that the additional OH-16 has an α-configuration. The NMR data was compared with literature data [19].

Compound 2: Vernoniamyoside D was obtained as a yellow powder from the Si-gel CC eluted with EtOAC: MeOH (3:2).IR (KBr)ν_{max}(cm^{-1}): 3404 (OH), 2936/2878 (sp^3-CH stretch), 1771 (conjugated lactone C=O stretch), 1705 (C=O stretch), 1636/1609, 1516 (C=C stretch), 1447 (CH_2 bend), 1377 (CH_3 bend), 1261/1142 (ester C(O)-C stretch), 1078/1055 (alcohol C-O stretch). The ^{13}C NMR data indicated 35 carbon signals, and also comparing both ^{1}H and ^{13}C NMR data (Table 3.3) shows compound 2 to be vernoniamyoside D. The result is in tandem with literature [21].

Compound 3: Luteolin-7-O-β-glucoside was eluted as a yellow powder from the Si-gel CC with EtOAC: MeOH (5.5:4.5).IR (KBr)ν_{max}(cm^{-1}): 3397 (OH), 2934/2878 (sp^3-CH stretch), 1707 (C=O stretch), 1630/1605, 1518 (C=C stretch), 1447 (CH_2 bend), 1375 (CH_3 bend), 1267/1159 (ester C(O)-C stretch), 1078/1055 (alcohol C-O stretch). Through the analysis of the NMR data (Table 1) and spectra comparison of a compound in Boudoukha et al. (2018) literature [22], the isolated compound was identified as luteolin-7-β-glucoside.

Compound 4: Vernilorinoside obtained via the elution on Si-gel CC produced a yellow powder (17.66 mg). IR (KBr)ν_{max}(cm^{-1}): 3258 (OH), 1636 (C=O stretch), 1409 (CH_3 bend), 1264 (ester C(O)-C stretch), 1059 (alcohol C-O stretch).

Table 1. ^{1}H and ^{13}C (400MHz) NMR Data of Compounds 1-4 in DMSO-*d6*

No.	1		2		4		No.	3	
	δ_H	δ_C	δ_H	δ_C	δ_H	δ_C		δ_H	δ_C
1	1.21, 1.34[a], d, 2H	31.1	1.00, 1.98, 2H	31.1	4.29[a], 1H	75.7	1′		121.4
2	1.20, 1.30[a], 2H	30.0	1.20, 1.75, 2H	29.2	3.57[a], 1H	64.8	2′	7.03, d, 1H	120.0
3	3.40, 1H	77.5	3.39, 1H	69.4	4.27[a], 1H	82.1	3′	6.92, d, 1H	116.2
4	1.90, 2H	34.9	1.19, 2H	33.5		174.5	4′		143.0
5	1.10, 1.40 1H	41.2	1.65, 1.8, 1H	36.0	1.85, 3H	22.3	5′		136.2
6	1.63, 1.98[a], 2H	29.8	1.00, 2.05, 2H	30.0			6′	7.02, 1H	114.9
7	4.42,1H	125.3	5.32, 1H	116.1			2		167.2
8		136.1		130.0			3	6.95, 1H	103.0
9		144.0		145.9			4		182.3
10		36.0		34.5			5		148.7
11	4.34, d, 1H	119.5	5.42[a], 1H	115.0			6	6.74[a], 1H	99.6
12	2,02, 2.06, 2H	42.2	1.48, 2H	44.2			7		166.0
13		45.3		48.8			8	6.74[a], 1H	97.0
14	2.27[a], 1H	46.3	2.88[a], 1H	51.4			9		145.2
15	1.90, 2.06[a], 2H	34.2	1.40[a], 2H	29.2			10		104.0
16	3.89, 1H	73.9	1.32, 1.75[a], 2H	23.5			1″	5.36, d, 1H	102.0
17	2.87, 1H	47.9	2.02[a], 1H	50.9			2″	3.15[a], 1H	75.8
18	0.42, 3H	14.3	1.01, 3H	12.5			3″	3.52[a], 1H	81.3
19	0.78, s, 3H	18.6	1.01, 3H	17.5			4″	3.30[a], 1H	70.0
20	2.17[a], 1H	56.8		129.9			5″	3.72[a], 1H	76.8
21	4.42, 1H	99.9					6″	3.66, 3.80, 2H	61.0
22	4.51[a], 1H	90.9	7.48, 1H	148.9					
23	4.51[a], 1H	81.5	5.10, 1H	82.0					
24		84.0		83.0					
25	2.17[a], 1H	33.8	2.30[a], 1H	31.0					
26	0.80, 3H	19.5	0.44, 3H	19.5					
27	0.50, 3H	21.0	0.79, 3H	21.8					
28		110.9							
29	1.78, 3H	17.0	2.18, 3H	29.0					
OCH_3	3.13, 3H	49.3			3.13, s, 3H	49.4			
Glucose									
1′	4.03, 1H	103.9	4.37, 1H	102.1	4.90, 1H	102.5			
2′	3.20[a], 1H	71.2	3.06[a], 1H	75.5	3.52[a], 1H	76.3			
3′	3.32[a], 1H	74.0	3.24[a], 1H	75.9	3.26[a], 1H	75.7			

4′	3.30 [a], 1H	70.2	3.14 [a], 1H	70.1	3.57 [a], 1H	70.6
5′	3.36 [a], 1H	76.8	3.43 [a], 1H	76.7	3.44 [a], 1H	81.7
6′	3.60, 3.70[a], 2H	63.5	3.35,3.61[a], 2H	63.2	3.39, 3.81[a], 2H	63.8

[a]Resonance pattern unclear due to overlapping.

Results of the Alpha-amylase Assay

The result of the alpha-amylase inhibition potential is as presented (Table 2).

Table 2. Inhibitory Effect of the Crude Extracts and Compounds 1-4

Sample	**IC_{50}±SEM** (µg/mL)
VARAQ	103.7±4.862
VARMEOH	227.9±0.817
VARNHEX	46.22±2.226
VARETOAC	115.0±1.357
Vernoamyoside C	143.8±2.681
Vernoniamyoside D	175.4±1.465
Luteolin-7-o-glucoside	234.0±6.725
Vernilorinoside	118.8±3.822
Acarbose[a]	143.2±5.823

Data are expressed as mean ± standard error of mean of triplicate determinations.

VARAQ - V. amygdalina root aqueous crude extract; VARMEOH - V. amygdalina root methanol crude extract; VARNHEX - V. amygdalina root n-hexane crude extract; VARETOAC - V. amygdalina root ethyl acetate crude extract; [a] α-amylase standard.

5. Discussion

The results of α-amylase inhibitory activity showed that all the crude extracts inhibited amylase activity (Table 2). The n-hexane crude extract exhibited the highest inhibitory activity (IC_{50} = 46.22±2.226 µg/mL) suggesting an improved activity compared to other crude extracts, the standard, acarbose with IC_{50} = 143.2±5.823 µg/mL) against α-amylase and methanol extract (IC_{50} =227.9±0.817 µg/mL) showed the least inhibitory activity. Similarly, isolated bioactive compounds 1-4 showed varied IC_{50} values (Table 2). With reference to the standard, data obtained were not significantly different at $P<0.05$. Compound 4, vernilorinoside, a new compound with IC_{50} =118.8±3.822 µg/mL), exhibited the highest inhibitory activity while compound 3 (IC_{50} =234.0±6.725 µg/mL) exhibited the least inhibitory activity. Although the mechanism of action of the compounds has not been studied, the small size of the Compound 4, importantly the aglycone unit may enhance the potency of the compound. All samples including the crude extracts and bioactives showed a concentration-dependent α-amylase inhibitory activity. In order to corroborate the results obtained in the studies, the evaluation of the isolated compounds in animal model is recommended.

5. Conclusion

In this study, four compounds (1-4) were isolated and purified from the root of *V. amygdalina* and characterized using spectra data obtained. To the best of our knowledge, this is the first report confirming the presence of compounds 1, 2, 3, and 4 in the root of the plant. The analysis of the results showed that the crude extracts and isolated phyto-compounds from *V. amygdalina* root are potent α-amylase inhibitors. It further suggests that *V. amygdalina* holds promise in the overall treatment or management of Type 2 diabetes by decreasing postprandial hyperglycaemia through the inhibition of the α-amylase enzymatic pathway. The crude extracts and the isolated compounds subjected to DNSA assay suggest the possibility of the amelioration of Type 2 diabetes disease via mechanisms that may be evaluated in the future. Compounds 1-4 which are glycosides may be further studied as a possible biomarker of the plant in addition to the pharmacological potentials exhibited. Future studies should be directed to exploring the *in vivo* potentials of the compounds.

6. Acknowledgment

Authors acknowledge the plant material donation from African Centre for Herbal Research, Ilorin (ACHRI), University of Ilorin, Nigeria.

7. Conflict of Interest

Authors declares no conflict of interest.

8. References

1. Kazi S. Use of traditional plants in *Diabetes mellitus*: A review. *Int. J. Pharm.*, 2014, 4(4), 283-289.
2. Farzaei F, Morovati MR, Farjadmand F, Farzaei MH. A mechanistic review on medicinal plants used for *Diabetes mellitus* in traditional Persian medicine. *J. Evidence-Based Complementary Altern. Med.*, 2017, 22(4), 944-955.
3. Skalli, S, Hassikou R, Arahou M. An ethnobotanical survey of medicinal plants used for diabetes treatment in Rabat, Morocco. *Heliyon*, 2019, 5, 1-24.
4. Oyagbemi AA, Salihu M, Oguntibeju OO, Esterhuyse AJ, Farombi EO.

Some selected medicinal plants with antidiabetic potentials. *Antioxid.-Antidiabetic Agents Hum. Health*, 2014, 1, 95-113.

5. Meresa A, Gemechu W, Basha H, Fekadu N, Teka F, Ashebir R, Tadele A. Herbal medicines for the management of *Diabetes mellitus* in Ethiopia and Eretria including their phytochemical constituents. *Am. J. Adv. Drug Delivery*, 2017, 5(1), 40-58.
6. Shin HJ, Kim JH, Yi JH, Han SW, Kim HJ. Polyuria with the concurrent manifestation of Central *Diabetes insipidus* (CDI) & Type 2 *Diabetes mellitus* (DM). *Electrolytes Blood Pressure*, 2012, 10(1), 26-30.
7. Kushawaha DK, Yadav M, Chatterji S, Srivastaval AK, Watal G. α-amylase and α-glucosidase inhibitory activity assessment of *Cucurbita maxima* seeds - A LIB STUDY. *Int. J. Phytomed.*, 2016, 8, 312-318.
8. Jaiswal P, Kumar P. Alpha amylase inhibitory activity of different extract of bark of *Albizia lebbeck* (L.) Benth. *Int. J. Pharm. Pharm. Sci.*, 2017, 9(8), 119-122.
9. Visvanathan R, Qader M, Jayathilake C, Liyanage R, Jayawardana BC, Sivakanesan R. Critical review on conventional spectroscopic α-amylase activity detection methods: Merits, demerits, and future prospects. *J. Sci. Food Agric.*, 2020, 100, 2836-2847.
10. Visvanathan R, Jayathilake C, Liyanage R. A simple microplate-based method for the determination of α-amylase activity using the glucose assay kit (GOD method). *Food Chem.*, 2016, 211, 853-859.
11. Egharevba C, Osayemwenre E, Imieje V, Ahomafor J, Akunyuli C, Udu-Cosi AA, Theophilus O, James O, Ali I, Falodun A. Significance of bitter leaf (*Vernonia amagdalina*) in tropical diseases and beyond: A review. *Malar. Chemother., Control Elimination*, 2014, 3(1), 1-10.
12. Anh HLT, Vinh LB, Lien LT, Cuong PV, Arai M, Ha TP, Lin HN, Dat TTH, Cuong LCV, Kim YH. *In vitro* study on α-amylase inhibitory and α-glucosidase of a new stigmastane-type steroid saponin from the leaves of *Vernonia amygdalina*. *Nat. Prod. Res.,* 2019, 35(5), 873-879.
13. Halim AM, Sirajuddin S, Bahar B, Jafar N, Syam A, Masni. The effect of African leaf herbal tea on fast blood glucose on centration of pre-diabetes teachers in Makassar city. *Enfermería Clín.*, 2020, 30, 261-264.
14. Ejiofor II, Das A, Mir SR, Ali M, Zaman K. Novel phytocompounds from *Vernonia amygdalina* with antimalarial potentials. *Pharmacogn. Res.*, 2020, 12, 53-59.
15. Alara OR, Abdurahman NH, Olalere OA. Ethanolic extraction of flavonoids, phenolics and antioxidants from *Vernonia amygdalina* leaf using two-level factorial design. *J. King Saud Univ., Sci.*, 2020, 32(1), 7-16.
16. Divneet K, Navpreet K, Anuja C. A comprehensive review on phytochemistry and pharmacological activities of *Vernonia amygdalina*.- *J. Pharmacogn. Phytochem.*, 2019, 8(3), 2629-2636.
17. Adeoye AT, Oyagbemi AA, Adedapo AD, Omobowale TO, Ayodele AE, Adedapo AA. Antidiabetic and antioxidant activities of the methanol leaf extract of *Vernonia amygdalina* in alloxan-induced diabetes in Wistar rats. *J. Med. Plants Econ. Dev.*, 2017, 1(1), 30.

18. Wong FC, Woo CC, Hsu A, Huat Tan BK. The anti-cancer activities of *Vernonia amygdalina* extract in human breast cancer cells are mediated through caspase-dependent and p53-independent pathways. *PLOS One*, 2013, 8(10), 7801.
19. Quasie O, Zhang Y, Zhang H, Luo J, Kong L. Four new steroid saponins with highly oxidized side chains from the leaves of *Vernonia amygdalina*. *Phytochem. Lett.*, 2016, 15, 16-20.
20. Kushawaha DK, Yadav M, Chatterji C. α-Amylase and α-glucosidase inhibitory activity assessment of *Cucurbita maxima* seeds – A LIBS based study. *Int. J. Phytomed.*, 2016, 8, 312-318.
21. Wang J, Song H, Wu X, Zhang S, Gao X, Li F, Zhu X. Steroidal saponins from *Vernonia amygdalina* Del. and their biological activity. *Molecules*, 2018, 23, 579.
22. Boudoukha C, Bouriche H, Elmastas M, Aksit H, Kayir O, Genc N, Senator A. Antioxidant activity of polyphenolic leaf extract from *Santolina chamaecyparissus* L. (*Asteraceae*) and the isolated luteolin 7-o-glucoside. *J. Pharm. Res. Int.*, 2018, 22(3), 1-12.

The Chemist
Journal of the American Institute of Chemists

Phytochemistry and Pharmacology of *Anogeissus leiocarpus* (DC.) Guill. & Perr. - A Review

[1,2]Ifeoluwa Samuel Adedotun, [3]Mohammad Torequl Islam, [2]Olubunmi Atolani

[1]Department of Pure and Applied Chemistry, Osun State University
P.M.B 4494, Osogbo, Nigeria
[2]Department of Chemistry, University of Ilorin P.M.B 1515, Ilorin, Nigeria.
[3]Department of Pharmacy, Life Science Faculty, Bangabandhu Sheikh Mujibur Rahman Science and Technology University Gopalganj (Dhaka)-8100, Bangladesh

**Corresponding author: Ifeoluwa Samuel ADEDOTUN*
**Corresponding author's (E-mail: ifeoluwa.adedotun@uniosun.edu.ng)*

Abstract: The relevance of medicinal plants as a primary source of therapeutic agents in the modern world cannot be overemphasized. *Anogeissus leiocarpus (A. leiocarpus)*, of the family *Combretaceae*, is a renowned medicinal plant used in folkloric medicine for the management of various illnesses, particularly in developing countries. In African traditional medicine, the edible stem bark used as a chewing stick reportedly possesses numerous biological activities. Stem bark extract from *A. leiocarpus* exhibits anti-parasitic, anti-hypertensive, and anti-tubercular effects. Additionally, *A. leiocarpus* bark extract is used in traditional medicine in Sudan to alleviate cough and in Ivory Coast to treat parasitic diseases. The plant reportedly possesses other medicinal properties, including anti-diabetic, anti-inflammatory, anti-malarial, and anti-cancer activities due to the presence of important phytochemicals, such as phenols, flavonoids, saponins, and alkaloids. Compounds including, serinic acid, arjungenin, isoquercetin, vitexin, kaempferol and some others have been identified as bioactives from various parts of the plant.

Key Words: *Anogeissus leiocarpus*, secondary metabolites, anti-malarial, antioxidant, anti-cancer

1. Introduction

Indigenous plants are a primary source of secondary metabolites, which play an intriguing role in traditional medicine [1]. The presence of several bioactive chemicals with chemo-preventive, antioxidant, antifungal, anti-inflammatory, antibacterial, analgesic, and other activities is what gives these plants their medical relevance [2].

Africa and other developing nations still rely heavily on medicinal plants as a therapeutic option for the management of variety of illnesses and diseases [3]. Recently, more attention has been directed at finding new drugs from a plant origin. Hence, there is a compelling need to find new bioactive compounds and new "leads" with vital pharmacological activities from herbal plants, such as the *Anogeissus leiocarpus*, a tropical indigenous medicinal plant in Africa. *A. leiocarpus* is the most abundant tree species in the woodland [4], which can be used in the production of charcoal [5]. *A. leiocarpus* is consumed as herbal tea and used for therapeutic purposes in the treatment of many ailments [6]. The leaf of *A. leiocarpus* has been found to be effective in treating sickle cell anemia [7]. The stem bark and leaf of *A. leiocarpus* offers potential alternatives and conveniently accessible sources of antibacterial compounds for the treatment of numerous bacterially induced illnesses [8-10]. The stem bark extract of *A. leiocarpus* has been utilised for a long time in conventional tanneries as a native agent for softening hide and skin [11].

2. Methodology

Data were gathered from various online databases such as ScienceDirect, PubMed, Scopus, Google Scholar and Web of Science by selecting the most comprehensive, recent and relevant articles on *Anogeissus leiocarpus* from the year 2014 to 2023.

3. Plant Profile

Occurrence and Distribution

A. leiocarpus, a deciduous tree (Figure 1) native to Asia and Africa belonging to the *Combretaceae* family, flourishes in a variety of environments, including forests, savannas, bushlands, semiarid grasslands, and drylands [12-14]. *A. leiocarpus*, also called African birch or axle wood, is called Ayin in the South-West region of Nigeria.

Figure 1. Pictures of *A. leiocarpus*

The *A. leiocarpus* are endemic in the forests and savanna zones of the Sudanese region. Its extensive biological activities extend from the edge of the Sahara to the uppermost layer of wet tropical forests. Senegal to Cameroon in West Africa, as well as Ethiopia and East Africa, are other places where it can be found or grown. in they thrive well at both dry forests and at the riverbank of wet regions [15].

Botanical Description

A. leiocarpus is a deciduous tree that typically reaches heights of 15 to 18 m and has light green foliage. In form, leaves range from elliptic to ovate-lanceolate, alternating to subopposite, and are 2 to 8 cm long by 1.5 to 3.5 cm wide [16]. The bark is fibrous with tiny scales, grey to beige in colour, and becomes blackish with age. The stems are coarsely pubescent. There are around 40 seeds of 10 g each that are spread by wind in an *A. leiocarpus* [16]. The leaves are attenuated at the base, pointed at the apex, and hairy below. The flowers lack petals and are bisexual; two-centimetre-wide, yellow inflorescence globose heads. The fruits are globose cone-like heads that are extensively winged, dark grey, and 3 cm in diameter. It reproduces both vegetatively and by seeds [12].

Ethnobotanical Uses

A. leiocarpus has a long history of being used as an infusion to treat a number of diseases. Extracts from the roots, leaves, stem bark, and twigs are used to treat illnesses, such as gonorrhoea, wounds, acute respiratory tract infections, stomach infections, TB, dysentery, and malaria. The stem bark, which is typically consumed as chewing sticks or used as home beverages, is known to contain wound-healing, anti-pneumonia, anti-arthritis, antibacterial, anti-malaria and antitrypanosomal effects [2,12,17-19]. Crude extract from this plant has been investigated to be effective in termite control [20]. Stem bark extracts have also been demonstrated to have the ability to protect liver function [21] and act as anti-parasitic, anti-hypertensive and anti-tuberculosis agents [22-25]. The aqueous extract of *A. leiocarpus* could be utilised as an alternate treatment and control method for coccidiosis [26].

Traditional Sudanese medicine uses a decoction of the bark to treat coughs [27]. The herb is used by traditional healers in the Ivory Coast to cure parasitic illnesses such malaria, trypanosomiasis, helminthiasis, and diarrhoea [28]. In traditional Togolese medicine, the decoction of the leaves is used to cure stomach problems and fungi infections including dermatitis and mycosis [29]. The plant extracts are effective in treating diabetes, ulcers, generalised body aches, blood clots, asthma, coughing, and tuberculosis [30].

4. Phytochemical Profile

Many potent phytochemical components found in *A. leiocarpus* have been demonstrated to be responsible for the therapeutic properties of the plant [31-34]. Secondary metabolites found in *A. leiocarpus* stems include alkaloids, tannins, flavonoids, cardiac glycosides, and saponins [35, 36]. Preliminary phytochemical screening of the *Anogeissus leiocarpus* stem bark for the major secondary constituents revealed that the plant, which was obtained from a local farm in Jigawa, Nigeria, was abundant in tannins and contained significant amounts of flavonoids, terpenes, and saponins, but was devoid of anthraquinones [12]. According to Hussaini *et al.* [37], the stem bark extract contained saponins, tannins, phenols, phytosterols but was devoid of flavonoids.

Despite its widespread use, only a few studies have established the phytochemical profile of *A. leiocarpus* stem bark to date [23,38]. In a qualitative chemical assessment of *A. leiocarpus* leaf and stem bark extracts by HPLC-ESI-MSn analysis, a significant number of phenolic components, including ellagitannins **1**, and some flavonoids were identified [38].

The stem bark of *A. leiocarpus* contains two oleanane-type compounds (4S, 6aR, 6bS, 8aR,14bR)-4-(hydroxymethyl)-4, 6a, 6b, 8a, 11,11,14b-heptamethyl-1, 2, 3, 4, 4a, 5, 6, 6a, 6b, 7, 8, 8a,9,10,11,12,12a,14,14a,14b-icosahydropicen-3-ol **2** and methyl 10-hydroxy-2-(hydroxymethyl)-2, 6a, 6b, 9, 9, 12a - hexamethyl-1, 2, 3, 4, 4a, 5, 6, 6a, 6b, 7, 8, 8a, 9, 10,11,12,12a,12b,13,14b-icosahydropicene-4a-carboxylate **3**, as well as other triter penoids, including sericoside **4**, serinic acid **5** and arjungenin **6** [39,40]. Several ellagic acid compounds, including 2,3,7,8-tetrahydroxychromeno[5,4,3-cde] chromene-5,10-dione **7**, were identified [23].

Polyphenolic substances found in the stem bark included 3, 3, 4-tri-o-methylellagic acid **8**, 3, 3, 4 - tri-o-methylellagic acid – 4 - d-glucoside **9**, gentisic **10**, protocatechuic acid **11**, gallic acid **12**, chebulagic acid **13** and chebulinic acid **14**. The stem bark also contained flavogallonic acid **15**, bislactone **16**, castalagin **17**, and ellagic acid **7**, [12]. 4H-1-Benzopyran-4-one **18**, and (S)-7-((2-O-(6-Deoxy-alpha-L-mannopyranosyl)-beta-D-glucopyranosyl)oxy)-2,3-dihydro-5-hydroxy-2-(4-methoxy-3(phenylmethoxy)phenyl) -4H – 1 - benzopyran-4-one **19**. The leaf contained -5-hydroxy-2-(4-methoxyphenyl)-4-oxo-4H-chromen-7-olate **20**, catechin **21**, quercetin **22**, isoquercetin **23**, rutin **24**, vitexin **25**, kaempferol **26**, and procyanidin B2 **27** [12]. Analysed essential oils with the aid of GC-MS obtained by hydro-distillation using a Clevenger-type apparatus from the leaf, stem bark and root of *A. leiocarpus* revealed the prominence of z-9-octadecenoic acid **28**, n-hexadecanoic acid **29**, n-octadecanoic acid **30** and methylhexadecanoate **31** [13].

Table 1. Some Phytochemical Compounds in *A. leiocarpus*

Compound ID	Structure	Name	Plant part
1	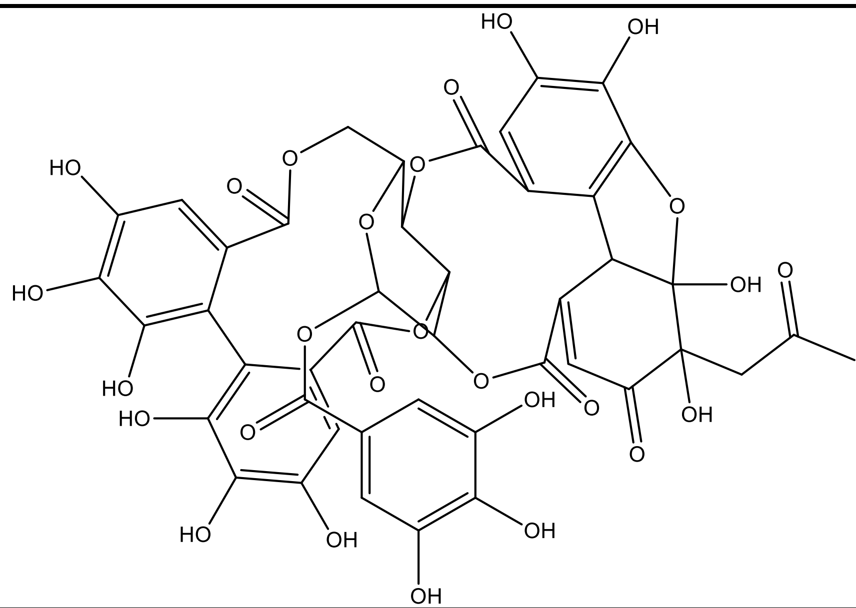	Ellagitannin	Leaf and Stem bark
2	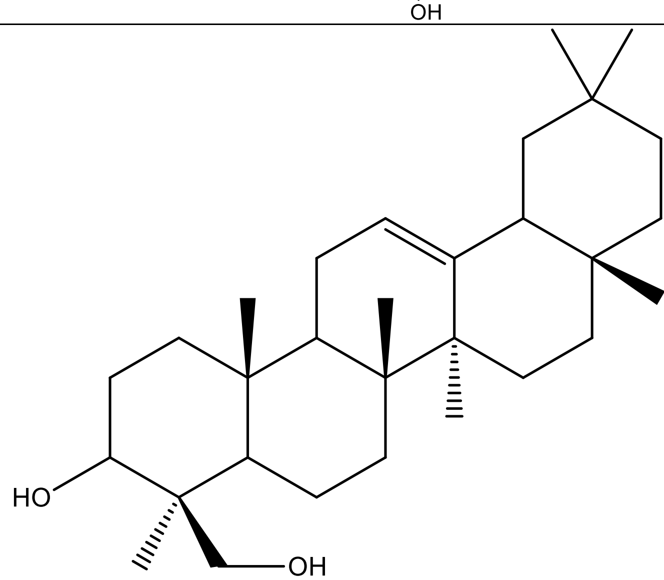	(4S,6aR,6bS,8aR,14bR)-4-(hydroxymethyl)-4,6a,6b,8a,11,11,14b-heptamethyl-1,2,3,4,4a,5,6,6a,6b,7,8,8a,9,10,11,12,12a,14,14a,14b-icosahydropicen-3-ol	Stem bark

3	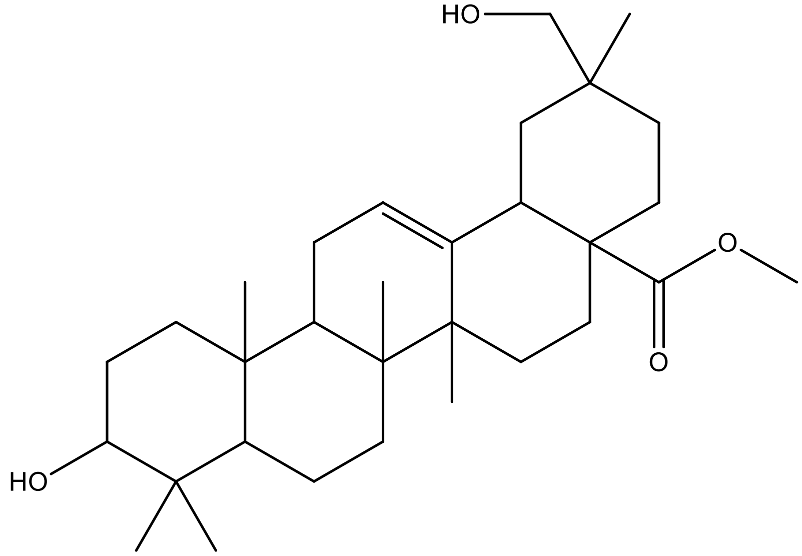	methyl 10-hydroxy-2-(hydroxymethyl)-2,6a,6b,9,9,12a-hexamethyl-1,2,3,4,4a,5,6,6a,6b,7,8,8a,9,10,11,12,12a,12b,13,14b-icosahydropicene-4a-carboxylate	Stem bark
4	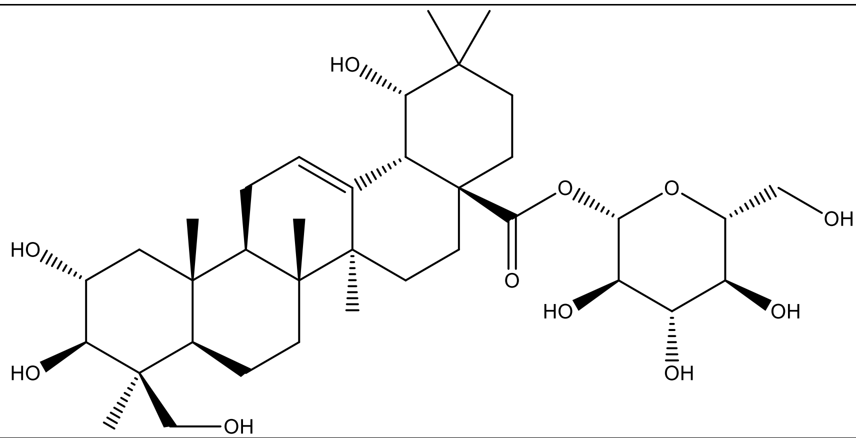	Sericoside	Stem bark
5	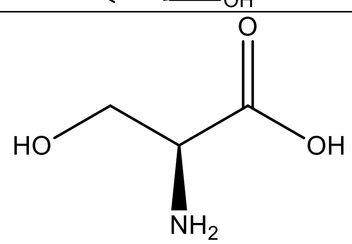	Serinic acid	Stem bark

6	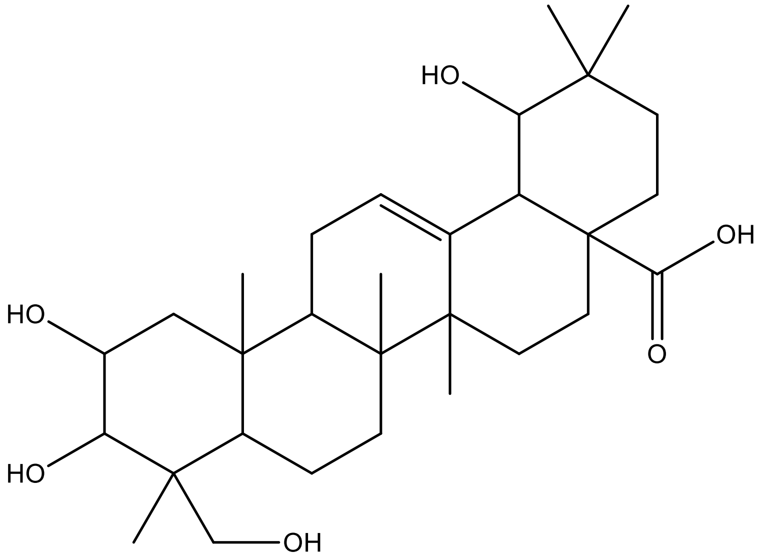	Arjungenin	Stem bark
7	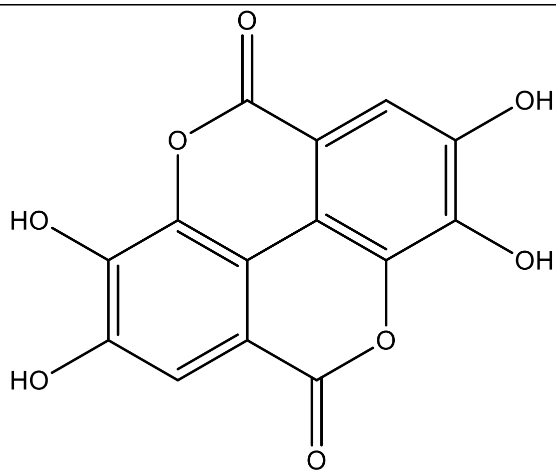	2,3,7,8-tetrahydroxychromeno [5,4,3-cde] chromene-5,10-dione	Stem bark
8	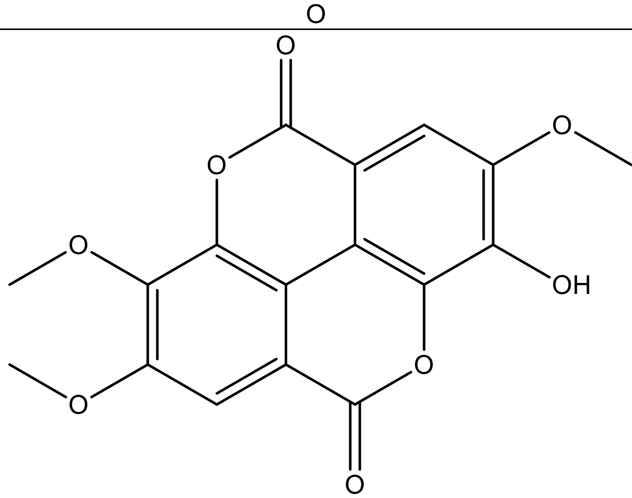	3,3,4-tri-o-methylellagic acid	Stem bark

9	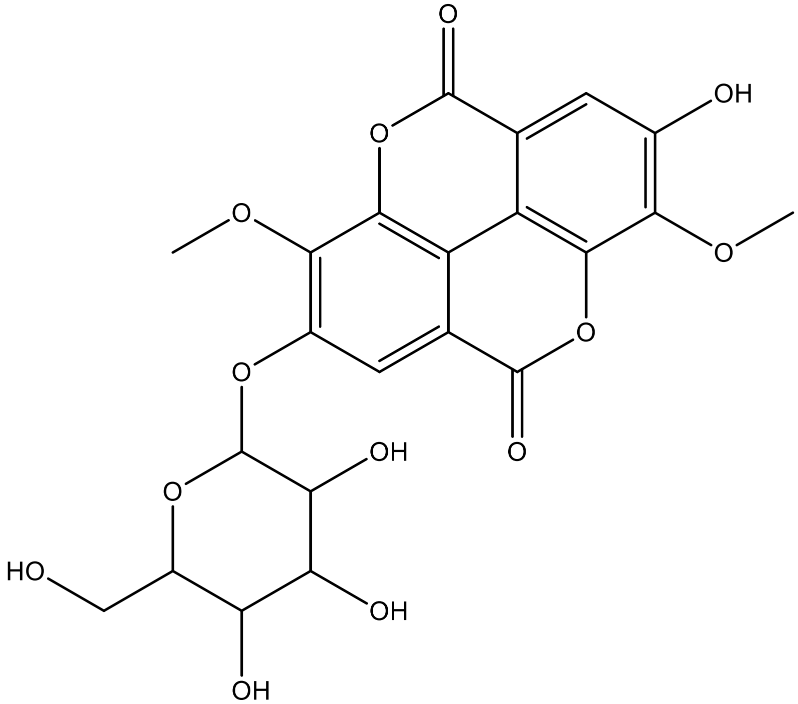	3,3,4-tri-o-methylellagic acid-4-d-glucoside	Stem bark
10	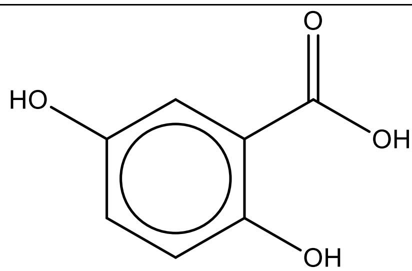	Gentisic	Stem bark
11	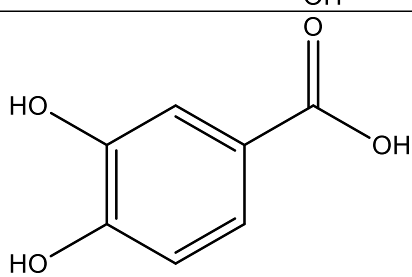	Protocatechuic acid	Stem bark
12	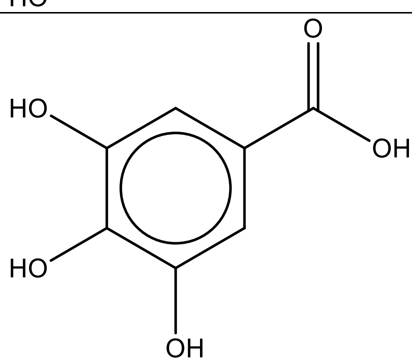	Gallic acid	Stem bark

13	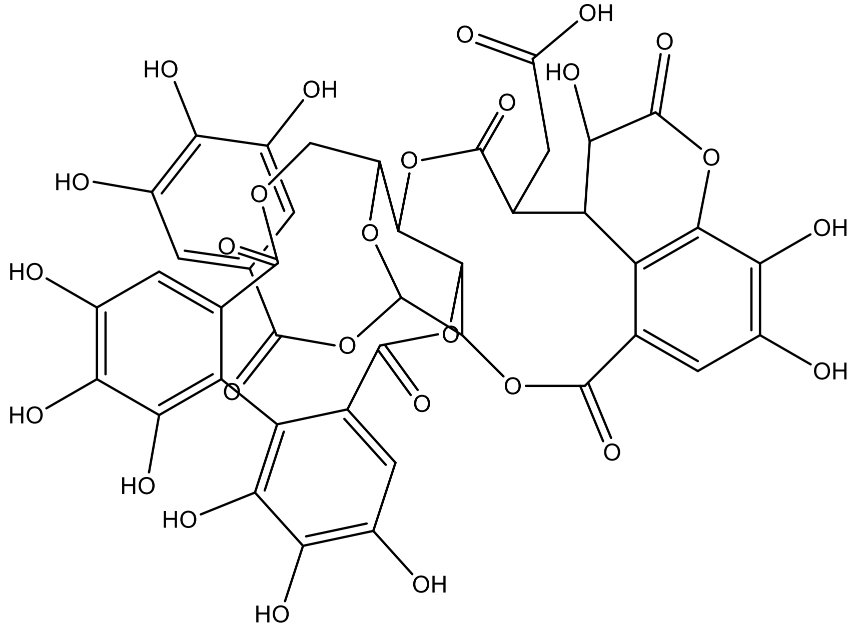	Chebulagic acid	Stem bark
14	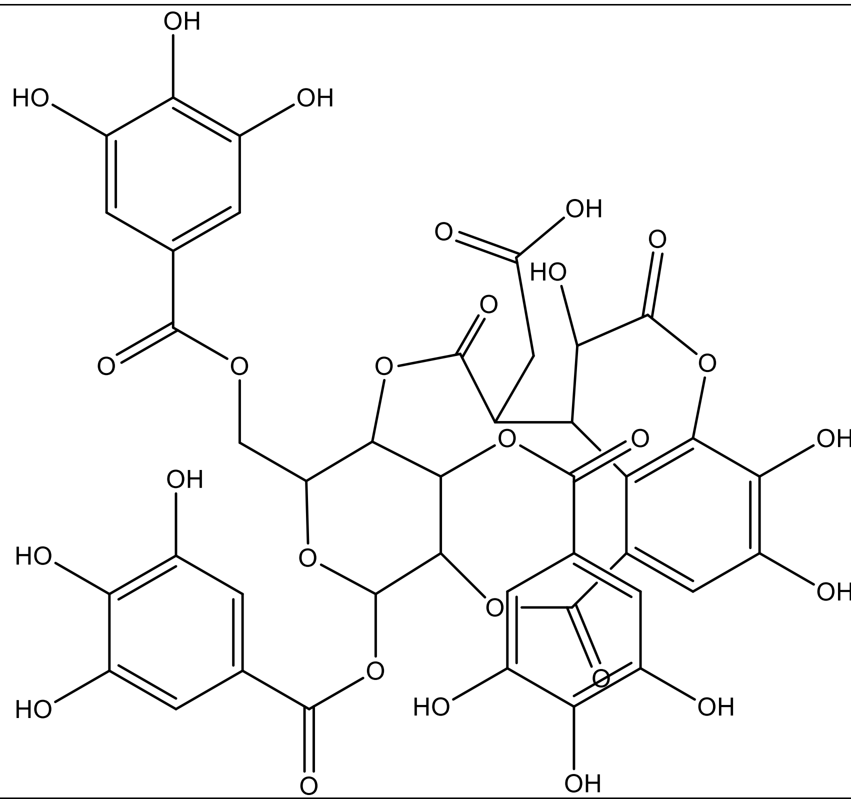		

15	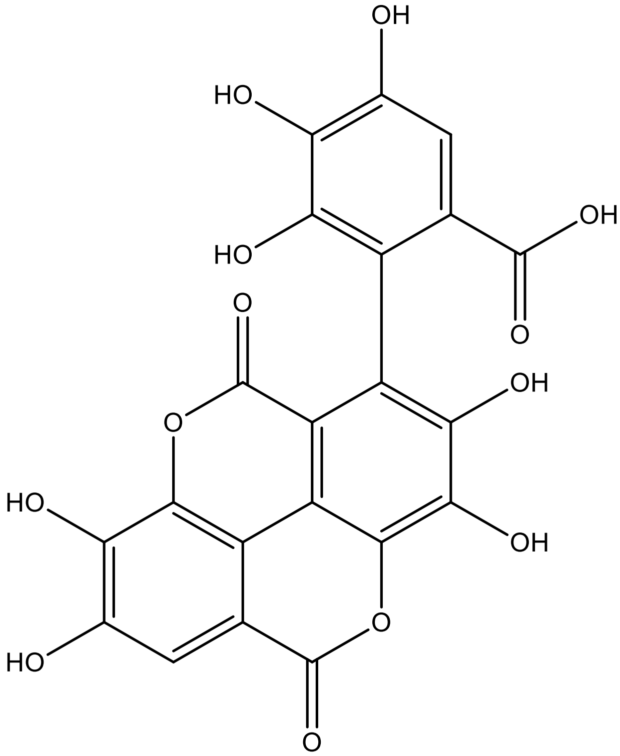	Flavogallonic acid	Stem bark
16	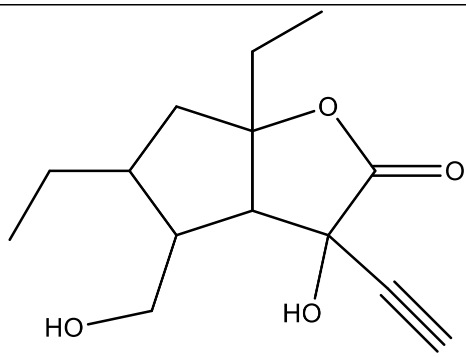	Bislactone	Stem bark

17	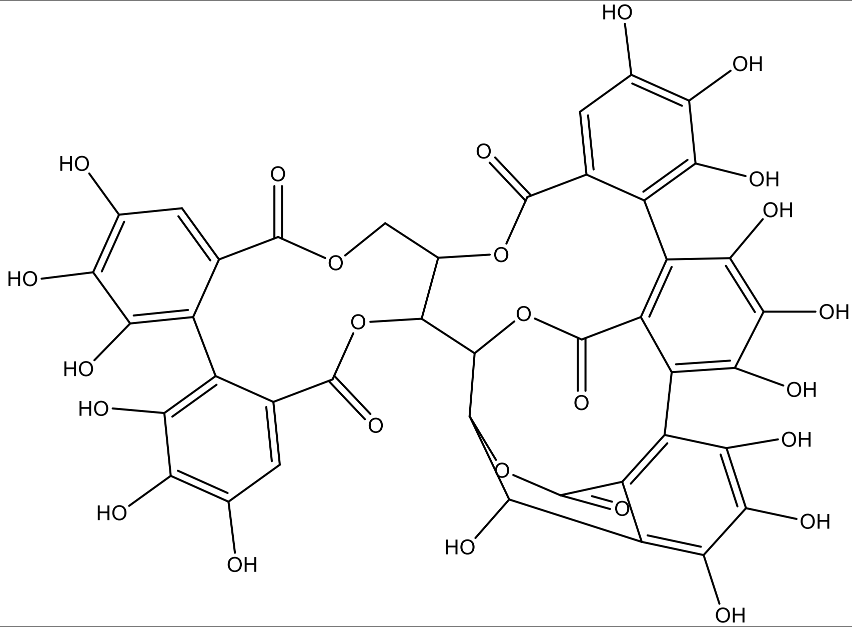	Castalagin	Stem bark
18	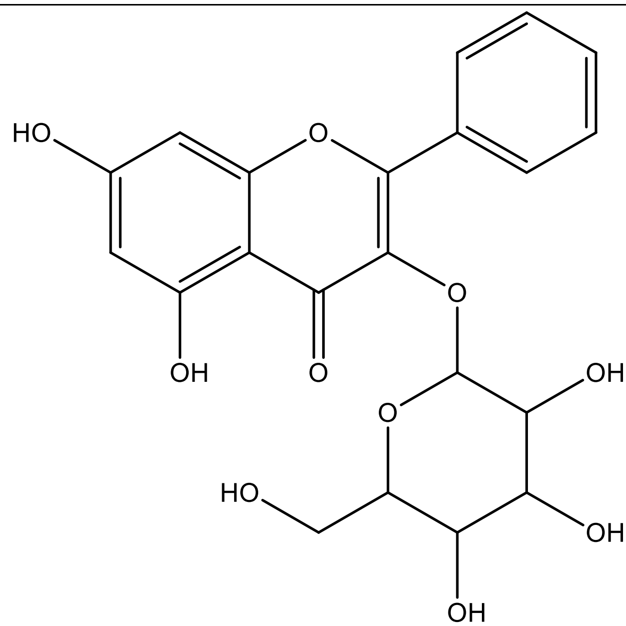	4H-1-Benzopyran-4-one	Stem bark
19	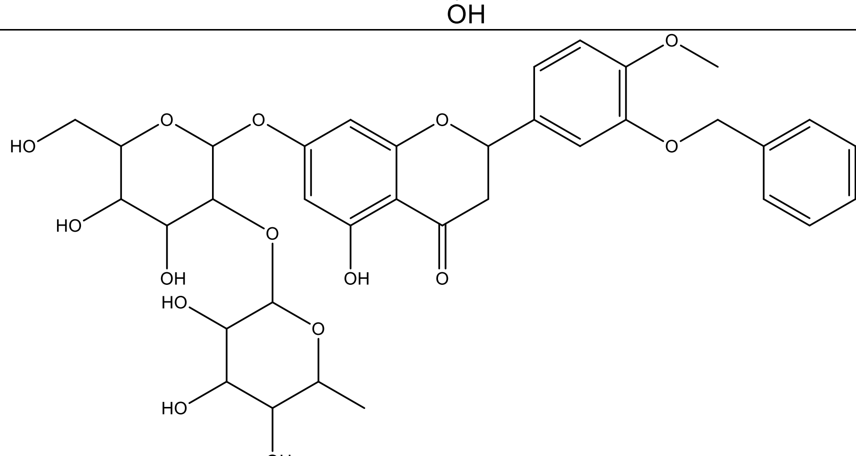	(S)-7-((2-O-(6-Deoxy-alpha-L-mannopyranosyl)-beta-D-glucopyranosyl)oxy)-2,3-dihydro-5-hydroxy-2-(4-methoxy-3(phenylmethoxy)phenyl) -4H-1-benzopyran-4-one	Stem bark

20	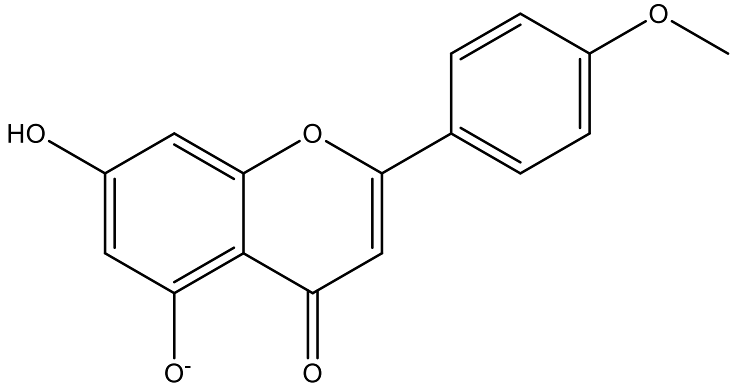	-5-hydroxy-2-(4-methoxyphenyl)-4-oxo-4H-chromen-7-olate	Leaf
21	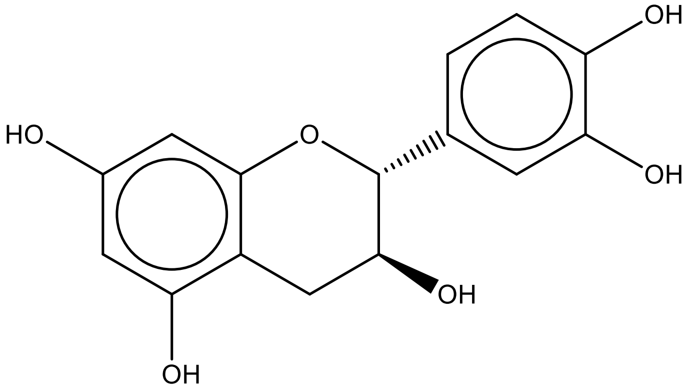	Catechin	Leaf
22	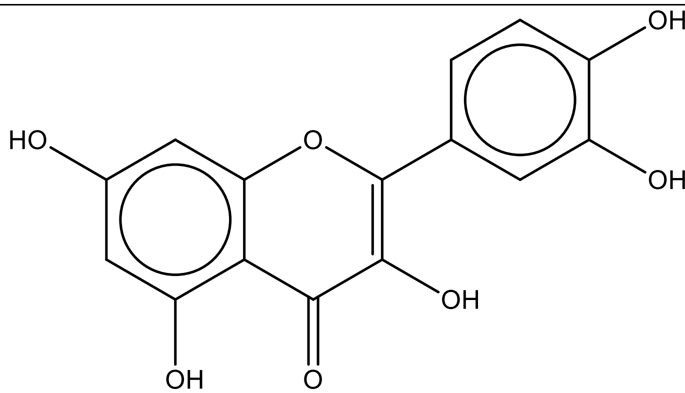	Quercetin	Leaf

23	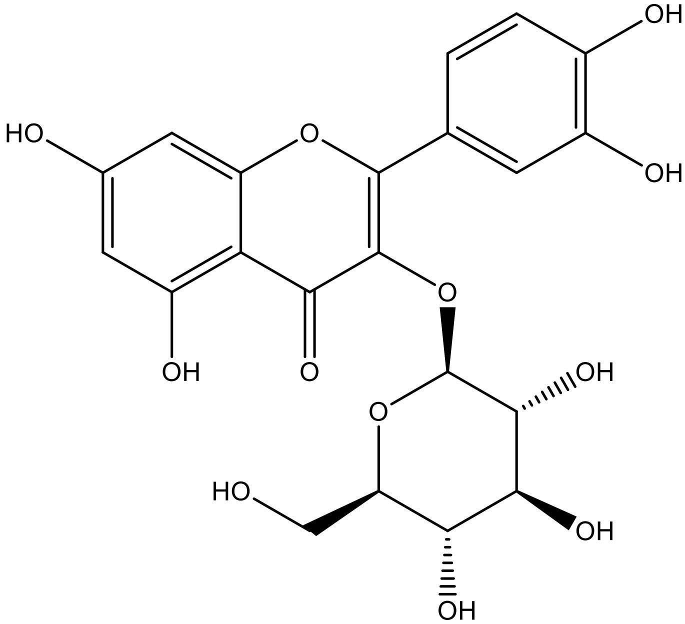	Isoquercetin	Leaf
24	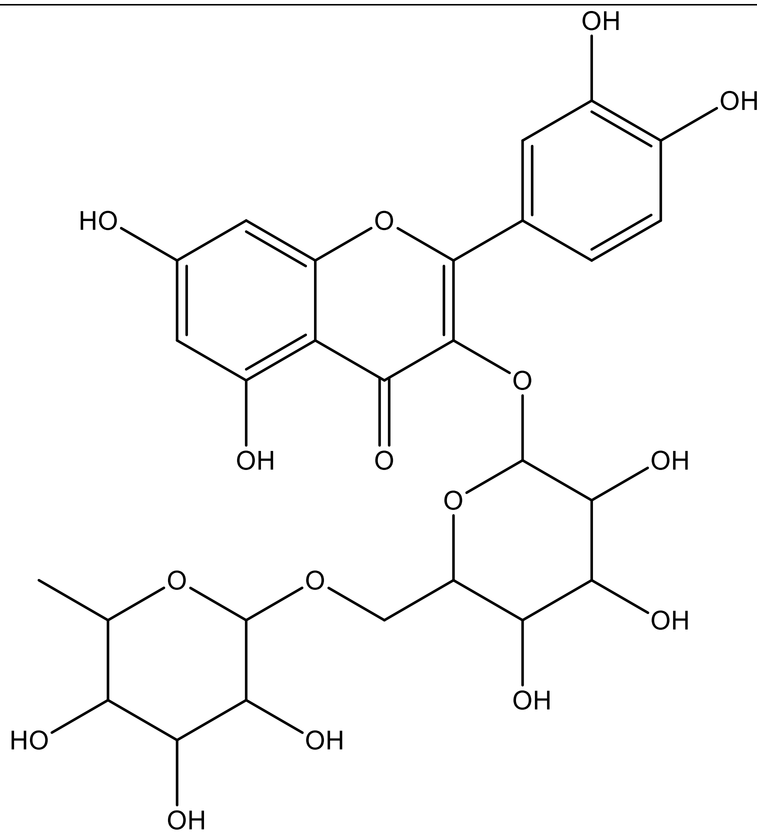	Rutin	Leaf

25	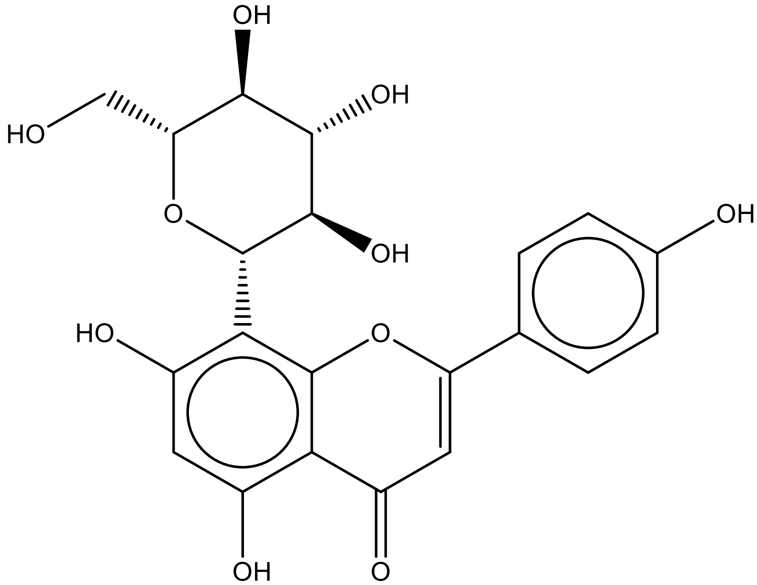	Vitexin	Leaf
26	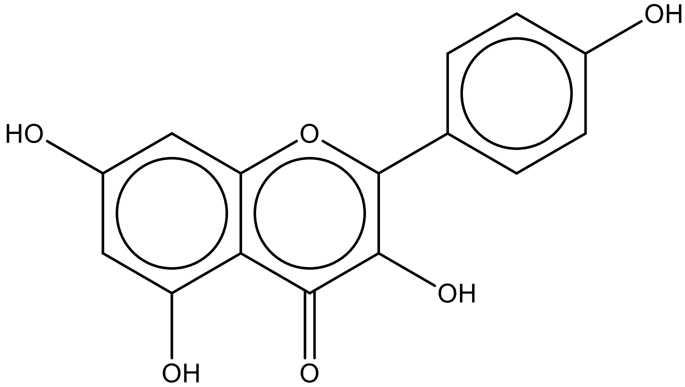	Kaempferol	Leaf
27	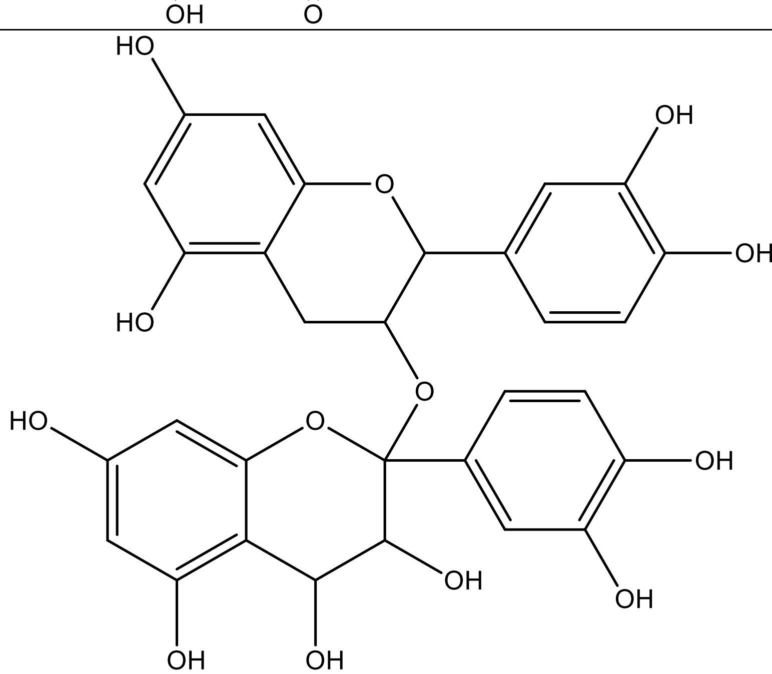	Procyanidin B2	Leaf

28	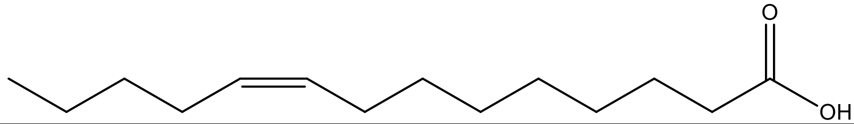	z-9-octadecenoic acid	Leaf, Stem bark and Root
29	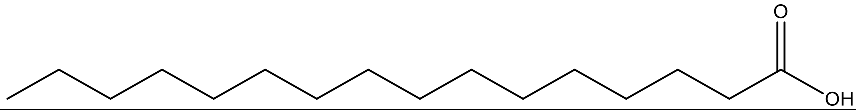	n-hexadecanoic acid	Leaf, Stem bark and Root
30	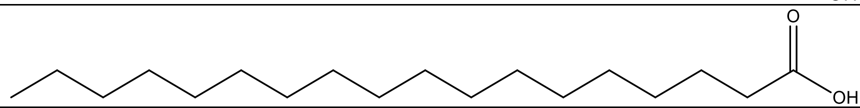	n-octadecanoic acid	Leaf, Stem bark and Root
31	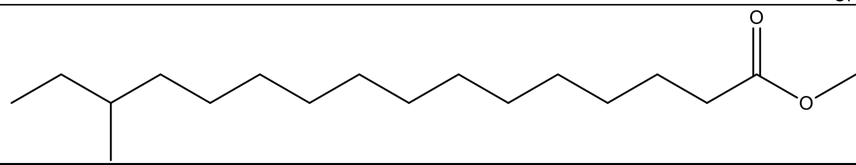	Methylhexadecanoate	Leaf, Stem bark and Root

5. Nutritional Values

The proximate analysis of the leaf of *A. leiocarpus* revealed a high content of crude protein (17.31%). The mineral analysis showed high levels of calcium and potassium, moderate levels of magnesium, iron and zinc, and low levels of copper and manganese [41]. Sawdust from *A. leiocarpus* (Hardwood) is more beneficial for growing mushrooms with a good nutritional composition that can promote good health in man [42].

6. Pharmacological Activities

A. leiocarpus has been subjected to a variety of *in vivo* and *in vitro* biological evaluations. This plant is equally known as a source of antimicrobial agents and for treatments of a variety of infection-related ailments [43]. Some of the pharmacological evaluations of the plant are as highlighted.

Antioxidant and Anti-hyperlipidaemic Characteristics

The aerial plant extract and supernatant of *A. leiocarpus* root bark significantly reduced serum and hepatic triglyceride levels, the amount of VLDL (Very Low-Density Lipoprotein) cholesterol and hyperlipidemic levels in mice. The crude extract and constituent fractions showed significant overall antioxidant activity [44]. It was discovered that *A. leiocarpus* crude extract and fractions possessed strong antioxidant [45] and anti-hyperlipidemic properties. The polyphenolic-rich extract of the plant may be useful in treatment of *Diabetes mellitus* [46]. *A. leiocarpus* leaves and stem bark extracts were similarly found to inhibit glucosidase activity [47]. The extract and the supernatant fraction of the roots of *A. leiocarpus* demonstrated a strong antidiabetic potential by hyperglycemia reduction, hyperlipidemia and glucose intolerance in rats induced with diabetes [48,49]. In cases when insulin is unaffordable, *A. leiocarpus* can be used as an unconventional treatment for diabetes-related oxidative stress [50,51]. In diabetic patients, a crude ethanol extract of *A. leiocarpus* stem bark lowers blood glucose levels [52,53].

Antimicrobial Potentials

The antimicrobial properties of *A. leiocarpus* support the beliefs of traditional healers that the plant's roots and stem bark can treat a variety of diseases [54,55]. Various antimicrobial activities which include antibacterial and antifungal activities of the plant have been established as highlighted.

Antibacterial effects

The root of the plant reportedly possesses huge antibacterial potential against pathogenic organisms which include *Escherichia coli*. The root material is sold in Nigeria as chewing sticks for the prevention of oral infections and mouth odour. The study suggested that plants with huge antibacterial potential against oral germs could also possess extended activities against throat infections, gum disease, and tooth decay [56,57]. In another evaluation, the tested isolates exhibited resistance to the crude leaf extract of *A. leiocarpus* [58,59]. The *in vitro* susceptibility of five bacteria, including *Staphylococcus aureus, Escherichia coli, Klebsiella aerogens, Pseudomonas aeruginosa,* and *Salmonella typhi* to the leaf, bark, and root extracts of *A. leiocarpus* revealed the strong antibacterial properties of the extracts [60,61].

Anti-fungal effects

A plant source of antifungal activity is *A. leiocarpus* [62-64]. The *in vitro* antifungal activity of root extracts from *Anogeissus leiocarpus* against *Aspergillus niger*, *Aspergillus fumigatus*, *Penicillium species*, *Microsporum audouinii*, and *Trichophyton rubrum* was investigated using the radial growth technique. The extracts inhibited the growth of all the test organisms significantly. The minimum inhibitory concentrations (MIC) and minimum fungicidal concentrations (MFC) of the extracts ranged from 0.03 to 0.07 g/mL and 0.04 to 0.08 g/mL, respectively. *A. leiocarpus* appears to be effective as an antifungal drug [65]. The *in vitro* susceptibility of two fungi, *Candida albicans* and *Aspergillus niger*, to the leaf, bark, and root extracts of *A. leiocarpus* revealed the strong antifungal properties of the extracts [60].

Anti-plasmodial Activities

A. leiocarpus stem bark fractions and crude methanol extracts were found to be highly effective against a field isolate of *Plasmodium falciparum*. The study therefore validated the traditional use of this herb as an effective malaria treatment option [66]. The methanolic extract of *A. leiocarpus* has been considered locally to have the same antimalarial activities as artemisinin derivatives in malaria-infected organisms [67,68].

Antidiarrheal Effects

The aqueous extract of *A. leiocarpus* leaves exhibited antidiarrheal properties by delaying intestinal peristalsis and decreasing gastro-intestinal output of fluids and electrolytes. This explains why this plant is used to treat diarrhoea in conventional medicine [69,70].

Anticancer and Anti-ulcerogenic Effects

A possible source of anticancer through the angiogenesis pathway is *A. leiocarpus* [71]. According to Olugbami *et al*. [72], extracts from the leaves and roots of *A. leiocarpus* can inhibit the rapid replication of cancer cells. Ehrlich ascites carcinoma cell lines were prevented from proliferating by the root extract of *A. leiocarpus*, whilst liver cancer HepG2 cell proliferation was equally inhibited by the ethanolic leaf extract [73]. Bioactive compounds which include elagic acid, castalagin, and flavogallonic acid from *A. leiocarpus*, have been demonstrated to inhibit the proliferation of cancer cells *in vitro* [74]. Methanol extract of *A. leiocarpus* leaves inhibited cholinesterase activity while the tyrosinase activity was suppressed by a methanol extract of the stem bark [38].

The effects of acetic acid-induced ulcerative colitis in rats were studied in relation to *A. leiocarpus* leaf aqueous extract. The aqueous extract of *A. leiocarpus* leaves exhibited anti-colitis actions by increasing superoxide dismutase (SOD) and catalase (CAT) levels, decreasing glutathione (GSH) levels, and elevating superoxide dismutase (GSH) levels while lowering MDA (Malonidialdehyde) and NO (Nitric oxide) levels. The extract preserved normal haematological parameters and treated inflammation brought on by acetic acid at doses of 100 and 200 mg/kg [75,76].

Antinociceptive and Anti-pyretic Activities

In a recent study involving acid-induced writhing in Wistar rats' model, the anti-nociceptive and antipyretic properties of *A. leiocarpus* aqueous leaf extract were examined. The extract was also assessed for safety using the median lethal dose (LD_{50}). The extract significantly ($p < 0.05$) reduced/eliminated the induced pain and pyrexia at doses of 200 and 400 mg/kg in a way that was equivalent to the positive controls. *A. leiocarpus* aqueous leaf extract reportedly possesses antinociceptive and antipyretic properties [77].

Effects on Reproductive System

A. leiocarpus stem bark extract significantly modifies the activities of phosphodiesterase-5, arginase, and acetylcholinesterase in male rats receiving paroxetine treatment thereby altering sexual behaviour and boosting anti-oxidant status, as well as biomolecules such as total thiol, malondialdehyde, nonprotein thiol and nitric oxide levels. These actions indicate some potential mechanisms that may under-line their application in the treatment of erec-tile dysfunction induced by anti-depressants [78,79,80]. *A. leiocarpus* extract has a pro-fertility effect. As a result, it serves as a good alternative for treating male infertility [80].

7. Conclusion

A. leiocarpus, a ubiquitous plant in the tropical woodlands and savannas is a multi-medicinal plant. Its folkloric applications which include the management of cough, wounds, stomach infections, tuberculosis, diarrhoea, and malaria make it highly desirable. Its other applications in the management of erectile dysfunction, antimicrobial, antibacterial, anticancer, antifungal, antioxidant, antinociceptive and antipyretic, anti-plasmodial activities among others makes it a target plant for more extensive investigations. Alkaloids, tannins, terpenoids, flavonoids, cardiac glycosides, and saponins are the secondary metabolites that have been found in *A. leiocarpus*. While the compounds identified in the plant include gentisic, gallic acids, chebulagic acid, bislactone, castalagin, catechin, quercetin and some others, many more chemical compounds are yet to be identified and characterized particularly from the root, wood, fruit and flower which have been grossly underexplored. The increasing demand for more potent antimicrobial agents makes the investigation of important underexplored folkloric medicinal plant such as *A. leiocarpus* more imperative particularly for the discovery of a drug lead. Future work should focus on the establishment of the possible mechanism of action of the identified compounds, discovery of potential drug leads and establishment of the toxicity of the extracts and constituent compounds. Apparently, more robust *in vivo* and holistic clinical studies are necessary to fully validate the traditional claims on the plant.

8. Conflict of Interest

The authors declare that there is no conflict of interest.

9. References

1. Cragg GM, Newman DJ. Natural products: A continuing source of novel drug leads. *Biochim. Biophys. Acta, Gen. Subj.*, 2013, 1830(6), 3670-3695.
2. Salih EYA, Kanninen M, Sipi M, Luukkanen O, Hiltunen R, Vuorela H, Julkunen-Tiitto R, Fyhrquist P. Tannins, flavonoids and stilbenes in extracts of African savanna woodland trees *Terminalia brownii*, *Terminalia laxiflora* and *Anogeissus leiocarpus* showing promising antibacterial potential. *S. Afr. J. Bot.*, 2017, 108, 370-386.
3. Akande A, Ahmad M, Majid U. A qualitative meta-synthesis on how autonomy promotes vaccine rejection

or delay among health care providers. *Health Promot. Int.*, 2022, 37(1), daab099.
4. Adenıjı O, İrunokhai E, Adigun J, Olorunfemi S. Diversity and abundance of tree species of a protected woodland: Southern Guinea savanna zone (Nigeria). *Turk. J. Biodiversity*, 2021, 4(2), 69-76.
5. Adenıjı O, Zaccheaus OS, Ojo BS, Adedeji AS. Charcoal production and producers' tree species preference in Borgu Local Government Area of Niger State, Nigeria. *J. Energy Technol. Policy*, 2015, 5(11), 1-8.
6. Niass O, Diop A, Samb I, Diop A, Dieng A, Diop YM. Antibacterial and antifungal activity essay of alkaloids extracted from four *Combretaceae* used in Senegal. *Int. J. Chem.*, 2022, 14(2), 59-62.
7. Elufioye TO, Williams BM, Cyrl-Olutayo MC. Identification of the anti-sickling activity of *Anogeissus leiocarpus* and *in silico* investigation of some of its phytochemicals. *Avicenna J. Med. Biochem.*, 2020, 8(1), 1-14.
8. Muhammad HA, Yusha'u M, Taura DW, Aliyu AM. Antibacterial activity and phytochemical constituents of African birch (*Anogeissus leiocarpus*) stem bark extracts. *Bayero J. Pure Appl. Sci.*, 2022, 13(1), 447-454.
9. Agada JO, Gberikon GM, Amuta, EU. Antibacterial Actions of *Anogeissus leiocarpus* and *Morinda lucida* leaves, stems and roots extracts against some enteric bacteria. *Int. J. Innovative Res. Adv. Stud.*, 2019, 6(9), 160-163.
10. Dayok O, Dawang DN, Da'am CE. Antimicrobial activity of leaf extract of *Anogeissus leiocarpus* (African birch) on some selected clinical isolates. *IOSR J. Pharm. Biol. Sci.*, 2018, 13(4), 36-40.
11. Audu BS, Wakawa IA, Oyewole OJ, Changdaya PZ. Histopathological alterations in the gills and liver of *Clarias gariepinus* juveniles exposed to acute concentrations of *Anogeissus leiocarpus*. *Jordan J. Biol. Sci.*, 2021, 14(3), 537-543.
12. Arbab AH. Review on *Anogeissus leiocarpus* a potent African traditional drug. *Int. J. Res. Pharm. Chem.*, 2014, 4(3), 496-500.
13. Singh D, Baghel US, Gautam A, Baghel DS, Yadav D, Malik J, Yadav R. The genus *Anogeissus*: A review on ethnopharmacology, phytochemistry and pharmacology. *J. Ethnopharmacol.*, 2016, 194, 30-56.
14. Ezuruike UF, Prieto JM. The use of plants in the traditional management of diabetes in Nigeria: Pharmacological and toxicological considerations. *J. Ethnopharmacol.*, 2014, 155(2), 857-924.
15. Ouédraogo DY, Mortier F, Gourlet-Fleury S, Freycon V, Picard N. Slow-growing species cope best with drought: Evidence from long-term measurements in a tropical semi-deciduous moist forest of Central Africa. *J. Ecol.*, 2013, 101(6), 1459-1470.
16. Klaus C, Plaimauer B, Studt J-D, Dorner F, Lämmle B, Mannucci PM, Scheiflinger F. Epitope mapping of ADAMTS13 autoantibodies in acquired thrombotic thrombocytopenic purpura. *Blood*, 2004, 103(12), 4514-4519.
17. Abubakar U, Yusuf K, Abdu G, Saidu S, Jamila G, Fatima A. Ethnopharmacological survey of medicinal plants used for the management of pediatric ailments in

Kano State, Nigeria. *Res. J. Pharmacogn.*, 2017, 4(3) 29-39.
18. Awobode HO, Fagbemi FT, Afolayan FID. Antitrypanosomal activity of *Khaya senegalensis* and *Anogeissus leiocarpus* stem bark on *Trypanosoma brucei brucei* infected rats. *Afr. J. Biotechnol.*, 2015, 14(6), 525-529.
19. Tauheed AM, Mamman M, Ahmed A, Suleiman MM, Balogun EO. *In vitro* and *in vivo* antitrypanosomal efficacy of combination therapy of *Anogeissus leiocarpus*, *Khaya senegalensis* and potash. *J. Ethnopharmacol.*, 2020, 258.
20. Ekhuemelo DO, Onuche MU, Tembe ET. Crude extracts of *Eucalyptus camaldulensis* (Dehnh) leaves and bark on *Anogeissus leiocarpus* (DC.) Guill. & Perr. and *Daniellia oliveri* Rolfe, hutch wood in control of termite (Isoptera: *Termitidae*). *Int. J. Sci. Eng. Invest.*, 2017, 6, 66.
21. Akanbi OM, Omonkhua AA, Cyril-Olutayo MC. Effect of methanolic extract of stem bark of *Anogeissus leiocarpus* on liver function of mice infected with *Plasmodium berghei*. *J. Herbs, Spices Med. Plants*, 2014, 20(4), 350-358.
22. Shuaibu MN, Wuyep PT, Yanagi T, Hirayama K, Ichinose A, Tanaka T, Kouno I. Trypanocidal activity of extracts and compounds from the stem bark of *Anogeissus leiocarpus* and *Terminalia avicennoides*. *Parasitol. Res.*, 2008, 102(4), 697-703.
23. Salih EY, Julkunen-Tiitto R, Luukkanen O, Sipi M, Fahmi MK, Fyhrquist PJ. Potential anti-tuberculosis activity of the extracts and their active components of *Anogeissus leiocarpa* (DC.) Guill. and Perr. with special emphasis on polyphenols. *Antibiotics*, 2020, 9(7), 364.
24. Belemnaba L, Ouédraogo S, Nitiéma M, Chataigneau T, Guissou IP, Schini-Kerth VB, Bucher B, Auger C. An aqueous extract of the *Anogeis-sus leiocarpus* bark (AEAL) induces the endothelium-dependent relax-ation of porcine coronary artery rings involving predominantly nitric oxide. *J. Basic Clin. Physiol. Pharmacol.*, 2018, 29(6), 599-608.
25. Sombié BC, Claude J, Ouédraogo W, Nitiema M. Standardization of extracts from trunk's barks of *Lannea macrocarpa* Engl. and K. Krause (*Anacardiaceae)* and *Anogeissus leiocarpus* (DC.) Guill. and Perr. (*Combretaceae*) for the formulation of antihypertensive herbal medicines. *Int. J. Pharm. Sci. Rev. Res.*, 2018, 48(1), 92-97.
26. Konan KS, Tiekpa WJ, Moroh AJ-L. Anticoccidial activity of the aqueous extract of *Anogeissus leiocarpus* leaves in broiler chickens. *J. Pharmacogn. Phytochem.*, 2020, 9(6), 41-44.
27. El Ghazali G, Adam I, Hamad A, El Bashir MI. *Plasmodium falciparum* infection during pregnancy in an unstable transmission area in eastern Sudan. *East. Mediterr. Health J.*, 2003, 9(4), 570-580.
28. Okpekon T, Yolou S, Gleye C, Roblot F, Loiseau P, Bories C, Grellier P, Frappier F, Hocquemiller R. Antiparasitic activities of medicinal plants used in Ivory Coast. *J. Ethnopharmacol.*, 2004, 90(1), 91-97.
29. Batawila K, Kokou K, Koumaglo K, Gbéassor M, de Foucault B, Bouchet P, Akpagana, K. Antifungal activities of five *Combretaceae* used in Togolese traditional medi-

cine. *Fitoterapia*, 2005, 76(2), 264-268.

30. Barku VY, Boye A, Ayaba S. Phytochemical screening and assessment of wound healing activity of the leaves of *Anogeissus leiocarpus*. *Eur. J. Exp. Biol.*, 2013, 3(4), 18-25.
31. Timothy SY, Mashi FI, Helga BI, Galadima IH, Midala TAS. Phytochemical screening, antibacterial evaluation and *in vitro* spasmodic effect of the aqueous and ethanol leaf and bark extracts of *Anogeissus leiocarpus* (DC.) Guill. & Perr. *Asian J. Pharm. Sci. Technol.*, 2015, 5(4), 302-308.
32. Osuntokun OT, Oluwafoise BO. Phytochemical screening of ten Nigerian medicinal plants. *Int. J. Multidiscip. Res. Dev.,* 2015, 2(4), 390-396.
33. Dahiru MM, Badgal EB, Musa N. Phytochemical profiling and heavy metals composition of aqueous and ethanol extracts of *Anogeissus leiocarpus*. *Ankara Univ. Eczacilik Fak. Derg.*, 2022, 47(2), 1-13.
34. Ezeonu CS, Ejikeme CM. Qualitative and quantitative determination of phytochemical contents of indigenous Nigerian softwoods. *New J. Sci.*, 2016, 2016, 1-9.
35. Namadina MM, Mukhtar AU, Karaye SI, Musa FM, Bah IH, Maitama FY. Phytochemical constituents and antibacterial activities of indigenous chewing stick (*Anogeissus leiocarpus*) stem. *Bayero J. Pure Appl. Sci.*, 2021, 14(1), 85-94.
36. Ogunjobi KM, Abdulwahab SO, Gakeno OF, Thompson OE, Olorunfemi O. Qualitative and quantitative evaluation of the phytochemical constituents of three wood species in Ogun state, Nigeria. *Trop. Plant Res.*, 2020, 7(3), 627-633.
37. Hussaini Y, Bello RY, Mustapha T. Preliminary phytochemical screening and GC-MS analysis of *Anogeissus leiocarpus* stem bark extract. *Pharm. Innovation J.*, 2022, 11(11), 113-117.
38. Orlando UD, Castillo AF, Medrano MAR, Solano AR, Maloberti PM, Podesta EJ. Acyl-CoA synthetase-4 is implicated in drug resistance in breast cancer cell lines involving the regulation of energy-dependent transporter expression. *Biochem. Pharmacol.*, 2019, 159, 52-63.
39. Chaabi M, Benayache S, Benayache F, N'Gom S, Koné M, Anton R, Weginer B, Lobstein A. Triterpenes and polyphenols from *Anogeissus leiocarpus* (*Combretaceae*). *Biochem. Syst. Ecol.*, 2008, 36(1), 59-62.
40. Hamzaoui M, Renault J-H, Nuzillard J-M, Reynaud R, Hubert J. Stepwise elution of a three-phase solvent system in centrifugal partition extraction: A new strategy for the fractionation and phytochemical screening of a crude bark extract. *Phytochem. Anal.*, 2013, 24(4), 367-373.
41. Agaie BM, Onyeyili PA. *In vitro* anthelmintic activity of the aqueous leaf extract of *Anogeissus leiocarpus* and its phytochemical, proximate and elemental contents. *J. Med. Plants Res.*, 2011, 5(30), 6656-6661.
42. Ogundele G, Salawu S, Abdulraheem I, Bamidele O. Nutritional composition of oyster mushroom (*Pleurotus ostreatus*) grown on softwood (*Daniella oliveri*) sawdust and hardwood (*Anogeissus leiocarpus*) sawdust. *Br. J. Appl. Sci. Technol.,* 2017, 20(1), 1-7.

43. Aburjai T, Darwish RM, Al-Khalil S, Mahafzah A, Al-Abbadi A. Screening of antibiotic resistant inhibitors from local plant materials against two different strains of *Pseudomonas aeruginosa*. *J. Ethnopharmacol.*, 2001, 76(1), 39-44.
44. Salau AK, Yakubu MT, Oladiji AT. Effects of aqueous root bark extracts of *Anogeissus leiocarpus* (DC.) Guill. & Perr. and *Terminalia avicennioides* Guill. & Perr. on redox and haematological parameters of diethylnitrosamine-administered rats. *Iran. J. Toxicol.*, 2018, 10(1),21-29.
45. Eltayeb IM, Ali HAR, Muddather AK, Ayoub SMH. Antioxidant activity and cytotoxic studies of *Anogeissus leiocarpous* root, leaf and stem. *Am. J. Res. Commun.*, 2016, 4(3), 52-57.
46. Onoja US, Ugwu CC, Uzor PF, Nweze IE, Omeje EO, Nnamani PO, Nwachukwu E, Njoku I, Effiong EJ. Effect of *Anogeissus leiocarpus* Guill. and Perr. leaf on hyperglycaemia and associated dyslipidaemia in alloxan-induced diabetic rats. *Dhaka Univ. J. Pharm. Sci.*, 2018, 17(1), 65-72.
47. Idakwoji PA, Agatemor UM-M, Akuba BO, Oniemola JM, Momoh TB. Effect of aqueous leaf extract of *Anogeissus leiocarpus* against experimental models of pain and pyrexia. Screening of medicinal plants for anti-diabetic properties (View project). Molecular identification, structure elucidation and characterization of bioactive principles in medicinal plants using FTIR, GC-MS, UPLC-PDA-QTOF-ESI-MS/MS and NMR techniques: Investigation of in vitro and in vivo bioactivities (View project). *Article in Int. J. Adv. Res. Biol. Sci.*, 2019, 6(6), 181-188.
48. Motto, AE, Lawson-Evi P, Kantati Y, Eklu-Gadegbeku K, Aklikokou K, Gbeassor M. Antihyperglycemic activity of total extract and fractions of *Anogeissus leiocarpus. J. Drug Delivery Ther.*, 2020, 10(3), 107-113.
49. Motto AE, Lawson-Evi P, Eklu-Gadegbeku K. Antidiabetic and antioxidant potential of total extract and supernatant fraction of the roots of *Anogeissus leiocarpus* in HFD-fed and *Streptozocin*-induced diabetic rats. *Biomed. Pharmacother.*, 2022, 154, 113578.
50. Ogbuagu NE, Aluwong T. Antidiabetic and antioxidant activities of ethanolic extract of *Anogeissus leiocarpus* in alloxan-induced type 1 diabetes mellitus in Wistar rats. *Cronicon Ec Diabetes Metab. Res.*, 2022, 6.1, 38-49.
51. Adefegha SA, Oboh G, Omojokun OS, Jimoh TO, Oyeleye SI. *In vitro* antioxidant activities of African birch (*Anogeissus leiocarpus*) leaf and its effect on the α-amylase and α-glucosidase inhibitory properties of acarbose. *J. Taibah Univ. Med. Sci.*, 2016, 11(3), 236-242.
52. Num-Adom SM, Adamu S, Aluwong T, Ogbuagu NE, Umar IA, Esievo KAN. Ethanolic extract of *Anogeissus leiocarpus* ameliorates hyperglycaemia, hepato-renal damage, deranged electrolytes and acid-base balance in alloxan-induced diabetes in dogs. *Sci. Afr.*, 2022, 16.
53. Omeje E, Osadebe P, Obonga W, Ugwuoke C. Phytochemical and pharmacological basis for the ethnomedicinal use of root extracts from *Anogeissus leiocarpus* as an antidiabetic in Eastern Nigeria. *Br. J. Pharm. Res.*, 2016, 9(4), 1-8.

54. Magashi LA, Nuhu I. Antimicrobial activity of the roots and stem bark of *Ceiba pentandra* and *Anogeissus leiocarpus* grown in Bauchi, North Eastern Nigeria. *J. Pharmacogn. Phytochem.*, 2017, 6(5), 865-870.
55. Ali EO, Tor-Anyiin TA, Hammuel C. Antimicrobial activity of *Anogeissus leiocarpus* stems bark extracts and an isolate from the plant against some microbes. *Am. J. Res. Commun.*, 2017, 5(8), 9-25.
56. Gbadamosi IT, Ogunsuyi AO. An appraisal of the potency of roots of *Anogeissus leiocarpus* (DC.) Guill. & Perr. and *Terminalia glaucescens* Benth. in the management of *E. coli* related infections. *J. Appl. Biosci.*, 2014, 78, 6646-6653.
57. Lawal TO, Bamiduro TB, Ofonmbuk JM, Elufioye TO, Adeniyi BA, Mahady GB. Antibacterial effects of *Anogeissus leiocarpus* (DC.) Guill. & Perr. and *Terminalia glaucescens* Planch. Ex Benth. on rapidly growing mycobacteria species. *Afr. J. Microbiol. Res.*, 2017, 11(12), 495-503.
58. Harisu YU, Muhammad AI. Antibacterial activity of leaves extract of *Anogeissus leiocarpus* and *Vitex doniana* against some bacteria. Control of malaria (View project). Study of Biochemical and Hematological Markers in Malaria-Malnutrition Co-Morbidity among Children Under 5 Years of Age in Kano State Nigeria (View project). *Am. J. Innovative Res. Appl. Sci.*, 2015, 1(10), 284-288.
59. Edewor TI, Akpor OB, Owa SO. Determination of antibacterial activity, total phenolic, flavonoid and saponin contents in leaves of *Anogeissus leiocarpus* (DC.) Guill. and Perr. *J. Coastal Life Med.*, 2016, 4(4), 310-314.
60. Elsiddig IME, Muddather AK, Ali HAR, Ayoub SMH. A comparative study of antimicrobial activity of the extracts from root, leaf and stem of *Anogeissus leiocarpous* growing in Sudan. *J. Pharmacogn. Phytochem.*, 2015, 4(4), 107-113.
61. Mann A, Yusuf A, Daniyan S. TLC analysis and bioactivity screening of the stem bark extract of *Anogeissus leiocarpus* against multi-resistant Staphylococcus aureus and quantification of its phytoconstituents. Screening of Indigenous Plants with Hypoglycemic and Antimicrobial Potentials (View project). Evaluating Effects of feeding detoxified *Jatropha curcas* meal and oil on the survival, growth and body compositions of *Clarias gariepinus* (View project). *Res. J. Pharm. Biol. Chem. Sci.*, 2014, 5(2), 187-203.
62. Muhammad FJ, Yafu MA, Yakubu M, Enemaku OF, Anthonia AB. Nigerian plants with anti-inflammatory and antifungal potential. *J. Adv. Biopharm. Pharmacovigilance*, 2019, 1(2), 40-48.
63. Maigari AK, Mukhtar Y Abubakar A, Muhammad B, Adamu A, Malami AI, Baura MS, Yaro MA, Harazimi AC, Umar RB, Barkindo MA. Antifungal activities of *Anogeissus leiocarpus* (African birch) against *Aspergillus niger* and *Rhizoctonia* species. *Int. J. Health Pharm. Res.*, 2017, 3(2), 30-39.
64. Elsiddig IME, Muddathir, AK, Ali HAR, Ayoub SMH. *In vitro* susceptibility of *Madurella mycetomatis* to the extracts of *Anogeissus leiocarpus* leaves. *Int. J. Biol. Biomolec. Agric. Food Biotechnol. Eng.*, 2015, 9(12), 1039-1050.

65. Mann A, Banso A, Clifford LC. An antifungal property of crude plant extracts from *Anogeissus leiocarpus* and *Terminalia avicennioides*. *Tanzania J. Health Res.*, 2008, 10(1), 34-38.
66. Gara TY. *In-vitro* activity of methanolic extract of stem bark of *Anogeisuss leiocarpus* (African birch) on *Plasmodium falciparum*. *Int. J. Appl. Biol. Res.*, 2020.
67. Akanbi OM, Omonkhua AA, Cyril-Olutayo CM, Fasimoye RY. The antiplasmodial activity of *Anogeissus leiocarpus* and its effect on oxidative stress and lipid profile in mice infected with *Plasmodium bergheii*. *Parasitol. Res.*, 2012, 110(1), 219-226.
68. Akanbi O. Antiplasmodial potential of combination therapy of methanolic bark extracts of *Terminalia avicennioides* and *Anogeissus leiocarpus* and its effect on haematological parameters on mice infected with *Plasmodium berghei*. *J. Adv. Med. Pharm. Sci.*, 2017, 15(2), 1-9.
69. Tagne MAF, Rékabi Y, Noubissi PA, Fankem GO, Akaou H, Wambe H, Kamgang, R. Evaluation of antidiarrheal activity of aqueous leaf extract of *Anogeissus leiocarpus* on castor oil-induced diarrhea in rats. *Am. J. Biomed. Sci. Res.*, 2019, 3(1), 27-34.
70. Irinmwinuwa EO, Adolphus MC, Ibeabuchi KC, Benard GO. Evidence based medicinal plant possessing anti-diarrhea activity: A review. *Natl. J. Adv. Res.*, 2023, 9(1), 1-6.
71. Hassan LEA, Al-Suade FS, Fadul SM, Abdul Majid AMS. Evaluation of antioxidant, antiangiogenic and antitumor properties of *Anogeissus leiocarpus* against colon cancer. *J. Angiother.*, 2018, 1(2), E056–E066.
72. Olugbami JO, Damoiseaux R, France B, Onibiyo EM, Gbadegesin MA, Sharma S, Gimzewski JK, Odunola OA. A comparative assessment of antiproliferative properties of resveratrol and ethanol leaf extract of *Anogeissus leiocarpus* (DC.) Guill. and Perr. against HepG2 hepato-carcinoma cells. *BMC Complementary Altern. Med.*, 2017, 17(1), 1-11.
73. Ukwade CE, Ebuehi OAT, Adisa RA. Phytochemical and cytotoxic screening of selected medicinal plants (*Byrsocarpus coccineus*, *Terminalia avicennioides* and *Anogeissus leiocarpus*) using brine shrimp (*Artemia salina*) lethality assay. *Eur. J. Nutr. Food Saf.*, 2020, 60-71.
74. Ohiagu FO, Chikezie PC, Chikezie CM, Enyoh CE. Anticancer activity of Nigerian medicinal plants: A review. *Future J. Pharm. Sci.*, 2021, 7(1), 1-21.
75. Tagne MAF, Noubissi PA, Gaffo EF, Fankem GO, Mukam JN, Kamgang R, Oyono J-LE Effects of aqueous extract of *Anogeissus leiocarpus* (DC.) Guill. Et Perr. (*Combretaceae*) leaves on acetic acid-induced ulcerative colitis in rats. *Adv. Tradit. Med.*, 2021, 1-10.
76. Rufa'i H, Nzelibe HC, Musa AM. Gastroprotective effect of aqueous stem bark extract of *Anogeissus leiocarpus* against ethanol-induced gastric ulcer in rats. *Sci. World J.*, 2022, 17(1), 11-16.
77. Idakwoji PA, Atanu FO, Nweje-Anyalowu PC, Momoh TB, Oniwon WO, Elazab ST, Sharkawi SMZ, Waheed RM, Youssef A, Batiha GE-S. Pharmacological studies of anti-inflammatory, anti-nociceptive and anti-pyretic compounds found in

chromatographic fractions of *Anogeissus leiocarpa* (DC). Guill. & Perr. leaves. *J. Pharm. Pharmacogn. Res.*, 2022, 10(3), 459-468.

78. Ademosun AO, Adebayo AA, Oboh G. *Anogeissus leiocarpus* attenuates paroxetine-induced erectile dysfunction in male rats via enhanced sexual behavior, nitric oxide level and antioxidant status. *Biomed. Pharmacother.*, 2019, 111, 1029-1035.
79. Oboh G, Adebayo AA, Ademosun AO, Boligon AA. *In vitro* inhibition of phosphodiesterase-5 and arginase activities from rat penile tissue by two Nigerian herbs (*Hunteria umbellata* and *Anogeissus leiocarpus*). *J. Basic Clin. Physiol. Pharmacol.*, 2017, 28(4), 393-401.
80. Ahmed OM, Ozikio EN, Agatemor UM-M Olubiyo GT, Momoh TB. Pro-fertility effect of the aqueous leaf extract of *Anogeissus leiocarpus* in albino Wistar rats. Pharmacological and Toxicological Profiling of Common Polyherbal Formulations (View project). Neuropharmacological Profile of *Leptadenia hastata* (View project). *Int. J. Curr. Res. Med. Sci.*, 2020, 6(5), 1-6.

The Chemist
Journal of the American Institute of Chemists

Qualitative Chemical Analysis of Some Aqueous Plant Extracts and Studying Their Biological Effectiveness on Germination and Growth of Maize (*Zea mays* L.) Seeds

Manar Abdullah Abou Hassan[1*], Mariam Abdul Razak Drakli[2]

1. Department of Chemistry, Faculty of Medicine, Syrian Private University, Syria
(E-mail: manarah87@hotmail.com)

2. Department of Chemistry, Faculty of Medicine, Syrian Private University, Syria
(E-mail: maria99913@hotmail.com)

**Corresponding Author*

Abstract: Medicinal plant extracts have a wide variety of chemical compounds. In this research, a qualitative study was conducted to reveal the chemical composition of the aqueous extract of figs (*Ficus carica* L.), mulberry (*Morus alba* L.) and eucalyptus (*camaldulensis* L.) leaves. This study included the detection of proteins, carbohydrates, phenols, flavonoids, glycosides, alkaloids, tannins, steroids, and saponins. The phytochemical analysis of the aqueous extracts from the studied plants leaves showed the presence of bioactive constituents like proteins, carbohydrates, phenols, flavonoids, glycosides and tannins in all mentioned extracts, while revealing the absence of alkaloids from mulberry and eucalyptus extracts, steroids from fig extract, and saponins from mulberry extract.

Different concentrations of aqueous extracts (5, 10, 15, 25, 50 and 75%) were evaluated for efficiency against germination and growth of *Zea mays* L. Using distilled water as a control, the germination percentage, and root and shoot length were observed. The results showed beneficial effects and a slight improvement in the percentage of germination and the above growth parameters compared with the control using mulberry extract at 5% and eucalyptus extract at 10%; however, higher concentrations of the extracts showed a negative effect.

Key Words: *Zea mays* L., germination, growth, medicinal plant, aqueous extract, eucalyptus

Abbreviations: WHO: World Health Organization, NaOCl: Sodium hypochlorite, ISTA: International Seed Testing Association, °C: Celsius degree, v/v: Volume Percentage

1. Introduction

Currently, use of phytochemicals, which are derived from medicinal plants, has gradually increased in many countries [1]. Medicinal plants have a wide variety of chemical compounds, resulting in different types of medicines and various bioactive molecules [2]. According to the World Health Organization (WHO), medicinal plants will be the best source for a variety of medicines and natural antioxidants, as they have long played important roles in the treatment of diseases throughout the world [1]. Some of the properties that the medicinal plants have are antimicrobial, anti-cancer, anti-diabetic, anti-atherosclerosis, and immunomodula-tory, and even have reno-protective or hepato-protective effects [3]. Figs (*Ficus carica* L.), mulberry (*Morus alba* L.) and eucalyptus (*camaldulensis* L.) are among these medicinal plants whose aqueous ex-tracts are of great importance because they contain many important biochemical com-pounds. The fig plant has a wide range of medicinal and nutritional values [4]. Its fruit, roots and leaves are used in native medicine for different disorders, such as colic, indigestion, diarrhea, sore throats, coughs, bronchial problems, inflammatory and cardiovascular disorders, ulcerative diseases, and cancers [5]. Clinical studies have shown that fig leaves extract has anti-tumor, hypolipidemic, antioxidant, antibacterial, hypoglycemic, and other functions. Because fig leaves contain a large number of flavonoids, they have a variety of pharmacological activities [4].

Mulberry trees are deciduous plants belonging to the genus *Morus* (family Moraceae), The most common species are *Morus alba* (white mulberry) and *Morus nigra* (blackberry) [6]. *Morus alba* L. leaves have an antiparasitic activity [7] and contain active ingredients showing a high nutritional importance and pharmaceutical effects among the genus *Morus*. They have long been used as traditional medicine for diabetes, arthritis, rheumatism, and other disorders for thousands of years in East Asia [6].

Eucalyptus (*camaldulensis* L.) is one of the important genera of the Myrtaceae family, a large genus of evergreen trees; it has been used as a medicinal plant for ages because of its various properties [8]. Eucalyptus' therapeutic properties include antiseptic, antiparasitic, insect repellent, anti-rheumatism, anti-migraines, anti-urinary tract infections, anti-ulcer burns, febrifuge, and anti-fatigue [9].

The present study was conducted to investigate the effects of fig (*Ficus carica* L.), mulberry (*Morus alba* L.) and eucalyptus (*camaldulensis* L.) leaves extracts on the germination and growth of maize (*Zea mays* L.) seeds due to it being one of the most economically important food crops in the world. It possesses high nutritive value and is important as a coarse grain. Germination is the first stage and one of the important and sensitive stages of the plant life cycle; it is an important process in seedling growth. This stage of growth is strictly influenced by environmental factors [10]. Additionally because these medicinal plant leaves are widely used in multiple fields, it was important to identify their chemical constituents.

2. Materials and Methods

This study was conducted in the laboratories of Syrian Private University, Syria, in 2022.

Preparation of Plant

The plant materials, fig (*Ficus carica* L.), mulberry (*Morus alba* L.) and eucalyptus (*camaldulensis* L.) leaves, were collected from the experimental fields of Tish-reen Park, Damascus City, Syria in June 2022.

The experiments were performed in a completely randomized design with three replications.
The seeds of maize (*Zea mays* L. Ghouta 82) were obtained from the General Institution for Plenitude of Seeds (Aleppo - Syria

Preparation of Extracts

Fresh leaves of fig, mulberry and eucalyptus plants were picked and cleared of any foreign materials, then rinsed with distilled water and dried with absorbent paper for 15 days in the shade. They were then grinded with an electric grinder to a fine powder that was used for the extraction [11].

Extraction was done using the method described by Dzimitrowicz *et al.* [12] with some modification. Twenty grams of fine powder of each plant were mixed separately in 400 mL of distilled water for one hour at room temperature with continuous stirring by a magnetic stirrer. The extracts were heated to 60°C for one hour, and after, were gradually cooled with continuous stirring until room temperature was reached, then left to stand for 24 h at 4°C. The resulting aqueous plant solutions were filtered twice with multi-layer tissue, then with Buchner funnels containing (Whatman® filter paper no. 5) and connected to a vacuum pump. Finally, the filtrates of the aqueous plant extracts were stored in the dark at 4°C until further used in bioassay and phytochemical characterization. Figure 1 shows the dried plants leaves before and after grinding, as well as the plant extract.

Fig 1. Plants Leaves and Extract

Qualitative Analysis

Preliminary qualitative phytochemical screening was carried out for proteins (Biuret's test) and glycosides (Salkowski's test) [13], carbohydrates (Molisch's test) [14], phenols [15,16], flavonoids (Alkaline reagent test) and alkaloids (Mayer's test) [17], tannins (Ferric chloride test) [18], steroids (Lieberman-Burchard test) [15,17], and saponins (Frothing test) [19], following the standard protocols.

Maize (*Zea mays* L.) Seeds Germination Experiment

For bioactivity study, healthy maize seeds of uniform size were used for the experiment. Surfaces were sterilized with 0.1% NaOCl, then they were washed thoroughly with distilled water [20].

The seeds were soaked for 24 h at room temperature (24°C) in different concentration of fig, mulberry and eucalyptus leaves extracts (5, 10, 15, 25, 50 and 75% v/v), using the distilled water as the control, then allowed to germinate on moist paper towels in petri dishes at 37°C in darkness for six days (144 h). The experimental seeds were kept moist by regularly adding of test solution, if required [21,22].

The germination percentage is the proportion, expressed as percentage of germinated seeds to the total number of viable seeds that were tested by the following formula according to ISTA [23].

$$G\% = Number\ of\ germinated\ seeds / Total\ number\ of\ planted\ seeds \times 100$$

The seedling growth was harvested after six days. The root length and shoot length were measured by using a centimeter scale, root length was measured from the main apex to the crown, whereas shoot length was measured from the crown to the main apex [24].

Statistical Analyses

The data was subjected to one way-ANOVA IBM SPSS software package for Windows (Version 20, SPSS Inc., Chicago, IL), the statistical significance was evaluated at $P \leq 0.05$. The results were presented as mean ± standard deviation based on three replications

3. Results and Discussion

Effects of the different concentrations (5, 10, 15, 25, 50 and 75% v/v) of fig, mulberry and eucalyptus leaves extracts were studied on germination percentage of maize seeds (*Zea mays* L.); distilled water was used as the control.

Results showed that seed germination of maize was promoted or inhibited to different degrees depending on the concentrations of aqueous extracts. This indicates that maize has a strong adaptability, which plays a pivotal role in it becoming a dominant species. At low concentrations of plant extracts (5%), the mulberry extract showed the highest germination percentage of 96.75%, followed by eucalyptus extract with a germination percentage close to that of the control (91.21%), while the fig extract at the same concentration reached 69.80%. By increasing the concentration of all plant extracts to 10%, a significant improvement and significant differences were observed for each of the extracts of fig and eucalyptus compared to the previous concentration, where the percentage of germination reached 89.96% and 97.42%, respectively. The percentage of germination of mulberry extract decreased to 60.44% with clear significant differences compared to the control and at the previous concentration. This may be due to the increased osmotic pressure of plants cells, which increases the water absorption capacity of cells. It may also be that the trace inorganic ions in maize cells have a stimulating effect on respiratory enzyme activity, which improves the ability of plants to generate nutrients, therefore promoting seed germination of maize [25]. Allelochemicals are usually called secondary plant products of the main metabolic pathway in plants, most of them originate from the shikimic acid and acetate pathway. They are often water-soluble substances and present in almost all plants and in many tissues. Allelochemicals that inhibit the growth of some species at certain concentrations might in fact stimulate the growth of the same or different species at different concentrations [26]. The increase in the concentrations of the plant extracts led to a clear decrease in the germination percentage of maize seeds. At the concentration of 15%, the germination percentage of figs, mulberry and eucalyptus was 52.74% and 43.31% and 67.74%, respectively, and at the concentration of 25% was 18.75% and 27.02% and 37.14%, respectively. The inhibition in the ability to germinate was more evident at the 50% concentration, where the percentage of germination was 18.75% and 27.02% and 37.14% for each of the extracts of figs, mulberry and eucalyptus, respectively. While the germination and growth of maize seeds were completely inhibited at 75% concentration.

The allelochemical content increased with the increase of the concentrations of the studied plants leaves aqueous extracts, resulting in an enhanced inhibition effect. Certain plant allelochemicals have hormone-like effects or promote the growth of the recipient plant by changing its hormone composition and concentration [25].

Table 1 shows the germination percentage of maize seeds, and root and shoot lengths of maize seedling when using distilled water as a control and at different concentrations of extracts of leaves of fig, mulberry and eucalyptus.

Table 1. Effect of Different Concentrations of the Fig, Mulberry and Eucalyptus Aqueous Leaves Extracts on the Seed Germination and Seedling Growth of Maize (*Zea mays* L.)

Plant Species	Concentration	Germination percentage	Length shoot	Length root
Control	0	93.12^{a}±3.97	8.96^{a}±0.273	9.50^{a}±0.512
Fig	5	69.80^{b}±1.06	5.50^{b}±0.506	4.00^{b}±0.284
	10	89.96^{c}±0.83	7.76^{a,c}±0.174	7.46^{c}±0.331
	15	52.74^{d}±2.13	6.33^{c}±0.532	3.53^{b}±0.121
	25	18.75 ^{e}± 1.89	1.83^{d}±0.328	1.33^{d}±0.118
	50	7.33^{f}±0.46	0.60^{e}±0.09	0.33^{e}±0.103
	75	0^{g}±00	0.00^{f}±0.00	0.00^{f}±0.00
Control	0	93.12^{a}±3.97	8.96^{a}±0.273	9.50^{a}±0.512
Mulberry	5	96.75^{a}±1.85	9.03^{a}±0.121	7.33^{b}±0.153
	10	60.44^{b}±2.13	6.20^{b}±0.145	4.06^{c}±0.227
	15	43.31^{c}±4.11	4.76^{c}±0.101	3.43^{c}±0.186
	25	27.02^{d}±0.46	4.33^{c}±0.098	2.43^{d}±0.121
	50	9.86^{e}±1.30	0.93^{d}±0.107	0.56^{e}±0.085
	75	0^{f}±00	0.00^{e}±0.00	0.00^{f}±0.00
Control	0	93.12^{a,b}±3.97	8.96^{a}±0.273	9.50^{a}±0.512
Eucalyptus	5	91.21^{a}±3.08	7.60^{b}±0.649	6.33^{b}±0.156
	10	97.42^{b}±1.11	8.96^{a}±0.323	10.1^{a}±0.447
	15	67.74^{c}±2.92	6.80^{b}±0.503	6.76^{b}±0.513
	25	37.14^{d}±1.84	4.90^{c}±0.226	6.66^{b}±0.501
	50	13.74^{e}±2.44	1.70^{d}±0.076	4.50^{c}±0.433
	75	0^{f}±00	0.00^{e}±0.00	0.00^{d}±

* Values are mean ± standard deviation.
* Different letters within column indicate significant differences between the concentrations at every plant (P ≤ 0.05).

By studying the effect of different concentrations of extracts of leaves of fig, mulberry and eucalyptus plants on the growth of seedlings of maize plant, the change in shoot and root length was recorded with the change in the concentration of each of the extracts. The results showed that the shoot length under the influence of each of the extracts of fig and eucalyptus leaves ranged between 7.76 cm and 0.60 cm for fig and between 8.96 cm and 1.70 cm for eucalyptus, and the length of the root ranged between 7.46 cm and 0.33 cm for fig and between 10.1 cm and 4.50 cm for eucalyptus, where these values were recorded at concentration 10% and 50%, respectively. Whereas, with the effect of mulberry leave extract, it was observed that the highest growth of shoot and root was recorded at the concentration 5% where the length of each of the shoot and root was 9.03 cm and 7.33 cm, respectively.

From the above, it is noted that the toxicity of fig and eucalyptus extracts on both the shoot and root started at a concentration of 15%, while the toxicity of the mulberry extract started at 10%, and this toxicity increased with increasing concentration. Germination and seedling growth are the screening criteria which are widely used to investigate the effects of allelopathy. Morphological changes, in response to allelochemicals, could be due to effects on the cellular or molecular level. The effects of the allelochemicals' action have been detected at molecular, structural, physiological, biochemical and ecological levels of plant organization. Allelochemicals restrict plant growth through negative interactions with some physiological processes such as suppression of cell division, changes in cell wall structure and activity of some enzymes [27]. Also, the effect of allelopathy on germination and growth of plants may occur through a variety of mechanisms, including a reduced mitotic activity in root and hypocotyls, suppressed hormone activity, reduced rate of nutrient uptake, inhibited protein formation, decreased permeability of cell membranes and inhibition of enzyme action which may be attributed to the reduction of (N, P, K) content in the tested seeds of maize. The tested seeds differed in their responses, which may be due to the effect of the extracts on the cell permeability to the nutrient's uptake, or the genetic effect, because the inhibitory compounds might have reduced the uptake of nutrient, which ultimately reduced shoot growth [28].

This study has revealed the presence of phytochemicals considered as active medicinal chemical constituents. Some of the phytochemicals were found in abundance while others in trace amounts. Table 2 showed preliminary phytochemical screening of the fig, mulberry and eucalyptus leaves aqueous extracts.

Table 2. Preliminary Phytochemical Screening of the Fig, Mulberry and Eucalyptus Aqueous Leaves Extracts

Plant	proteins	carbohydrates	phenols	flavonoids	glycosides	alkaloids	tannins	steroids	saponins
figs	++	+	++	++	++	+	++	-	++
mulberry	+	+	+++	++	+	-	+	++	-
eucalyptus	+	++	+++	+++	++	-	+	+	+

Legend: +=Low concentration, ++ = Moderate concentration, +++ = High concentration, - = Absent

Phytochemical studies and qualitative phytochemical investigation discovered the presence of proteins, carbohydrates, phenols, flavonoids, glycosides and tannins in all mentioned extracts of plant. Steroids are found in all extracts except for those obtained from figs extract. Alkaloids were found in figs extract, while other plant extracts did not contain this type of compound. Saponins were not found in mulberry extract.

Plant cells produce two types of metabolites. Primary metabolites are involved directly in growth and metabolism (carbohydrates, lipids and proteins). Secondary metabolites are considered products of primary metabolism and are generally not involved in metabolic activity (alkaloids, phenolics, essential oils and terpenes, sterols, flavonoids, lignins, tannins, etc.). These secondary metabolites are the major source of pharmaceuticals, food additives, fragrances and pesticides, and herbicides. The composition of bioactive compounds present in plants are influenced by the genotype, extraction procedure, geographic and climatic conditions, and the growth phase of the plants [15].

Saponins have anti-inflammatory and antifungal effects, hemolytic activity, and cholesterol binding properties. Tannins have been reported to prevent the development of microorganisms by precipitating microbial protein and making nutritional proteins unavailable for them. Also, tannins exhibit antioxidant and antiviral effects [15,18]. Steroids are known to produce an inhibitory effect on inflammation and are very important compounds, especially due to their relationship with compounds such as sex hormone [15,29]. Alkaloids have been reported to exert analgesic, antispasmodic and antibacterial activities [30]. Phenolic compounds like phenolic acids, polyphenols and flavonoids are very important plant components called antioxidants, which scavenge free radicals such as peroxide, hydroperoxide of lipid hydroxyl and therefore halt the oxidative mechanism that leads to degenerative diseases. Flavonoids have anti-inflammatory, anti-angiotic, antimicrobial, antioxidant, and reduced hypertension effects, and have anti-cholesterol properties [16].

The phytochemical analysis of the medicinal plants is also important and has commercial interest from both research institutes and pharmaceuticals companies for the manufacturing of the new drugs for treatment of various diseases.

4. Conclusion

In the present study, the phytochemical screening for leaves extracts of figs, mulberry and eucalyptus showed the presence of active component like phenols, flavonoids, glycolsides and tannins from aqueous extracts. These extracts have an extremely strong effect on the seed germination of maize at different concentrations. The low concentrations of the leaves aqueous extracts of the studied plants showed an improvement in morphological growth and germination percentage, while the higher concentrations showed clear toxicity in the maize plant.

5. Funding

This research received no external funding.

6. Conflict of Interest

The manuscript was written through contributions of the two authors, and these two authors contributed equally. The authors have given approval to the final version of the manuscript.

The authors declare no conflict of interest.

7. Acknowledgments

The authors are thankful to the Syrian Private University and Atomic Energy Commission of Syria for providing the facility to conduct the experiments in laboratories.

8. References

1. Selvamohan T, Ramadas V, Kishore SSS. Antimicrobial activity of selected medicinal plants against some selected human pathogenic bacteria. *Adv. Appl. Sci. Res.*, 2012, 3(5), 3374-3381.
2. Borah R, Biswas SP. Tulsi (*Ocimum sanctum*), excellent source of phytochemicals. *Int. J. Environ. Agric. Biotechnol.*, 2018, 3(5), 1732-1738.
3. Rafieian-Kopaei M. Medicinal plants and the human needs. *J. HerbMed Pharmacol.*, 2012, 1(1), 1-2.
4. Li C, Yang X, Tian Y, Yu M, Shi S, Qiao B, Zhou C, Mao L. The effects of fig tree (*Ficus carica* L.) leaf aqueous extract on seed germination and seedling growth of three medicinal plants. *Agronomy*, 2021, 11(12), 2564.
5. Lee YS, Cha JD. Synergistic antibacterial activity of fig (*Ficus carica*) leaves extract against clinical isolates of methicillin-resistant *Staphylococcus aureus*. *Microbiol. Biotechnol. Lett.*, 2010, 38(4), 405-413.
6. Chang BY, Koo BS, Kim SY. Pharmacological activities for *Morus alba* L., focusing on the immune-stimulatory property from the fruit aqueous extract. *Foods*, 2021, 10(8), 1966.
7. Thagfan FA, Al-Megrin WA, Al-Quraishy S, Dkhil MAM. Mulberry extract as an ecofriendly anti-coccidial agent: *in vitro* and *in vivo* application. *Rev. Bras. Parasitol. Vet.*, 2020, 29(24).
8. Kaur S, Gupta S, Gautam PB. Phytochemical analysis of Eucalyptus leaves extract. *J. Pharmacogn. Phytochem.*, 2019, 8(1), 2442-2446.
9. Abbasi N, Khalighi Z, Eftekhari Z, Bahmani M. Extraction and phyto-analysis of chemical compounds of *Eucalyptus globulus* leaf native to Dehloran, Ilam province, Iran by HS-SPME and GC-MS. *Adv. Anim. Vet. Sci.*, 2020, 8(6), 647-652.
10. Sozharajan R, Natarajan S. Germination and seedling growth of *Zea mays* L. under different levels of sodium chloride stress. *Int. Lett. Nat. Sci.*, 2014, 7, 5-15.
11. Nangare S, Bhatane D, Rushikesh MALI, Shitole M. Development of a novel freeze-dried mulberry leaf extract-based transfersome gel. *Turk. J. Pharm. Sci.*, 2021, 18(1), 44-55.
12. Dzimitrowicz A, Jamroz P, Sergiel I, Kozlecki T, Pohl P. Preparation and characterization of gold nanoparticles prepared with aqueous extracts of Lamiaceae plants and the effect of follow-up treatment with atmospheric pressure glow micro-discharge. *Arabian J. Chem.*, 2019, 12(8), 4118-4130.
13. Panchal P, Parvez N. Phytochemical analysis of medicinal herb (*Ocimum sanctum*). *Int. J. Nanomater. Nanotechnol. Nanomed.*, 2019, 5(2), 008-011.

14. Prabhavathi RM, Prasad MP, Jayaramu M. Studies on qualitative and quantitative phytochemical analysis of *Cissus quadrangularis*. *Adv. Appl. Sci. Res.*, 2016, 7(4), 11-17.
15. Ndam LM, Mih AM, Fongod AGN, Tening AS, Tonjock RK, Enang JE, Fujii Y. Phytochemical screening of the bioactive compounds in twenty (20) Cameroonian medicinal plants. *Int. J. Curr. Microbiol. Appl. Sci.*, 2014, 3(12), 768-778.
16. Rao USM, Abdurrazak M, Mohd KS. Phytochemical screening, total flavonoid and phenolic content assays of various solvent extracts of tepal of *Musa paradisiaca*. *Malays. J. Anal. Sci.*, 2016, 20(5), 1181-1190.
17. Yadav P, Kumar A, Mahour K, Vihan VS. Phytochemical analysis of some indigenous plants potent against endoparasite. *J. Adv. Lab. Res. Biol.*, 2010, 1(1), 56-59.
18. Banso A, Adeyemo S. Phytochemical screening and antimicrobial assessment of *Abutilon mauritianum*, *Bacopa monnifera* and *Datura stramonium*. *Biokemistri*, 2006, 18(1), 39-44.
19. Nadeem A, Ahmad B, Imran M, Tabassum A, Craker LE. The phytochemical analysis, metabolic profiling, anti-bacterial and anti-oxidant activity of *Nepeta cataria*. *Research Square*, 2021. DOI: https://doi.org/10.21203/rs.3.rs-154568/v1
20. Aliu S, Rusinovci I, Fetahu S, Gashi B, Simeonovska E, Rozman L. The effect of salt stress on the germination of maize (*Zea mays* L.) seeds and photosynthetic pigments. *Acta Agric. Slov.*, 2015, 105(1), 85-94.
21. Dawood MG, Sadak MS, Reyad BY, El-Sayed ASM, El-Gayar SH. Changes in chemical composition during germination of some canola varieties changes in oil content and fatty acid composition. *Sci. Agric.*, 2013, 2(3), 77-82.
22. Parviz M, Resa SM, Asghar HA. Effects of aluminum toxicity on maize (*Zea mays* L.) seedlings. *Iran. J. Plant Physiol.*, 2015, 5, 1289-1296.
23. Abu-Hassan M, Malo A, Al-Muhanna N. Effect of untreated olive mill wastewater on seed germination, seedling growth and biochemical of *maize (Zea mays L.). Chem.: Bulg. J. Sci. Educ.*, 2018, 27(1), 93-108.
24. Houshmandfar A, Moraghebi F. Effect of mixed cadmium, copper, nickel and zinc on seed germination and seedling growth of safflower. *Afr. J. Agric. Res.*, 2011, 6, 1182-1187.
25. Li C, Yu M, Li S, Yang X, Qiao B, Shi S, Zhao C, Fu Y. Valorization of fig (*Ficus carica* L.) waste leaves: HPLC-QTOF-MS/MS-DPPH system for online screening and identification of antioxidant compounds. *Plants*, 2021, 10(11), 2532.
26. Naz R, Bano A. Effects of allelochemical extracts from medicinal plants on physiological and biochemical mechanisms of maize (Zea mays L.) seedlings. *Int. J. Agron. Agric. Res.*, 2014, 5(2), 31-39.
27. Morsi MM, Abdelmigid HM. Allelopathic activity of *Eucalyptus globulus* leaf aqueous extract on *Hordeum vulgare* growth and cytogenetic behavior. *Aust. J. Crop Sci.*, 2016, 10(11), 1551-1556.
28. Saeed AJ, Al-Rawi RE, Ibraheem KF. The effect of aqueous leaves extracts of *Eucalyptus camaldulensis* on germination and growth of three

weed species. *Rafidain J. Sci.*, 2013, 24(2), 1-10.
29. Shrivastava S, Leelavathi S. Preliminary phytochemical evaluation of leaf extracts of *Catunaregum spinosa* Thunb. *Int. J. Pharm. Sci. Rev. Res.*, 2010, 3(2), 114-118.
30. Wadood A, Ghufran M, Jamal SB, Naeem M, Khan A, Ghaffar R. Phytochemical analysis of medicinal plants occurring in local area of Mardan. *Biochem. Anal. Biochem.*, 2013, 2(4), 1-4.

The Chemist
Journal of the American Institute of Chemists

Review on Testing Methods for Permeability and Selectivity Measurements of Polymeric Membranes

Yousef Alqaheem*

Petroleum Research Center, Kuwait Institute for Scientific Research, Kuwait

** Corresponding author. Tel.: +965 24956929. Fax: +965 23980445*
(E-mail: yqaheem@kisr.edu.kw)

Abstract: Polymeric membranes can provide an energy-saving solution for gas separation. The technology is also compact and easy to maintain, though, for commercial applications, the membrane performance should be conscientiously tested as the data could vary significantly. Unfortunately, there is no standard procedure for evaluating the membranes for gas separation. This paper gives general guidelines on various methods for determining the membrane permeability and selectivity with the commonly used setup. The paper also discusses the measurements and calculations of product purity and gas recovery for better comparison with other separation technologies.

Key Words: Gas-separation membrane, gas permeability, real selectivity, time-lag method, gas recovery

1. Introduction

Polymeric membranes have been comer-cialized for gas separation since the 1980s [1]. The first application was for the removal of hydrogen from methane by a polysulfone membrane [2]. The applications were then expanded to cover acid gas remo-val, and oxygen enrichment [3]. The mem-brane is considered as an environmentally-friendly technology because it operates at low energy and it does not produce toxic wastes [4]. Furthermore, the membrane is easy to scale up and can have a continuous life of five years [5,6].

There are many materials for polymeric membranes and their performance varies broadly depending on the polymer and the gases to be separated. The widely accepted theory for gas transport through dense poly-meric membranes is the solution-diffusion model [7]. The model states that the gas is first absorbed on the membrane surface and then dissolved. The gas then diffuses inside the membrane by a means of free volumes. The gas is then desorbed on the low-pressure side. Their dominant factors that control the solution-diffusion model are solubility and diffusivity [8]. The perme-ability (P), which is one of the key parameters to describe the membrane per-formance, is the product of solubility and diffusivity:

$$P = K_A \times D_A \tag{1}$$

where K_i and D_i are the sorption and diffusion coefficients of gas a, respectively. The permeability gives information about the quantity of the produced gas (also known as the permeate). Experimentally, the perme-ability can be determined without the need for solubility and diffusivity measure-ments. There are typically three approaches to measure the permeability: using a bubble flowmeter, a mass flowmeter, and the time-lag technique. Each method will be dis-cussed in detail in the following sections. The permeability data is given in Barrer (named after Richard Barrer) and it is calculated by:

$$P\ (\text{Barrer}) = \frac{V_A \times l}{A \times \Delta P} 10^{10} \tag{2}$$

where V_A is the volume flowrate of the permeate of gas a ($cm^3\ s^{-1}$), l is the mem-brane thickness (cm), A is the active mem-brane area (cm^2), and ΔP is the pressure dif-ference across the membrane (cmHg). The mentioned techniques for permeability cal-culations actually measure the volume flowrate which will be used to calculate the permeability as given in equation 2. Because the volume of the gas depends on the pres-sure and temperature, the volume flowrate for equation 2 should be stated at STP (standard temperature and pressure of 0°C and 1 atm). STP should not be confused with NTP (normal temperature and pressure) where the temperature is 20°C instead of 0°C. The pressure in NTP is 1 atm which is very close to 1 bar (0.986 atm). Assuming ideal gas behavior, the volume flowrate can be converted from NTP to STP using the following equation:

$$V_{STP} = \frac{T_{STP}}{T_{NTP}} V_{NTP} = \frac{273}{293} V_{NTP} = 0.925 V_{NTP} \tag{3}$$

where T_{STP} and T_{NTP} , are the temperatures of 273 and 293K, respectively. This gives a correction factor of 0.925 when the flowrate is converted of NTP to STP.

The membrane thickness in equation 2 is commonly determined using a caliper in the case of a symmetric membrane which is made from a single material with a uniform structure (porous or dense). However, for asymmetric membranes made from two or more materials (composite), characterization techniques such as scanning electron micro-scopy (SEM) are needed to measure the thickness of the selective material which is usually the dense layer. Other techniques such as transmission electron microscopy (TEM) and atomic force microscopy (AFM) can be used as well [9]. It is worth mentioning that asymmetric membranes can be made as well from a single material using the phase-inversion method [10].

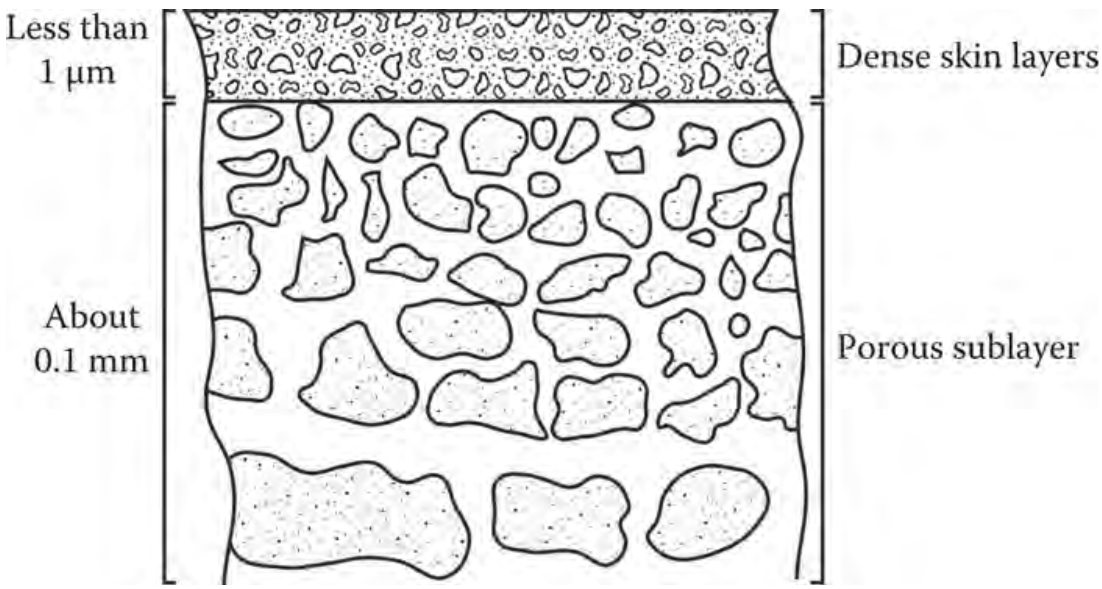

Figure 1. Structure of Asymmetric Membrane Made from One Material by the Phase-inversion Method [12]

The developed membrane will have two structures: porous and dense, as given in Figure 1, despite the use of one material. In this case, the membrane thickness is the skin of the dense layer similar to the composite membrane [11]. In literature, most of the membranes are made from the phase-inversion method and therefore, a spectroscopy technique is needed to measure the membrane thickness.

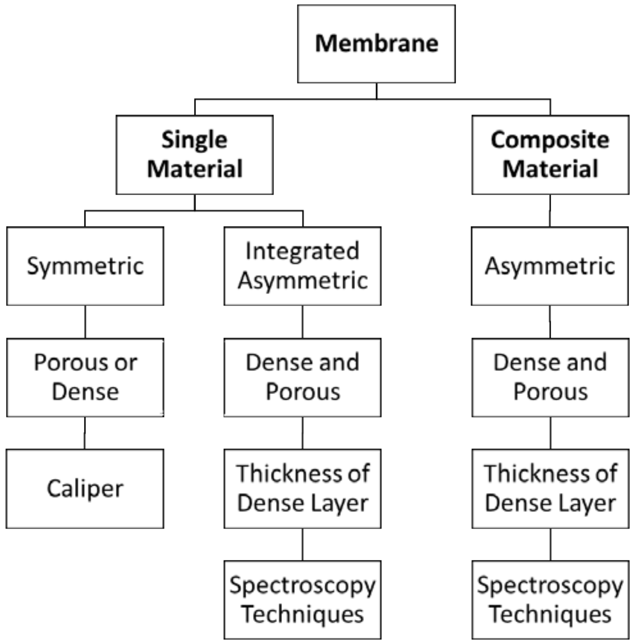

Figure 2. Determination of the Membrane Thickness for the Calculation of Gas Permeability in Barrer

Figure 2 gives general guidelines for determining the membrane thickness for calculating the permeability in Barrer. Sometimes is it difficult to measure the membrane thickness as it can vary notably along with the membrane structure. Furthermore, the spectroscopy technique maybe not available to measure the membrane thickness. Thus, a new unit for gas permeability was defined and it is known as permeance (Q). It is calculated similar to equation 2 but without the use of thickness:

$$Q\ (\text{GPU}) = \frac{V_A}{A \times \Delta P} 10^6 \qquad (4)$$

where V_A, A, and ΔP shares the same units as equation 2. The unit of permeance is the gas permeation unit (GPU).

Unfortunately, the units of Barrer and GPU cannot be converted if the membrane thickness was not stated. If the membrane thickness is known, the following equation can be used to convert the permeability from Barrer to GPU.

$$Q\ (\text{GPU}) = \frac{P\ (\text{Barrer})}{10{,}000 \times l} \qquad (5)$$

It should be noted that Barrer is considered as a more accurate unit than GPU for stating the permeability as it takes into consideration the membrane thickness. This will make the comparison with other reported data more reliable for the same membrane. However, industrially, the membrane performance is widely described by GPU unit rather than Barrer for easier calculations.

This paper reviews the methods for measuring the permeability in polymeric membranes using different approaches such as bubble flowmeter, mass flowmeter, and the time-lag method (also known as the closed volume technique). The paper also describes about calculations of solubility and diffusion coefficients. Furthermore, the paper discusses the determination of gas selectivity which represents the purity of the gas produced. The paper also differentiates between the ideal and real selectivities and the latter is a key parameter for determining the membrane performance for commercial applications. The calculations of product purity and gas recovery are also important to evaluate the membranes with other separation technologies such as the amine process.

2. Permeability Measurements

The permeability can be calculated based on the measured flowrate of the permeate. There are extensively three ways to measure membrane permeability: (1) bubble flowmeter, (2) mass flowmeter, and (3) time-lag technique. Before starting the evaluation, the membrane should be examined visually. Any visible holes or defects may cause incorrect value of the permeability. The membrane is then inserted in a cell, usually made of metal housing. Rubber rings (with o-shape) are traditionally employed to seal the membrane and prevent gas leakage. The gas is normally fed to the membrane by a gas cylinder equipped with a pressure regulator. A mass flow controller (MFC) is commonly used to control the feed flowrate. This device is used to set the volume flowrate of the feed gas. The output gas (after MFC) will be at atmospheric pressure and a pressure control valve can be employed to elevate the pressure. The feed gas will reach the membrane surface and the volume flowrate of the permeate will be measured to deter-mine the permeability. Figure 3 shows the common experimental setup for the permeability test.

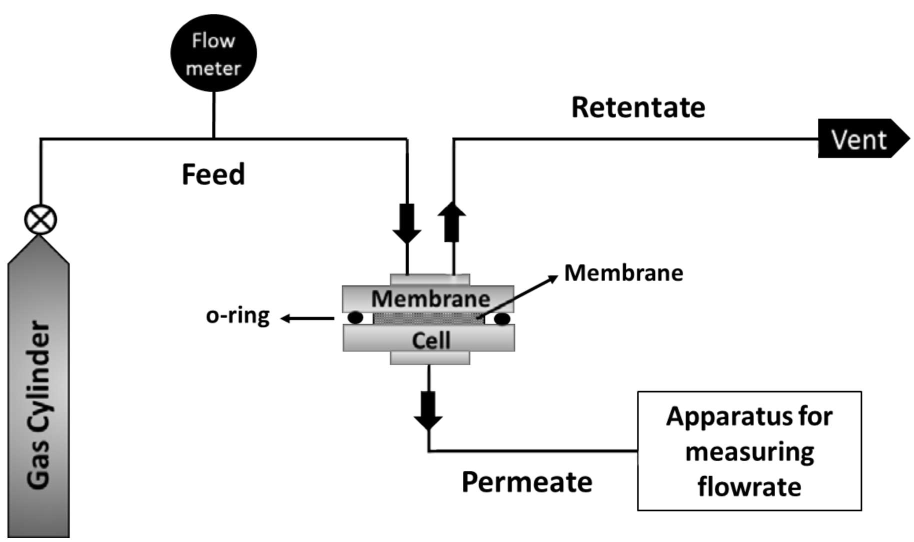

Figure 3. Experimental Setup for Determining the Gas Permeability of Polymeric Membranes

It should be noted that there are some inputs that should be defined before performing the membrane assessment. These inputs will significantly affect the permeability data. The parameters are the gas feed flowrate, temperature, pressure, membrane area, and membrane thickness. The area is calculated based on the cross-section area of the membrane as follows:

$$A = \pi \frac{d^2}{4} \tag{6}$$

where d is the diameter of the exposed area to the gas which is usually lower than the total diameter of the membrane as the o-rings will block some region for sealing.

Unfortunately, there are no standards for the input parameters, however, the following values are widely used in literature: feed flowrate of 0.1−1 $cm^3\ s^{-1}$, temperature of 25−35°C, pressure of 3−10 bar, area of 10−15 cm^2, membrane thickness of 10−300 μm as given in Table 1. The following sections will discuss the methods for determining the permeability using the bubble flowmeter, mass flowmeter, and the time-lag technique.

Table 1. Operating Conditions for Membrane Testing Used by Most Researchers [13-26]

Operating condition	Value
Feed flowrate	0.1 − 1 $cm^3\ s^{-1}$
Temperature	25 − 35°C
Pressure	3 − 10 bar
Membrane effective area	10 − 15 cm^2
Membrane thickness	10 − 300 μm

Bubble Flowmeter

The bubble flowmeter is considered as the oldest and the most cost-effective technique for measuring the permeability. Broadly, the system is suitable for measuring flowrates between 0.1 to 1000 $cm^3\ s^{-1}$. The instrument consists of a graded burette along with a rubber bulb and soap solution. The gas enters the side of the instrument and then the bulb is squeezed to create a soap film that will be lifted by the gas in the form of a bubble. The burette is marked with a starting point in which a stopwatch will be used to measure the time needed for the bubble to cross the final mark as shown in Figure 4. By dividing the volume by time, the volume flowrate can be determined. The error expected for this instrument is within ±5% [28]. Nevertheless, if the experiment was carried perfectly, the error can be reduced to ±1% [29].

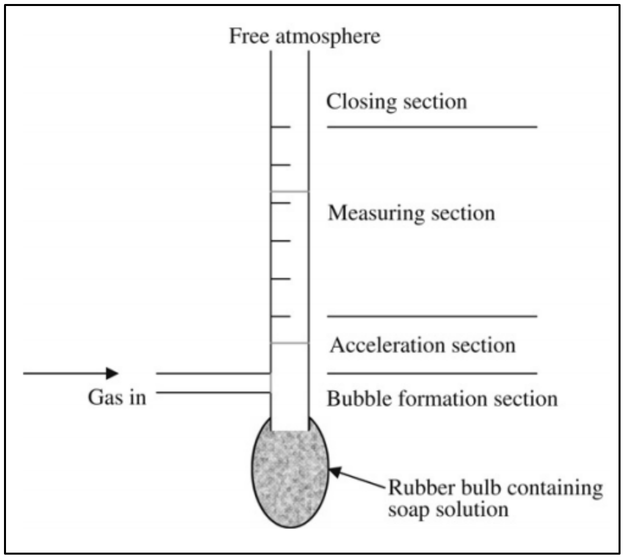

Figure 4. Components of the Bubble Flowmeter for Gas Permeability Measurements [27]

It should be noted that not all gases can be used in the bubble flowmeter. For example, high water-soluble gases such as ammonia and hydrogen chloride will be dissolved in the soap solution, and this will cause a significant error in the reading [30].

Mass Flowmeter

In the mass flowmeter approach, the volume flowrate of the permeate will be measured by an electrical signal. It is more accurate compared to the bubble flowmeter as the stopwatch will not be needed and this can minimize the uncertainty. Thermal mass flowmeters are widely used, and they work based on the thermal conductivity of the gas. The unit consists of a filament where its temperature is maximum when no gas is fed. When the gas enters the flowmeter, a drop in temperature will occur and this can be related to the volume of the gas (Figure 5).

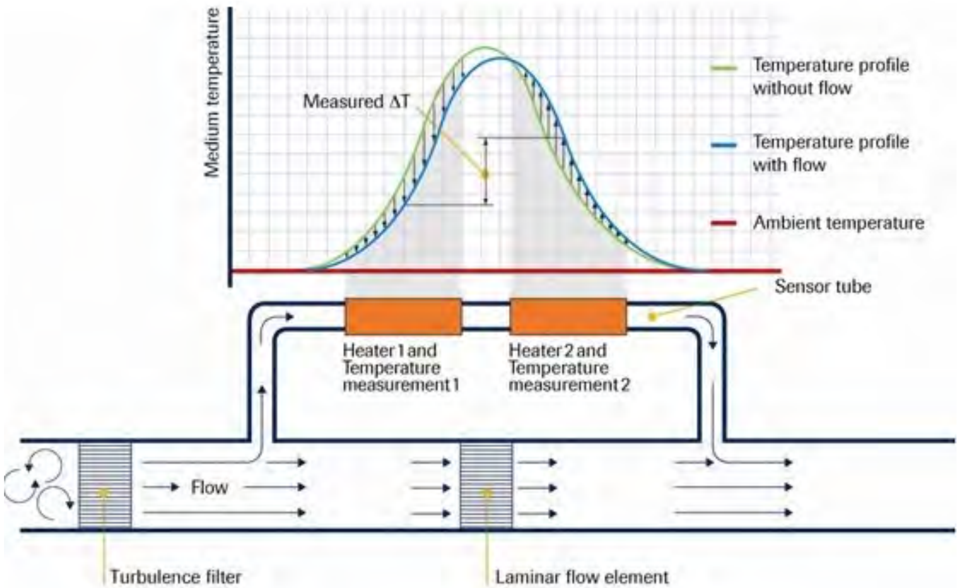

Figure 5. Operating Principle of the Thermal Mass Flowmeter [31]

It should be noted that the mass flowmeter is calibrated for specific gas and its accuracy is within ±1% [32]. However, using the same mass flowmeter for a different gas than the calibrated one may introduce an error in the measurement. For example, a calibrated mass flowmeter for nitrogen was tested for methane and the error reached 20.5% [33]. Yet, when the same mass flowmeter was used for hydrogen, the error was only 1%. It was found that the error depends highly on the specific heat of the gas which is defined as the required energy to raise the gas temperature by 1 K of a unit mass of gas at constant pressure (*Cp*). Table 2 shows the calculated correction factor (*CF*) for a nitrogen-calibrated mass flowmeter tested with other gases. The correction factor was calculated using the following equation:

$$CF = \frac{V_A}{V_B} = \frac{(C_p M)_A}{(C_p M)_B} \tag{7}$$

where B is the tested gas and A is the calibrated gas. M is the molecular weight and C_p is the specific heat at constant pressure. So, if the mass flowmeter is calibrated with methane, and butane is to be used, equation 7 will give a correction factor of 0.37. The absolute average error of the previous equation is 3.1%.

The data in some mass flowmeters are given in NTP while the others are given in STP. To calculate the permeability in Barrer or GPU, the data of volume flowrate should be converted to STP using equation 3. The mass flowmeters are capable of reading flows from 0.0003 to 40,000 cm^3 s^{-1} [34]. Furthermore, the technique can be used to monitor the membrane permeability for long-term operation.

Table 2. Correction Factor for the Conversion of a Nitrogen-calibrated Mass Flowmeter for Use with Other Gases [35]

Tested Gas	C_p (kJ kg^{-1} K^{-1})	M (g mol^{-1})	CF
Ammonia	2.19	17.03	0.78
Argon	0.52	39.95	1.40
Butane	1.67	58.12	0.30
Carbon dioxide	0.84	44.01	0.79
Ethane	1.75	30.07	0.55
Helium	5.19	4.02	1.40
Hydrogen	14.32	2.02	1.01
Methane	2.22	16.04	0.82
Nitrogen	1.04	28.02	1.00

Time-Lag Method

The time-lag method is based on a closed volume in which the permeate flowrate will cause an increase in the pressure with time. The volume of the closed system should be accurately determined taking into consideration the volume of pipes. Before the experiment, the system is vacuumed using a pump and a pressure gauge is utilized to monitor the pressure. The system should be leak-free otherwise, the permeability data will be incorrect. To make sure the setup is gas-tight, the system is kept under vacuum (with no gas fed) for about 24 h. First, the vacuum pump should be run for about 30 min, and then the valve before the pump is closed. Generally, the pressure gauge should give a reading below 3 mbar for the system to be considered gas-tight. Figure 6 shows the setup for the time-lag experiment.

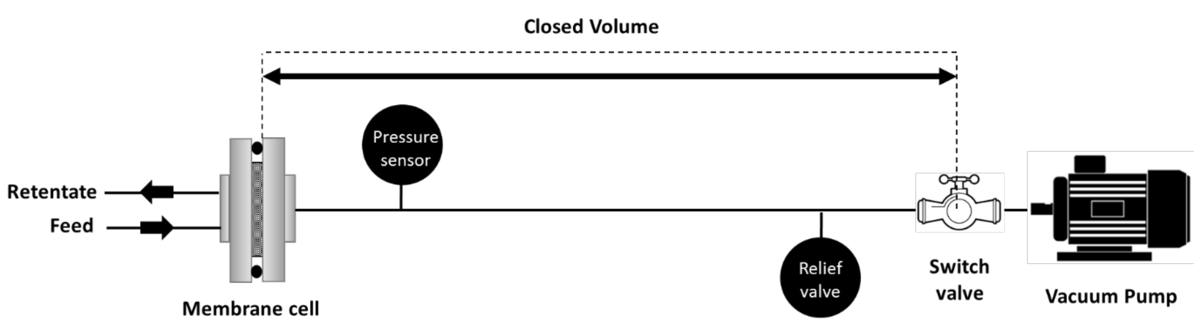

Figure 6. Experimental Setup for the Time-lag Method for Permeability Measurements [36]

After feeding the gas to the membrane, the permeated gas will cause a pressure buildup. The experiment is usually terminated when the pressure reaches 1 atm. Gauge-pressure data should be monitored along with the time on stream. The time starts at 0 s when the gas is fed to the membrane. The permeability (in Barrer) can be then calculated using [37]:

$$P\text{ (Barrer)} = \frac{273}{76}\left[\frac{V_b \times l}{A \times T \times p_a}\right]\frac{dp_b}{dt} \times 10^{10} \tag{8}$$

where V_b is the volume of the closed system (cm^3), T is the temperature (K), p_a is the pressure of the feed gas (cmHg), and dp_b/dt is the rate of change of the pressure in the permeate side with time (cmHg s^{-1}). The plot of the pressure in the permeate side along with time will give a straight-run and the slope is equal to dp_b/dt as given in Figure 7.

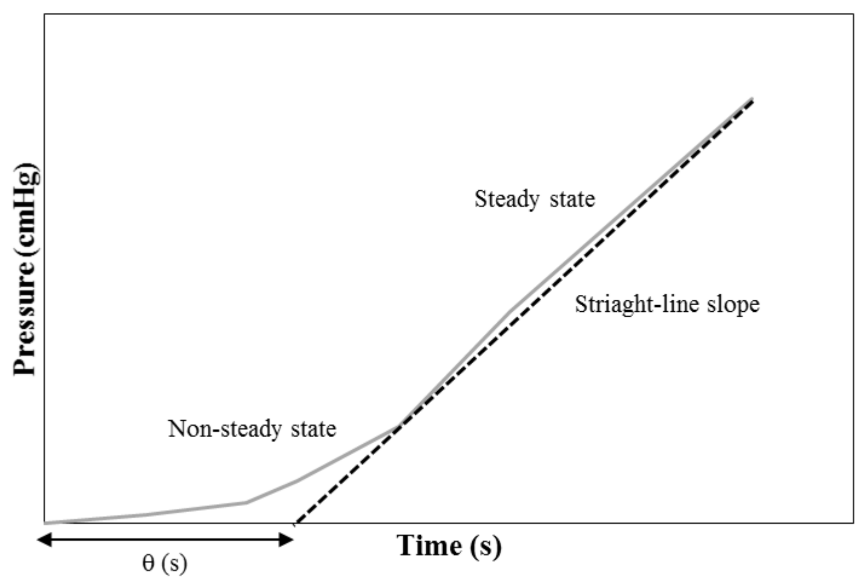

Figure 7. Plot of Pressure with Time in to Determine the Permeability and Diffusion and Solubility Coefficients [38]

For the first time of operation, it is expected to observe a non-steady-state line. After a certain time, a steady-state process is achieved and a straight slope line will be noticed which will be used to calculate dp_b/dt. The time-lag method is beneficial over the bubble and mass flowmeters for very low permeate flowrates. Furthermore, the time-lag technique can be used to determine the diffusivity (or diffusion coefficient, D) by the following correlation [16]:

$$D(\text{cm}^2\ \text{s}^{-1}) = \frac{l^2}{6\theta} \tag{9}$$

where l is the membrane thickness (cm) and θ is the time lag (s). The time lag is calculated based on the intercept of dp_b/dt line as shown in Figure 7. The solubility (K) can be then calculated from equation 1:

$$S[\mathrm{cm^3(STP)cm^{-3}cmHg^{-1}}] = \frac{P}{D} \quad (10)$$

where P is the permeability and D is the diffusion coefficient. The accuracy of the time-lag method can vary from 3 to 27% for permeability and diffusion/solubility coefficients [39]. Table 3 shows the advantages and limitations of bubble flowmeter, mass flowmeter, and the time-lag method for membrane permeability measurements.

Table 3. Comparison Between Different Techniques for Permeability Measurements in Membranes

Technique	Advantages	Limitations
Bubble Flowmeter	• Cost effective. • Good flowrate range.	• Requires a stopwatch. • Some gases can dissolve in the soap solution.
Mass Flowmeter	• Wide flowrate range. • Long-term experiments	• Use of a calibrated mass flowmeter for another gas may introduce error.
Time-lag	• Ability to measure very low flowrates. • Calculations of diffusion and solubility parameters.	• Not suitable for high flowrates. • Volume of the closed system should be accurately measured.

3. Selectivity Calculations

To study the membrane performance, the membrane should be tested with at least two gases. This is because the membrane defects (such as voids and cracks) may result in an increase in the membrane permeability as there will be no flow resistance. This can be reflected if the selectivity is very low or nearly 1. Usually, the permeability of gas *a* will be measured separately and then the permeability of gas *b* will be measured. Dividing the two permeabilities of gas *a* and *b* will give the ideal selectivity (α_{AB}):

$$\alpha_{AB} = \frac{P_A}{P_B} \quad (11)$$

where P_A is the permeability of gas a (the desired gas) and P_B is the permeability of gas b (the unwanted gas). Another way to calculate the selectivity is by introducing two or more gases at the same time. The user should define the gas mixture composition which is usually 50 vol% of gas a and 50 vol% of gas b. Because the permeate will have two or more gases, the produced gas should be analyzed to determine the composition so the flowrate of each gas can be calculated. This is necessary so that the permeability of each gas can be determined. Usually, a gas-chromatography (GC) is used for this purpose but other instruments such as mass spectrometers, infrared analyzers, and colorimetric tubes can be implemented as well. After determining the volume percentage (vol%) of each gas, the volume flowrate of each gas in the permeate can be quantified by:

$$(V_P)_A = V_P \times (\text{vol\%})_A \tag{12}$$
$$(V_P)_B = V_P \times (\text{vol\%})_B \tag{13}$$

where V_P is the volume flowrate of the total gas in the permeate, $(V_P)_A$ is the volume flowrate of the product gas a, and $(V_P)_B$ is volume flowrate of gas b. The real selectivity can be then calculated using equation 11. Industrially, real selectivity is a must as it gives the actual membrane performance. The real selectivity can significantly change when mixtures are introduced compared to the ideal selectivity. For example, a cellulose acetate membrane was used for carbon dioxide separation from methane and the ideal selectivity was greatly reduced from 35 to 15 when a gas mixture was used [40]. It was also found that the real selectivity is a function of the composition of the mixture gas. Therefore, the ideal selectivity should be only used for research purposes and the real selectivity should be measured using actual feeds. Table 4 shows that the real selectivity is always lower than the ideal selectivity. Generally, the real selectivity is reduced by 10 to 63% compared to the ideal selectivity.

Table 4. Reduction in the Selectivity of Polymeric Membranes Due to the Use of Mixed Feeds

Gas separation	Ideal selectivity	Real selectivity	Reference
H_2/N_2	281	250	[41]
H_2/CO_2	4.5	3.6	[42]
CO_2/CH_4	32−35	10−15	[40]
CO_2/N_2	38	35	[43]
Propylene/propane	31	18	[44]

4. Calculations of Gas Recovery and Product Purity

In literature, the membrane performance is described by permeability and selectivity and these parameters are advantageous in comparing the membrane with other reported data. Furthermore, permeability and selectivity are useful for membrane modeling and upscaling. However, to evaluate the membrane system with other gas-separation technologies such as amine scrubber and pressure swing adsorption (PSA), universal terms are preferred such as gas recovery and product purity. The following equation can be used then to calculate the gas recovery (R):

$$R(\%) = \frac{(V_P)_A}{(V_F)_A} \times 100 \tag{14}$$

where $(V_P)_A$ is the volume flowrate of gas a in the permeate and $(V_F)_A$ is the volume flowrate of the gas a in the feed. Normally, a commercial membrane is expected to have a recovery of 70 to 99%, depending on the separated gas [45]. For the product purity, mixed-gas experiments should be conducted and GC will determine the mol% of component a in the permeate. It should be noted that the gas recovery and product purity greatly depend on the operating conditions such as feed composition, feed flowrate, pressure, temperature, and membrane area.

Product purity of a binary system can be still estimated from the data of ideal selectivity [46]. Mole balance across the membrane is applied by the following equation (neglecting accumulation):

$$x_F n_F = y_P n_P + x_R n_R \tag{15}$$

where n is the number of moles, x_F is the mole fraction of component a in the feed, x_R is the mole fraction in the retentate, and y_P is the mole fraction in the product. Equation 15 can be rewritten as:

$$y_P n_P = x_F n_F - x_R n_R = QA(\overline{xP_F - yP_P}) \tag{16}$$

where Q is the permeance, A is the membrane area, and the last term is the trans-membrane pressure difference. P_F is the feed pressure while P_P is the permeate pressure. The trans-membrane pressure difference can be simplified to (assuming complete mixing, neglecting radial gradients, constant pressures, and no mass-transfer resistance):

$$(\overline{xP_F - yP_P}) \cong x_F P_F - y_p P_P \tag{17}$$

The flux of component a (J_A) can be calculated by combining equations 16 and 17:

$$J_A = Q_A(x_F P_F - y_p P_P) \tag{18}$$

where Q_A, x_F and y_P are properties of component *a*. For component *b*, the flux is:

$$J_B = Q_B\left[(1 - x_F)P_F - \left(1 - y_p\right)P_P\right] \tag{19}$$

The ratio of absolute pressures (R) is defined as:

$$R = \frac{P_P}{P_F} \tag{20}$$

Now, equations 18 and 19 can be rewritten as:

$$J_A = Q_A P_F(x_F - y_p R) \tag{21}$$
$$J_B = Q_B P_F\left[(1 - x_F) - \left(1 - y_p\right)R\right] \tag{22}$$

The mole fraction of component *a* in the permeate can be estimated by:

$$y_p = \frac{J_A}{J_A + J_B} = \frac{Q_A P_F(x_F - y_p R)}{Q_A P_F\left(x_F - y_p R\right) + Q_B P_F\left[(1 - x_F) - \left(1 - y_p\right)R\right]} \tag{23}$$

Use of ideal selectivity in equation 11 but in terms of permeances gives:

$$\alpha = \frac{Q_A}{Q_B} \tag{24}$$

Applying the previous equation in equation 23 leads to:

$$y_p = \frac{J_A}{J_A + J_B} = \frac{(x_F - y_p R)}{\left(x_F - y_p R\right) + \frac{\left[(1 - x_F) - \left(1 - y_p\right)R\right]}{\alpha}} \tag{25}$$

The above equation can be rearranged resulting in a quadratic equation:

$$(\alpha - 1)y_p^2 + \left[1 - \alpha - \frac{1}{R} - \frac{x_F(\alpha - 1)}{R}\right] y_p + \frac{\alpha x_F}{R} = 0 \tag{26}$$

$$a y_p^2 + b y_p + c = 0 \tag{27}$$

The solution for equation 27 is:

$$y_p = \frac{-b \pm \sqrt{b^2 - 4ac}}{2a} \tag{28}$$

So, to calculate the product purity for a binary system, the following data are needed: feed and permeate pressures, feed composition, and ideal selectivity value.

5. Conclusions

The membrane is an energy-efficient technology for gas separation. It requires minimum supervision and has a long operating life. The membrane performance is determined by measuring the gas permeability and selectivity. However, the data can change significantly based on the experimental setup. Permeability is defined as the product of solubility and diffusivity, and it can be calculated based on measuring the flowrate of the permeate. The user should define the operating conditions before performing the experiment, which generally are: feed flowrate of 0.1−1 $cm^3 s^{-1}$, temperature of 25−35°C, pressure of 3−10 bar, membrane effective area of 10−15 cm^2, and membrane thickness of 10 −300 μm. There are mainly three ways to measure the permeate flowrate: bubble flowmeter, mass flowmeter, and time-lag method. The bubble flowmeter provides a low-cost solution for flowrates ranging from 0.1 to 1000 $cm^3 s^{-1}$. The mass flowmeters are generally more accurate than the bubble flowmeters with a wider flow range. The time-lag method is useful for low flowrates, and it can be also used to determine the solubility and diffusion coefficients. The membrane should be tested for two or more gases to calculate the selectivity. If the gases were fed separately, this would give the ideal selectivity. However, for commercial applications, the mixed gas should be fed directly to the membrane and a gas chromatograph has to be used to determine the composition of the permeate. After that, the real selectivity can be stated. The real selectivity could vary significantly from the ideal selectivity, and this would seriously affect the membrane performance. To evaluate the membrane unit with other separation techniques, common terms are usually preferred such as gas recovery and product purity.

6. Funding

This research received no external funding.

7. Conflict of Interest

The authors declare no conflict of interest.

8. References

1. Baker R. Future directions of membrane gas separation technology. *Ind. Eng. Chem.*, 2002, 41, 1393-1411.
2. Henis J, Tripodi M. A novel approach to gas separations using composite hollow fiber membranes. *Sep. Sci. Technol.*, 1980, 15, 1059-1068.
3. Ismail A, Khulbe K, Matsuura T in Gas Separation Membranes: Polymeric and Inorganic, Springer International Publishing, US, 2015.
4. Ismail A, Matsuura T in Sustainable Membrane Technology for Energy, Water, and Environment, Wiley, 2012.
5. He X, Lie J, Sheridan E, Hägg M-B. CO_2 capture by hollow fibre carbon membranes: Experiments and process simulations. *Energy Procedia*, 2009, 1, 261-268.
6. Ball P. Scale-up and scale-down of membrane-based separation processes. *Membr. Technol.*, 2000, 2000, 10-13.
7. Wijmans J, Baker R. The solution-diffusion model: A review. *J. Membr. Sci.*, 1995, 107, 1-21.
8. Baker R in Membrane Technology and Applications, Wiley, 2012.
9. Lin L, Feng C, Lopez R, Coronell O. Identifying facile and accurate methods to measure the thickness of the active layers of thin-film composite membranes – A comparison of seven characterization techniques. *J. Membr. Sci.*, 2016, 498, 167-179.
10. Yang E, Goh K, Chuah C, Wang R, Bae T-H. Asymmetric mixed-matrix membranes incorporated with nitrogen-doped graphene nanosheets for highly selective gas separation. *J. Membr. Sci.*, 2020, 118293.
11. Marchese J, Pagliero C. Characterization of asymmetric polysulphone membranes for gas separation. *Gas Sep. Purif.*, 1991, 5, 215-221.
12. Matsuura T in Synthetic Membranes and Membrane Separation Processes, Taylor & Francis, 1993.
13. Scholes C, Chen G, Lu H, Kentish S. Crosslinked PEG and PEBAX membranes for concurrent permeation of water and carbon dioxide. *Membranes*, 2016, 6, 1.
14. Liu SL, Wang R, Liu Y, Chng M., Chung T. The physical and gas permeation properties of 6FDA-durene/2,6-diaminotoluene copolyimides. *Polymer*, 2001, 42, 8847-8855.
15. Basile A, Nunes S in Advanced Membrane Science and Technology for Sustainable Energy and Environ-

mental Applications, Elsevier Science, 2011.
16. Koolivand H, Sharif A, Kashani M, Karimi M, Salooki M, Semsarzadeh M. Functionalized graphene oxide/polyimide nanocomposites as highly CO_2-selective membranes. *J. Polym. Res.*, 2014, 21, 599.
17. Liu Y, Wang R, Chung T-S. Chemical cross-linking modification of polyimide membranes for gas separation. *J. Membr. Sci.*, 2001, 189, 231-239.
18. Calle M, Lozano A, de Abajo J, de la Campa J, Álvarez C. Design of gas separation membranes derived of rigid aromatic polyimides. 1. Polymers from diamines containing di-tert-butyl side groups. *J. Membr. Sci.*, 2010, 365, 145-153.
19. Espeso J, Lozano A, de la Campa J, de Abajo J. Effect of substituents on the permeation properties of polyamide membranes. *J. Membr. Sci.*, 2006, 280, 659-665.
20. David O, Gorri D, Nijmeijer K, Ortiz I, Urtiaga A. Hydrogen separation from multicomponent gas mixtures containing CO, N_2 and CO_2 using Matrimid® asymmetric hollow fiber membranes. *J. Membr. Sci.*, 2012, 419–420, 49-56.
21. Vaughn J, Koros W. Effect of the amide bond diamine structure on the CO_2, H_2S, and CH_4 transport properties of a series of novel 6FDA-based polyamide–imides for natural gas purification. *Macromolecules*, 45, 7036-7049, 2012.
22. Vaughn J, Koros W. Analysis of feed stream acid gas concentration effects on the transport properties and separation performance of polymeric membranes for natural gas sweetening: A comparison between a glassy and rubbery polymer. *J. Membr. Sci.*, 2014, 465, 107-116.
23. Ren X., Ren J, Deng M. Poly(amide-6-b-ethylene oxide) membranes for sour gas separation. *Sep. Purif. Technol.*, 2012, 89, 1-8.
24. Bernardo P, Drioli E, Golemme G. Membrane gas separation: A review/state of the art. *Ind. Eng. Chem. Res.*, 2009, 48, 4638-4663.
25. Flaconnèche B, Martin J, Klopffer M. Permeability, diffusion and solubility of gases in polyethylene, polyamide 11 and poly(vinylidene fluoride). *Oil Gas Sci. Technol.*, 2001, 261-278.
26. Scott K, Hughes R in Industrial Membrane Separation Technology, Springer Netherlands, 2012.
27. Lashkari S, Kruczek B. Development of a fully automated soap flowmeter for micro flow measurements. *Flow Meas. Instrum.*, 2008, 19, 397-403.
28. de Matos M, Rodrigues N. Gas mass-flow meters: Measurement and uncertainties. *Flow Meas. Instrum.*, 2013, 33, 45-54.
29. Levy A. The accuracy of the bubble meter method for gas flow measurements. *J. Sci. Instrum.*, 1964, 41, 449-453.
30. Nelson G in Gas Mixtures: Preparation and Control, CRC Press, 2018.
31. Bronkhorst. [last accessed 3/04/2022] https://www.bronkhorst.com/int/blog/good-to-know-thermal-mass-flow-sensor-bypass-versus-cta/
32. Flowmeters for system applications designer checklist: Flow meter designer checklist, Instrumentation Testing Association, 1999.
33. Sahshi G, Mahendra A, Gouthaman G. Understanding the compatibility

of thermal mass flow meter with various process gases. *J. Chem. Eng. Process Technol.*, 2012, S1, 1-7.
34. Bau H, DeRooij N, Kloeck B, Göpel W, Hesse J, Zemel J in Sensors, Mechanical Sensors, Wiley, 2008.
35. Lide D in Handbook of Chemistry and Physics, CRC Press, US, 2004.
36. Malagón-Romero D, Ladino A, Ortiz N, Green L. Characterization of a polymeric membrane for the separation of hydrogen in a mixture with CO_2. *Open Fuels Energy Sci. J.*, 2016, 9.
37. Wu H, Thibault J, Kruczek B. The validity of the time-lag method for the characterization of mixed-matrix membranes. *J. Membr. Sci.*, 2021, 618, 118715.
38. Ebadi A, Sanaeepur H, Kargari A, Moghadassi A. Direct determination of concentration-dependent diffusion coefficient in polymeric membranes based on the Frisch method. *Sep. Purif. Technol.*, 2011, 82, 102-113.
39. Ye X, Lv L, Zhao X, Wang K. Permeation time lag in polymeric hollow fiber membranes. *J. Membr. Sci.*, 2006, 283, 425-429.
40. Baker R, Low B. Gas separation membrane materials: A perspective. *Macromolecules*, 2014, 47, 6999-7013.
41. Yáñez M, Ortiz A, Gorri D, Ortiz I. Comparative performance of commercial polymeric membranes in the recovery of industrial hydrogen waste gas streams. *Int. J. Hydrogen Energy*, 2020.
42. Pesiri D, Jorgensen B, Dye R. Thermal optimization of polybenzimidazole meniscus membranes for the separation of hydrogen, methane, and carbon dioxide. *J. Membr. Sci.*, 2003, 218, 11-18.
43. Xin Q, Ma F, Zhang L, Wang S, Li Y, Ye H, Ding X, Lin L, Zhang Y, Cao X. Interface engineering of mixed matrix membrane via CO_2-philic polymer brush functionalized graphene oxide nanosheets for efficient gas separation. *J. Membr. Sci.*, 2019, 586, 23-33.
44. Zhang C, Dai Y, Johnson J, Karvan O, Koros W. High performance ZIF-8/6FDA-DAM mixed matrix membrane for propylene/propane separations. *J. Membr. Sci.*, 2012, 389, 34-42.
45. Alqaheem Y, Alomair A, Vinoba M, Pérez A. Polymeric gas-separation membranes for petroleum refining. *Int. J. Polym. Sci.*, 2017, 1-19.
46. McCabe W, Smith J, Harriott P in Unit Operations of Chemical Engineering, McGraw-Hill Education, 2005.

The Chemist
Journal of the American Institute of Chemists

Statistical Analysis Using Factorial Design Experiments for Developing Cellulose Acetate (CA) Hollow-fine-fibre Membranes

Akram Tawari [a,*], Bashir Brika [b]

[a] *Department of Process Engineering, Faculty of Engineering, Stellenbosch University Stellenbosch, South Africa*
(E-mail: tawari@live.com)

[b] *Libyan Advanced Center of Chemical Analysis, Libyan Authority for Scientific Research Tripoli, Libya*
(Tel. +218925411305; E-mail: bashirforlibya@gmail.com)

*Corresponding author

Abstract: Statistical analysis was used to generate a fabrication formulation for producing cellulose acetate hollow-fine-fibre membranes for brackish water desalination with improved salt retention and flux. A three-level three-factor factorial was used to the study of the effect of spinning parameters (solvent to non-solvent ratio, bore fluid ratio and air gap distance). A regression equation was successfully established and was used to predictably produce membranes with good performance within the limits of the factors studied. RO performance of these hollow-fine-fibre membranes was good: the salt retention ranged from 96 to 98% and the permeate flux ranged from 60 to 64 L/m^2.d.

Key Words: Hollow-fine fibre membrane, cellulose acetate, factorial design experiment, analysis of variance

1. Introduction

The development of hollow-fibre membranes during the 1970s helped reverse osmosis (RO) technology advance even further. Since the early development of RO membranes for sea water desalination, hollow-fibre membranes have been crucial to membrane separation technology. This is mainly because of their large surface area, which typically exceeds other membrane module configurations (104 m^2/m^3 per unit volume). They are also independent (there is no need for supporting material). To be able to endure high operating pressure for RO applications without collapsing, hollow-fibre membranes for RO desalination are typically of tiny fibre size in the range of 50 - 300 µm outer diameter [1].

The fibers are typically referred to as hollow-fine-fibers when their diameter falls between 50 and 500 µm. They can tolerate intense feed pressure (20 bar or higher) applied from the outside [2]. They are suitable for RO or high-pressure gas separation due to this characteristic. Hollow-fibers are frequently utilized for microfiltration (MF) or ultrafiltration (UF), which do not require significant operating pressure [3].

For the preparation of hollow-fiber membranes, the dry-wet spinning method is frequently used. This spinning process can be employed to obtain almost every known membrane morphology by controlling the phase separation processes that take place.

According to Tawari and Brika, 2018, three spinning parameters including solvent/non-solvent ratio, bore fluid composition and air gap distane may have an effect on the fibre morphology [1]. In order to investigate the effects of the spinning parameters (factors) on the fabrication process, factorial design was performed. Factorial design and the associated analysis of variance are useful tools to characterize processes which are influenced by a number of factors. The methods allow the determination of statistically important factors and enable the experimenter to study the joint effect of the factors on the response [4]. In this way, a regression model for each of the measured can be generated. In this study, a 3^3–factorial design [3] is used to identify which factors and their interactions have the most important effect of the performance of CA hollow-fine-fibre membrane for brackish water desalination.

2. Experimental Design

Based on literature and preliminary results obtained in previous work of the authors [1], three important factors which affect the fabrication process were considered: solvent/non-solvent ratio, air gap distance and bore fluid composition. Each factor will be studied at three levels, and a 3^3 full factorial design was selected to achieve this goal because it consists of all possible combinations of the levels for all factors. It is also useful for investigating quadratic effects, which is not possible with 2 level design. The responses of interest are (flux) and (retention). The list of factors and their chosen levels for the experiment are shown in Table 1. The hollow-fine-fibre membrane performance was determined using an applied pressure of 20 bar and a feed solution of 2,000 ppm (NaCl).

Table 1. Factors and Levels for 3^3 Levels Factorial Design

Label	Factors	Low level -1	Mid level 0	High level 1
A	Solvent/Non-solvent mass ratio (m/m)	0.847	1.147	1.447
B	Air gap distance (mm)	40	80	120
C	Bore fluid ratio Acetone/water (m/m)	50% acetone 50% water (1)	60% acetone 40% water (1.5)	70% acetone 30% water (2.3)

Each trial was replicated twice since replication permits more degrees of freedom in the estimation of error variance and provides the means to determine variability between treatments and that due to random variation. The Design-Expert Software 7.1 was used to analyze the experimental data. The experimental results of the 3^3–factorial design are shown in standard order in Table 2.

Table 2. Design Data of the Experiments and Their Replication with Response Values

	Factor 1	Factor 2	Factor 3	Response 1	Response 2
Trials	A: Solvent/Non-solvent ratio (m/m)	B: Air gap distance (mm)	C: Bore fluid ratio (m/m)	Salt retention (%)	Flux ($L/m^2.d$)
1	0	0	0	97.5	62.4
2	0	0	1	94.5	50
3	0	-1	-1	96.3	53.4
4	0	0	1	94.0	49.0
5	1	0	-1	95.0	51.2
6	-1	1	-1	95.8	55.6
7	-1	1	-1	96.3	53.4
8	-1	1	0	97.0	62.3
9	0	1	1	95.0	53.0
10	-1	0	-1	96.4	50.2
11	1	-1	1	92.4	41
12	1	1	-1	95.4	53.5
13	-1	0	0	96.7	58.0
14	1	-1	1	93.4	42.0
15	1	1	0	96.7	55.6
16	1	1	-1	95.3	55.7
17	0	-1	-1	97.5	55.7
18	-1	-1	-1	95.7	49.4
19	1	1	1	94.5	45
20	1	-1	0	96.0	53.4
21	0	1	0	98.5	64.6
22	0	1	-1	97.6	55.7
23	1	1	0	96.0	60.0
24	1	-1	-1	95.6	51.2
25	1	0	1	94.2	42.4
26	-1	0	0	96.7	55.6
27	-1	1	1	94.0	48.0
28	1	0	0	96.0	53.4
29	0	-1	1	94.4	48.0
30	0	0	-1	97.2	58.0
31	-1	-1	0	96.6	60.0
32	1	1	1	95.0	43.6
33	0	1	-1	97.5	58.0
34	1	0	-1	94.9	51.2
35	0	0	-1	96.8	51.2
36	0	1	1	94.7	52.3
37	1	-1	-1	96.0	49.0
38	-1	-1	1	94.0	44.0
39	0	-1	0	97.4	61.5
40	1	0	0	95.8	53.4
41	0	1	0	97.6	62.3
42	1	-1	0	95.2	53.0
43	-1	0	1	94.0	47.0
44	-1	-1	0	96.3	51.2
45	-1	0	1	93.7	47.0
46	0	-1	1	94.0	49.0
47	-1	0	-1	96.3	49.3
48	-1	-1	-1	96.4	48.7
49	0	-1	0	96.8	59.3
50	0	0	0	97.2	60.0
51	-1	-1	1	92.0	42.0
52	1	0	1	93.5	44.0
53	-1	1	0	97.2	57.0
54	-1	1	1	94.8	50.0

3. Results and Discussion

The salt retention and permeate flux responses for each experimental trial are shown in Table 2. These results were statistically analyzed using analysis of variance (ANOVA) to study the joint effect of each factor and their interactions on the membrane performance (retention and flux).

Analysis of Variance (ANOVA)

This method was first developed by Fisher in 1930 [5]. ANOVA is a statistical method used to evaluate which of the factors studied significantly affects the responses over the range studied [6]. The relative importance of each factor and factor-factor interaction can be ranked in terms of their effect on the process output. Thus, the information about how significant the effect of each factor on the experimental results can be concluded from ANOVA. Tables 3 and 4 summarize the ANOVA of the three factors studied.

Table 3. Analysis of Variance of the Regression Model for Retention

Source	Sum of squares	df	Mean square	*F-Value*	Prob > F	
Model	98.44	9	10.94	51.34	< 0.0001	significant
A	1.93	1	1.93	9.04	0.0044	significant
B	4.97	1	4.97	23.32	< 0.0001	significant
C	44.22	1	44.22	207.55	< 0.0001	significant
AB	0.00	1	0.0017	0.0078	0.9299	not significant
AC	1.29	1	1.29	6.06	0.0178	significant
BC	2.21	1	2.21	10.39	0.0024	significant
A^2	13.09	1	13.09	61.44	< 0.0001	significant
B^2	0.13	1	0.13	0.63	0.4325	not significant
C^2	21.39	1	21.39	100.41	< 0.0001	significant
Residual	9.37	44	0.21			
Lack of fit	3.56	17	0.21	0.97	0.51	not significant
Pure error	5.81	27	0.22			
Correct Total	107.81	53				
Standard deviation	0.46		R-squared R^2	0.91		
Mean	95.65		Adjusted R-squared	0.90		
Coefficient of variation C. V. %	0.48		Predicted R-squared	0.86		
PRESS	15.18		Adequate precision	23.88		

Table 4. Analysis of Variance of the Regression Model for Flux

Source	Sum of squares	df	Mean square	*F-value*	Prob > F	
Model	1732.21	9	192.47	49.13	< 0.0001	significant
A	29.66	1	29.66	7.57	0.0086	significant
B	138.98	1	138.98	35.47	< 0.0001	significant
C	355.32	1	355.32	90.69	< 0.0001	significant
AB	2.16	1	2.16	0.55	0.4617	not significant
AC	23.55	1	23.55	6.01	0.0183	significant
BC	0.19	1	0.19	0.05	0.828	not significant
A^2	318.61	1	318.61	81.32	< 0.0001	significant
B^2	10.58	1	10.58	2.70	0.1075	not significant
C^2	704.12	1	704.12	179.72	< 0.0001	significant
Residual	172.39	44	3.92			
Lack of fit	43.61	17	2.57	0.54	0. 9074	not significant
Pure error	128.78	27	4.77			
Correct total	1904.60	53				
Standard deviation	1.98		R-squared R^2	0.91		
Mean	52.48		Adjusted R-squared	0.89		
Coefficient of variation C. V. %	3.77		Predicted R-squared	0.87		
PRESS	251.84		Adequate precision	26.24		

Checking the Adequacy of Both Regression Models

In Tables 3, 4, the "Model F-values" are calculated from a model mean square divided by residual mean square; the residuals are defined as the differences between the experimental data and the predicted values for each point in the design. The Model F-value is the test for comparing model variance with residual (error) variance. If the variances are close to the same, the ratio will be close to one and it is less likely that any of the factors have a significant effect on the response. Similarly, an "F-value" for any individual factor terms is calculated from a term mean square divided by a residual mean square. It is a test that compares a term variance with a residual variance. If the variances are close to the same, the ratio will be close to one and it is less likely that the term has a significant effect on the response. In Table 3, a "Model F-values" of 51.34 with a "Model F-values" 49.13 in Table 4 imply that the selected models are significant and there is only a 0.01% chance that a "Model F-values" this large could occur due to noise. Prob > F represents the probability of seeing the observed F value if the null hypothesis is true (there is no factor effect). Small probability values call for a rejection of the null hypothesis. The probability equals the proportion of the area under the curve of the

F-distribution (with 9 and 27 degree of freedom) that lies beyond the observed F-value. Furthermore, the P-value is the probability that the test statistic will take on a value that is at least as extreme as the observed value of the statistic when the null hypothesis is true. Thus, a P-value conveys much information about the weight of evidence against null hypothesis, and so a decision maker can draw a conclusion at any specified level of significance. More formally, we define the P-value as the smallest level of significance that would lead to the rejection of the null hypothesis [7,8]. In other words, if the Prob > F value is very small (less than 0.05), then the terms in the model have a significant effect on the response, providing at least 95% confidence for results. If the Prob > F value is greater than 0.1 then this is an indication that the model terms are not significant. The "lack-of-fit F-values" for both models implies that the lack of fit is not significantly related to pure error. These values of lack of fit are desirable as we want to know how well the models fit the experimental data.

"R-squared", or more formally the coefficient of multiple determination, is defined as the sum of squares for the model divided by the total corrected sum of squares and indicates the proportion of the variability in the data explained by the analysis of variance model [9]. The R^2 values of models were calculated to be 0.91 in both instances, indicating that only 9% of the total variation was not explained. Thus, the models were able to explain about 91% of the variability in salt retention and permeate flux data. The closer the value of R^2 is to unity, the better is the correlation between the observed and predicted values [10]. In this study, the predicted R^2 of 0.86 and 0.87 are in reasonable agreement with the adjusted R-squared of 0.90 and 0.89 of both models. Adequate precision measures the signal to noise ratio. A ratio greater than 4 is desirable. Adequate precisions of 23.88 and 26.24 for both models indicate adequate model discrimination [4]. The coefficient of variation (CV) for the retention and flux were calculated to be 0.48 and 3.77%. The CV, the ratio of the standard error of estimate to the mean value of the observed response (as a percentage), is a measure of reproducibility of the model and, as a general rule, a model can be considered reasonably reproducible if its CV is not greater than 10% [11,12]. The predicted sum of squares (PRESS), which is a measure of how a particular model fits each point in the design, was 15.18 and 251.84. According to Table 3, the main factors of A, B, C, the interaction of AC, BC, and the second orders of A2, C2 are significant model terms. In Table 4, the main factors of A, B, C, the interaction of AC and the second orders of A2, C2 are significant model terms. The other factors are less significant but cannot be neglected due to their little influence on responses as well.

The results of each of these overall responses are included in the analysis procedure and an equation that describes the influence of the factors on the overall responses was found. The following equations are the final regression models in terms of the actual and coded factors. Table 5 tabulates the differences between the actual and predicted response values according to the equations.

$$\text{Salt retention (coded)} = 97.16 - 0.23 \times A + 0.37 \times B - 1.11 \times C + 0.00838 \times A \times B + 0.23 \times A \times C + 0.30 \times B \times C - 1.04 \times A2 + 0.11 \times B2 - 1.42 \times C2 \quad (1)$$

$$\text{Flux (coded)} = +\, 60.63 - 0.91 \times A + 1.97 \times B - 3.14 \times C - 0.30 \times A \times B - 0.98 \times A \times C + 0.088 \times B \times C - 5.15 \times A2 + 0.94 \times B2 - 8.16 \times C2 \quad (2)$$

Table 5. Comparison of the Actual and Predicted Responses of Retention and Flux

Trials	Actual retention	Predicted retention	Residual	Actual flux	Predicted flux	Residual
1	97.5	97.1	0.34	62.4	60.6	1.77
2	94.5	94.6	-0.13	50.0	49.3	0.67
3	96.3	96.8	-0.58	53.4	54.6	-1.26
4	94.0	94.6	-0.63	49.0	49.3	-0.33
5	95.0	95.3	-0.34	51.2	49.5	1.66
6	95.8	96.4	-0.64	55.6	55.4	0.13
7	96.3	96.4	-0.14	53.4	55.4	-2.07
8	97.0	96.8	0.18	62.3	60.5	1.72
9	95.0	95.4	-0.41	53.0	52.3	0.67
10	96.4	96.2	0.13	50.2	51.3	-1.17
11	92.4	93.0	-0.61	41.0	43.4	-2.42
12	95.4	95.5	-0.13	53.5	51.0	2.41
13	96.7	96.3	0.35	58.0	56.3	1.61
14	93.4	93.0	0.39	42.0	43.4	-1.42
15	96.7	96.3	0.33	55.6	56.2	-0.60
16	95.3	95.5	-0.23	55.7	51.0	4.61
17	97.5	96.8	0.62	55.7	54.6	1.04
18	95.7	96.3	-0.61	49.4	49.1	0.26
19	94.5	94.3	0.13	45.0	44.9	0.02
20	96.0	95.6	0.39	53.4	54.8	-1.41
21	98.2	97.6	0.86	64.6	63.5	1.06
22	97.6	97.0	0.57	55.7	58.4	-2.73
23	96.0	96.3	-0.37	60.0	56.2	3.80
24	95.6	95.3	0.23	51.2	49.8	1.32
25	94.2	93.5	0.62	42.4	43.2	-0.86
26	96.7	96.3	0.35	55.6	56.3	-0.79
27	94.0	94.3	-0.36	48.0	49.3	-1.37
28	96.0	95.8	0.11	53.4	54.5	-1.17
29	94.4	94.0	0.34	48.0	48.2	-0.20
30	97.2	96.8	0.35	58.0	55.6	2.39
31	96.6	96.0	0.51	60.0	54.0	5.93
32	95.0	94.3	0.63	43.6	44.9	-1.38
33	97.5	97.0	0.47	58.0	58.4	-0.43
34	94.9	95.3	-0.44	51.2	49.5	1.66
35	96.8	96.8	-0.05	51.2	55.6	-4.41
36	94.7	95.4	-0.71	52.3	52.3	-0.03
37	96.0	95.3	0.63	49.0	49.8	-0.88
38	94.0	93.0	0.97	44.0	42.8	1.32
39	97.4	96.8	0.51	61.5	59.6	1.90
40	95.8	95.8	-0.09	53.4	54.5	-1.17
41	97.6	97.6	-0.04	62.3	63.5	-1.24
42	95.2	95.6	-0.41	53.0	54.8	-1.81
43	94.0	93.5	0.41	47.0	45.0	1.92
44	96.3	96.0	0.21	51.2	54.0	-2.87
45	93.7	93.5	0.11	47.0	45.0	1.92
46	94	94.0	-0.06	49.0	48.2	0.80
47	96.3	96.2	0.03	49.3	51.3	-2.07
48	96.4	96.3	0.09	48.7	49.1	-0.44
49	96.8	96.8	-0.09	59.3	59.6	-0.30
50	97.2	97.1	0.04	60.0	60.6	-0.63
51	92.0	93.0	-1.03	42.0	42.8	-0.68
52	93.5	93.5	-0.08	44.0	43.2	0.74
53	97.2	96.8	0.38	57.0	60.5	-3.58
54	94.8	94.3	0.44	50.0	49.3	0.63

In order to check data for normality, even when there is fairly small number of observations, it is best to construct normal probability plots of the residuals. Here "residual" means the difference in the observed values (obtained from the experiments) and the predicted value or fitted values. The normal probability plot shows the residuals plotted against a cumulative normal percentile derived from the normal probability distribution for the ranking location of the residuals. This provides a visual method to illustrate if the residuals are actually normally distributed. If the residuals fall approximately along a straight line, the residuals are then normally distributed. In contrast, if the residuals do not fall fairly close to a straight line, the residuals are then not normally distributed and hence the data do not come from a normal population. In Table 5, the residuals are ranked in ascending order from the lowest to highest in order to plot the normal probability plot and their cumulative probability points are calculated Pk= (K – 0.5)/n, where K is the sequence number from 1 to n and n is the number of entries in the list.

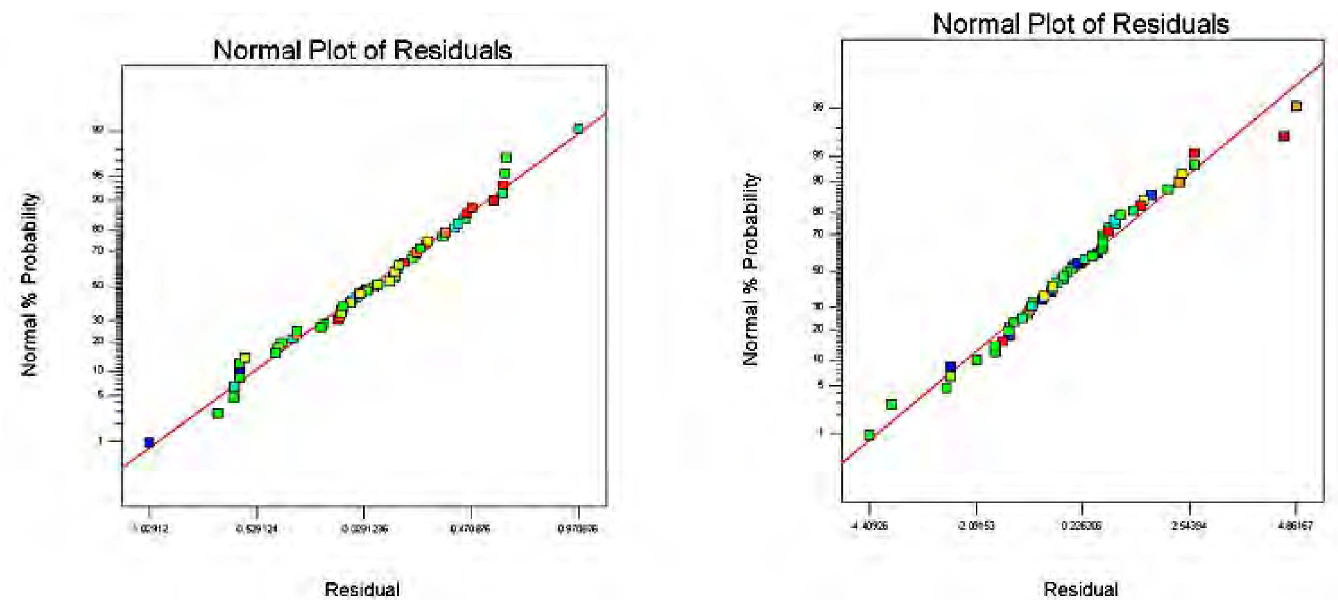

Figure 1. Normal Plot of Residuals for Retention (left) and Flux (right)

Figure 1 shows the normal probability plots of the residuals. There is no indication of nonnormality, nor is there any evidence pointing to possible outliers. It can be concluded that the normal distribution provides an excellent model for the data.

The next residual plot which we examine was the plot of residuals versus the predicted values in Figure 2. The plot of the residuals versus the ascending predicted response values indicated that there is no expanding variance phenomenon.

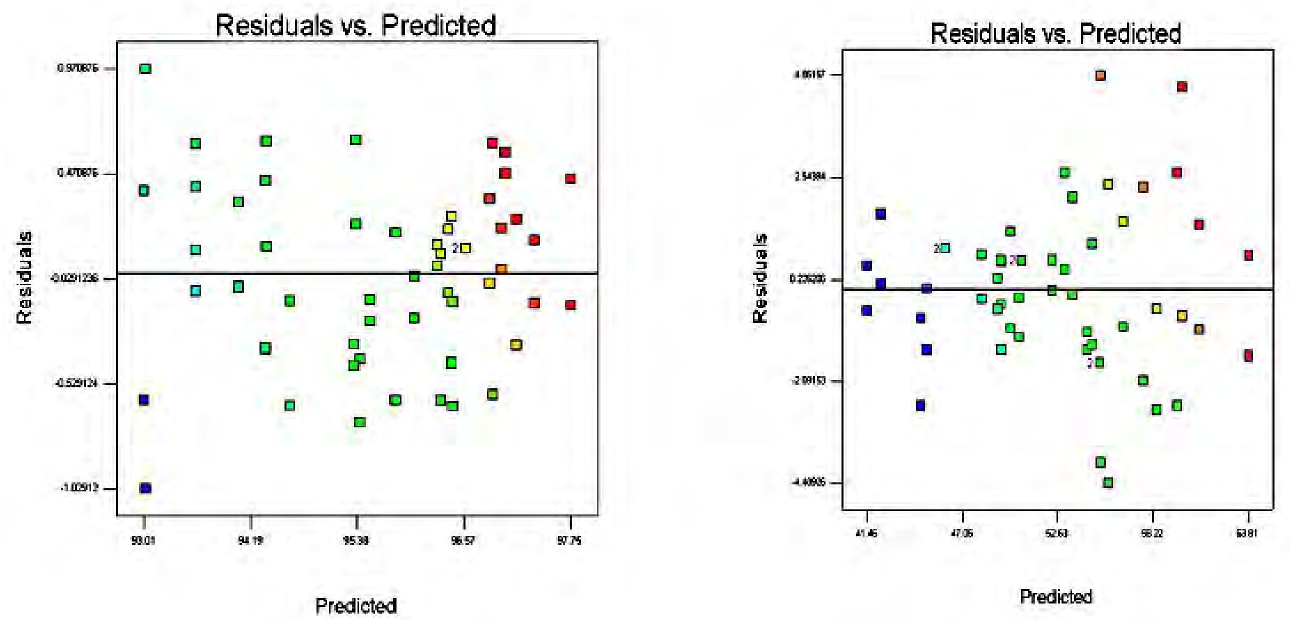

Figure 2. Plots of Residuals Verses Predicted Response Values for Retention (right) and Flux (left)

The residual values seem to be randomly scattered above and below zero over the range of the data and do not indicate any problems with the model. The reference line at 0 emphasizes that the residuals are split about 50-50 between positive and negative. There are no systematic patterns or unusual structures apparent in this plot. Plots in which the residuals do not exhibit any systematic structure indicate that the model fits the data well. In contrast, plots of the residuals that exhibit systematic structure indicate that the form of the function can be improved in some way [1]. Therefore, Figure 2 indicates that the model fits and there is no reason to suspect any violation of the independence or constant variance assumption.

Effect of Factors and Interactions on the Performance of CA Hollow-fine-fibre Membranes

The 3D response surface plots described by the regression models and these graphs were drawn to illustrate the effect of the independent factors and the interaction effects on the response variables. These graphs, in accordance with the regression model fitted, imply that the interaction between the two factors were significant. Figures 3 and 4 depict the effect of solvent/non-solvent and bore fluid ratio on both membrane retention and flux.

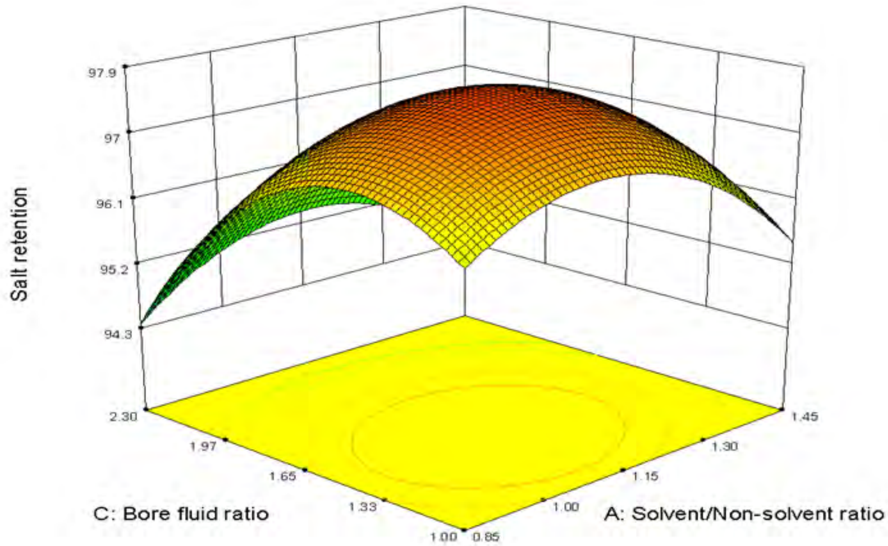

Figure 3. Effect of Solvent/Non-solvent and Bore Fluid Ratio on Salt Retention

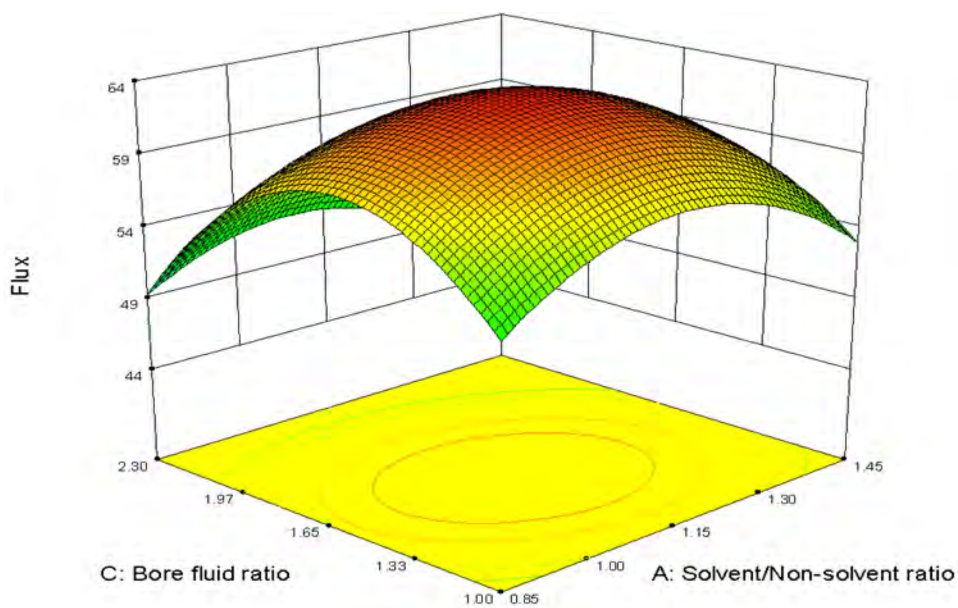

Figure 4. Effect of Solvent/Non-solvent and Bore Fluid Ratio on Water Flux

The retention and flux, obtained from earlier experiments, support the findings from the analysis of variance, which shows that solvent/non-solvent and bore fluid ratio are important factors that affect the membrane performance. The retention and flux plots show an improvement in salt retention and water flux as the solvent/non-solvent ratio in the solution was decreased from 1.447 to 1.147 (factor A) while decreasing the solvent concentration (factor c) in the bore fluid. The decrease in solvent/non-solvent ratio will result in a high formamide ratio in the spinning solution, which will shift the composition path of the spinning solution in the direction of the liquid-liquid demixing gap and as a result, a porous membrane will be produced. The decrease of acetone in the bore fluid from 70 to 60 and 50% (m/m) will improve the flux and retention of the produced hollow-fine fibres. High solvent concentration in the bore fluid and dope solution produced a very thick dense layer when the extruded fibres undergo rapid phase separation from both sides. The formation of an impermeable skin is due to the high gelation of supersaturated top layer of the spinning solution. Lowering the solvent concentration by increasing the non-solvent content in both bore fluid and the spinning solution will slow down and control the two different processes of gelation and the phase separation process and hence, more porous hollow-fine fibres could be produced with improved flux and retention.

Figures 5 and 6 illustrate the interaction plot between solvent/non-solvent ratio and air gap distance on both retention and flux.

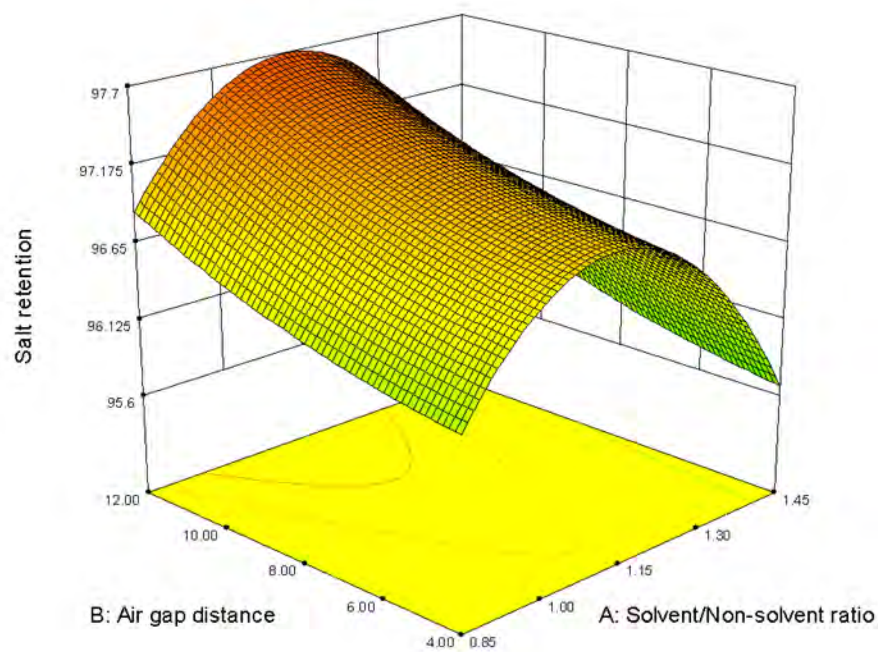

Figure 5. Response Surface Plot of the Effects of Solvent/Non-solvent Ratio and Air Gap Distance on Salt Retention of CA Hollow-fine-fibre Membranes

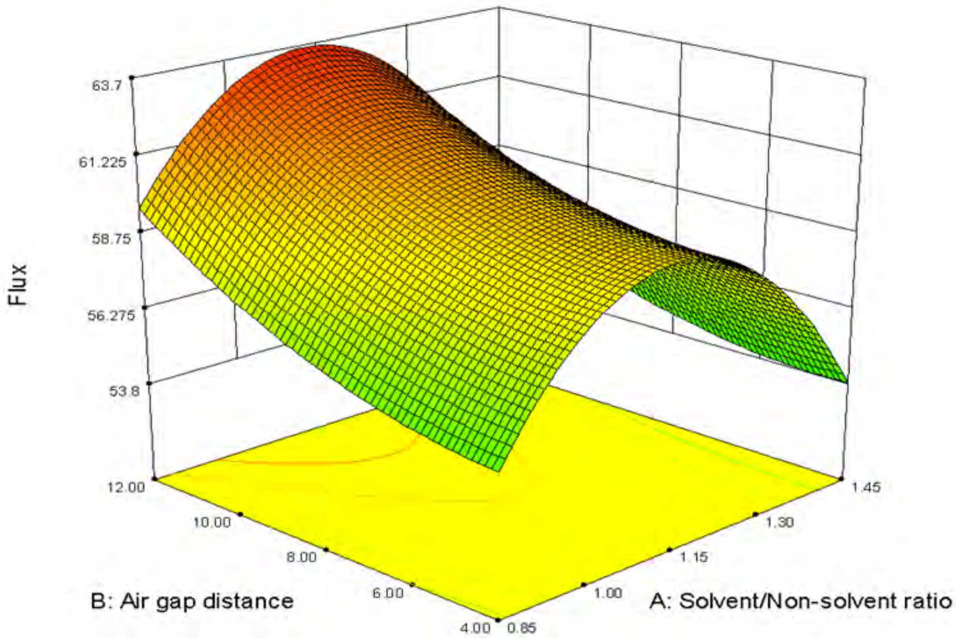

Figure 6. Response Surface Plot of the Effects of Solvent/Non-solvent Ratio and Air Gap Distance on Water Flux of CA Hollow-fine-fibre Membranes

It is clear that both flux and retention were increased with decreasing the solvent/non-solvent ratio and increasing the air gap distance to 120 mm. It was stated that the air gap is responsible for the formation of a thin skin on the outside of the fibre and the bulk of membrane structure is formed in the coagulation bath. Then increasing the non-solvent content in the spinning solution with 12 cm air gap distance will produce very thin skin layer with more pores in it. As the composition bath of the spinning solution will become close to the liquid-liquid demixing state with high non-solvent content, the spinodal outer layer should result in a microporous skin layer. Fibres spun with different air gap distances experience elongational stress with higher take-up speeds that induce molecular orientation and cause polymer molecules to pack more closely to one another. For a small air gap distance 4 cm, there was too little time for orientation and with a high take-up speed leading to a much tighter structure resulted. With an air gap of 12 cm the orientation will have small relaxation time before entering the gelation bath, leading to a less dense outer skin and subsequently high flux and retention.

Figure 7 and 8 illustrate the interaction plot between the air gap distances and bore fluid ratio on both retention and flux.

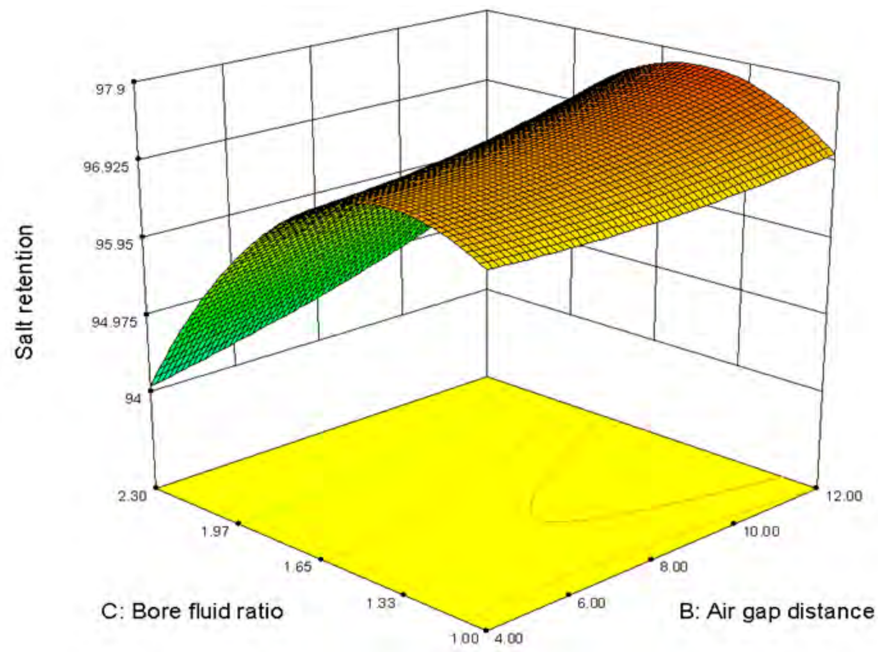

Figure 7. Response Surface Plot of the Effects of Air Gap Distance and Bore Fluid Ratio on Salt Retention of CA Hollow-fine-fibre Membranes

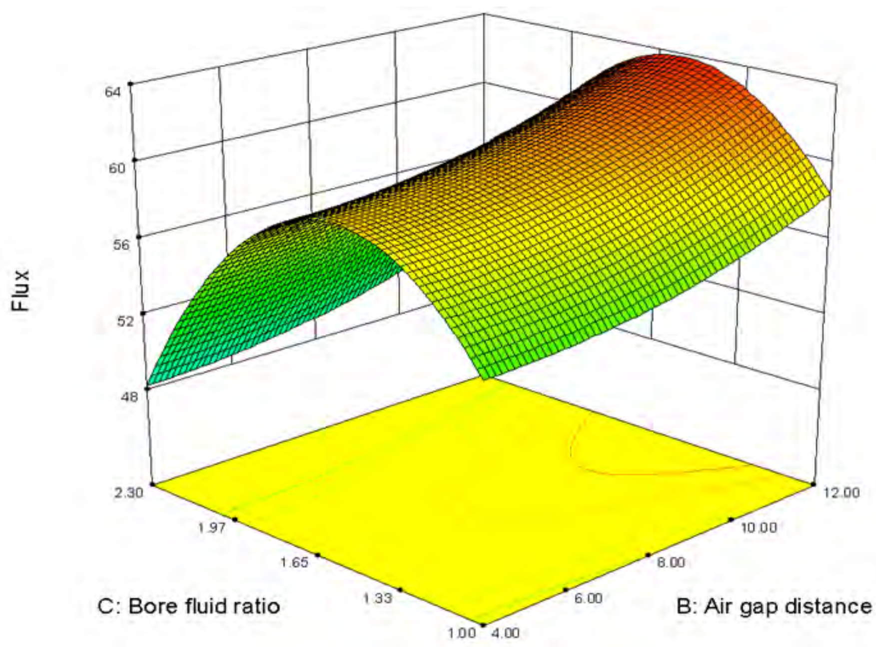

Figure 8. Response Surface Plot of the Effects of Air Gap Distance and Bore Fluid Ratio on Flux of CA Hollow-fine-fibre Membranes

It can be seen the bore fluid ratio had a large effect on flux. This can be explained that higher air gap distance results in enough time for the mass transfer at the inner surface, which means enough time for bore liquid/solvent exchange. As a result, an open porous structure will be formed on the inner surface leading to an increase in the flux.

4. Model validation

In order to verify the adequacy of the model developed, three confirmation experiments were conducted within the range of the levels studied. Each of the experiments was repeated three times from different dope solutions and the average was taken for the retention and flux of each experiment. For each of the confirmations, the responses were determined experimentally and calculated by using the regression equation. The results of these validation experiments and the model predicted values are shown in Table 6.

Table 6. Confirmation Runs with Their Responses

Solvent/Non-solvent (m/m)	Air gap distance mm	Bore fluid ratio (m/m)	Retention %	Flux L/m^2.d
1	60	1.2	97.92	60.14
1	60	1.2	97.68	62.36
1	60	1.2	97.43	59.52
1.147	80	1.5	98.04	60.14
1.147	80	1.5	97.80	64.59
1.147	80	1.5	98.17	62.36
1.302	100	1.8	97.56	55.68
1.302	100	1.8	97.07	55.68
1.302	100	1.8	96.82	57.91

Test conditions: (2,000 ppm NaCl and 20 bar)

The average values are shown in Table 7 for each set together with their predicted values calculated from the regression model. The results showed that our regression model yields reasonable results for the flux and retention with small residual between predicted and actual data. Therefore, our regression equation can be expected to apply in the preparation of CA hollow-fine-fibre membranes with better performance.

Table 7. Actual and Predicted Responses of Retention and Flux for the Confirmation Runs

Solvent/Non-solvent ratio %(m/m)	Air gap distance m/m	Bore fluid ratio %(m/m)	Actual retention %	Predicted retention %	Residual	Actual flux L/m^2.d	Predicted flux L/m^2.d	Residual
1	6	1.2	97.68 ± 0.25	97.15	0.66	60.67 ± 1.49	57.23	3.44
1.147	8	1.5	98.00 ± 0.19	97.34	0.53	62.36 ± 2.23	60.92	1.44
1.302	10	1.8	97.15 ± 0.38	96.56	0.58	56.42 ± 1.29	57.95	-1.52

5. Conclusions

In this study, the ability of a factorial design to perform a comparative investigation of the importance of individual factors and their interactions on the membrane performance was demonstrated. It was concluded in this statistical analysis that the solvent/non-solvent ratio, bore fluid ratio, air gap distance and the interaction between solvent/non-solvent and bore fluid, air gap distance, and bore fluid ratio had a significant influence on both the flux and retention of CA hollow-fine-fibre membranes for brackish water desalination. According to 3^3 factorial designs, the regression analysis showed a goodness of fit to the experimental data. Therefore, the model was considered adequate for the prediction of good membrane performance (salt retention in the range of 96 – 98% and permeate flux in the range of 60 – 64 L/m^2.d.

6. References

1. Tawari A, Brika B, Bradshaw SM, Jacobs EP. Development of a cellulose acetate hollow-fine-fibre membrane. *Acta Chem. Malays.*, 2018, 2(2), 15-30.
2. Tawari A, Brika B. Hollow-fine-fibre membranes: Collapse pressure and pressure drop analysis. *The Chemist*, 2020, 2(1), 1-17.
3. Riley RL in Membrane Separation Systems, eds. RW Baker, EL Cussler, W Eykamp, WJ Koros, RL Riley, H Strathmann, Noyes Data Corporation, New Jersey, 1991.
4. Montgomery DC in Design and Analysis of Experiment, John Wiley & Sons, New York, 1997.
5. Fisher F in The Design of Experiments, Hafner, New York, 1971.
6. Saisana M in Analysis of Variance, ed. AC Michalos, Encyclopedia of Quality of Life and Well-Being Research. Springer, Dordrecht, 2014. https://doi.org/10.1007/978-94-007-0753-5_83.
7. Thomas PR in Modern Engineering Statistics, John Wiley & Sons, New Jersey, 2007.
8. Ferreira JC, Patino CM. What does the p value really mean? *J. Bras. Pneumol*, 2015, 41(5), 485. doi: 10.1590/S1806-37132015000000215. PMID: 26578145; PMCID: PMC4635100.
9. Figueiredo Filho DB, Silva Júnior JA, Rocha EC. What is R2 all about? *Leviathan (São Paulo)*, 2011, 3, 60. https://doi.org/10.11606/issn.2237-4485.lev.2011.132282
10. Khuri AI, Cornell JA in Response Surfaces: Design and Analyses, Marcel Dekker, Inc., New York, 1987.
11. Beg Q, Sahai V Gupta R. Statistical media optimization and alkaline protease production from *Bacillus mojavensis* in bioreactor. *Process Biochem.*, 2003, 39, 203.
12. Masoumi HR, Kassim A, Basri M, Abdullah DK. Determining optimum conditions for lipase-catalyzed synthesis of triethanolamine (TEA)-based esterquat cationic surfactant by a Taguchi robust design method. *Molecules*, 2011, 16(6), 4672-4680. doi: 10.3390/molecules16064672. PMID: 21642941; PMCID: PMC6264298.

The Chemist
Journal of the American Institute of Chemists

Zinc and Copper Complexes of 4-Methylbenzoic Acid and 2-Methylimidazole: Synthesis, Characterization, Antimicrobial and Molecular Docking Studies

Hassan K. Busari[1,4]*, Luqmon A. Azeez[1], Harun K. Aremu[2], Sheriff O. Ayinla[3,4], Lukmon A. Jinadu[5], Joshua A. Obaleye[4]

[1]*Department of Pure and Applied Chemistry, Osun State University, Osogbo, Nigeria*
[2]*Department of Biochemistry, Osun State University, Osogbo, Nigeria*
[3]*Department of Chemical & Geological Sciences, Al-Hikmah University, Ilorin, Nigeria*
[4]*Department of Chemistry, University of Ilorin, Ilorin, Nigeria*
[5]*Department of Chemical Sciences, Fountain University, Osogbo, Nigeria*

** Corresponding author: Hassan K. Busari (0000-0002-0440-3056)*
(E-mail: hassan.busari@uniosun.edu.ng)

Abstract: This study introduces two new compounds: **(1)** $[Zn(4MBA)_2(2MIm)(H_2O)_3].H_2O$ and **(2)** $[Cu(4MBA)_2(2MIm)(H_2O)_3]$, with 4MBA representing 4-methylbenzoic acid and 2MIm denoting 2-methylimidazole. Synthesis of the compounds involved a 3-hour stirring at room temperature, followed by characterization through elemental analysis, molar conductance, melting point, FTIR, GC/MS, and PXRD techniques. FTIR analysis confirmed monodentate coordination of the metal ions with both the carboxylate group of 4MBA and the nitrogen atom of 2MIm in both complexes. Both complexes demonstrated heightened antibacterial effectiveness against *Staphylococcus aureus*, *Pseudomonas aeruginosa*, and *Escherichia coli* compared to the free ligands. Complex **2** showcased superior antifungal potential against all tested fungal organisms compared to complex **1** and the parent ligands. Molecular docking indicated complex **2** to have the highest binding energy of -8.6 kcal/mol, signifying superior antimicrobial attributes. In conclusion, copper-derived complex **2** could be considered a promising candidate for combatting pathogenic infections.

Key Words: Complex synthesis, pathogens, orthorhombic, cubic, molecular docking

1. Introduction

Pathogenic bacteria and fungi have emerged over time in our environment, posing a serious danger to public wellbeing [1]. Bacteria such as Shiga toxin-producing *Escherichia coli, Salmonella enterica, Listeria monocytogenes* and fungal pathogens such as *Aspergillus niger* and *Aspergillus flavus* have been linked to more serious illnesses, complications, and even deaths [2,3]. They are the major causes of acute health problems such as diarrhea, vomiting, nausea, stomach cramps, migraines, paralysis, and paresthesia [4]. Treatment of these infections has resulted in an increased economic burden on diverse parts of the world, especially in developing nations [2].

Despite the abundance of antimicrobial medications for treating illnesses resulting from bacterial and fungal infections, there are growing inefficacies in these treatment options due to the development of resistance caused by horizontal gene transfer as well as unregulated usage of antimicrobial drugs [5]. This has necessitated the need to improve or introduce a novel therapeutic regimen that could replace conventional drugs [6].

Recently, metal-ligand adducts have become of critical importance in the development of medication due to their therapeutic efficacy, which have been the subject of numerous studies [7,8]. The addition of metal ions to biologically active ligands has been shown in the literature to primarily improve their properties [6]. Several metal-ligand medications that primarily comprise pyrans, thiazole, imidazole, piperidines and other sulfur-, nitrogen-, or oxygen-containing heterocyclic compounds have recently been developed [9,10].

Nitrogen donor ligands, particularly imidazole derivatives, have shown to be appealing tools for coordinating metal ions in several ways. The electron-rich imidazole heterocyclics are able to build complexes with specific biological and redox functions due to their good donor properties [11]. Carboxylate ligands, such as 4-methylbenzoic acid, have also been reported in many studies such as coordination chemistry, materials chemistry, and supramolecular chemistry owing to their capacity to establish stable bonds with metal ions and display diverse coordination modes [12,13].

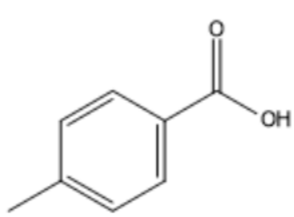

(a)

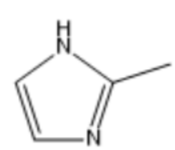

(b)

Figure 1. Structure Formula of 4-Methylbenzoic Acid (a) and 2-Methylimidazole (b)

In the present study, Zn (II) and Cu (II) complexes were synthesized using 4-methylbenzoic acid (Figure 1a) and a nitrogen donor heterocyclic ligand 2-methylimidazole (Figure 1b), they were structurally elucidated and their antimicrobial potentials against pathogenic organisms were investigated with both experimental and *in-silico* molecular docking studies.

2. Materials and Methods

All the reagents used were of analytical grade. The ligands were obtained from Sigma Aldrich, while the salts and solvents were obtained commercially. The compounds' IR spectra in KBr pellets were studied with a SHIMADZU FTIR (FTIR 8400s) in the frequency range of 400-4000 cm^{-1}. The complexes' molar conductance (1 x 10^{-3} $molL^{-1}$) was determined in DMSO at 25^{o}C using a HANNA conductivity meter with a cell constant of 0.83. The elemental analysis and melting point were performed on a CHNS/O Perkin Elmer Analyser (2400 series II) and MPA100 Optimelt Automated Melting Point System (SRS), respectively. The GCMS analysis was conducted by on an Agilent-Technologies 6890N Network GC system, equipped with an Agilent-Technologies 5975 inert XL Mass selective detector, located in Little Falls, CA, USA. The PXRD patterns were obtained using an Empyrean diffractometer in the angle range $2\theta = 0 - 70^{o}$ with Cu-Kα_1(λ = 1.5406) and Cu-Kα_2(λ = 1.5444).

Synthesis of [Zn(4MBA)$_2$(2MIm)(H_2O)$_3$].H_2O (1)

Complex **1** was prepared, as described by Chen et al. [14] by dissolving 1.0 mmol $ZnCl_2$ (136.3 mg), 1.0 mmol 4MBA (136.1 mg) and 1.0 mmol 2Mim (82.1 mg) in 10 mL distilled water. The mixture's pH was brought to a range of 8 to 10 with the addition of 0.5M KOH and stirred continuously for 3 hrs at room temperature. The resulting white precipitate was filtered, washed with distilled water, and then dried using anhydrous calcium chloride in a desiccator.

Analytical data for Complex 1: White powder, Yield: 67 %, m.pt.= 248^{o}C, Anal. Calcd. for $C_{20}H_{28}N_2O_8Zn$, (MW = 489.8 g/mol) %:C; 49.04, H; 5.76, N; 5.72, found C; 49.06, H; 5.73, N; 5.70.

Synthesis of [Cu(4MBA)$_2$(2MIm)(H_2O)$_3$] (2)

Complex **2** was prepared following the same procedure as complex **1**, with $CuCl_2.2H_2O$ (1.0 mmol; 170.5 mg) as the metal salt. The resulting blue precipitate was filtered, followed by a thorough wash with distilled water. It was subsequently dried using anhydrous calcium chloride in a desiccator.

Analytical data for Complex 2: Purple powder, Yield: 62 %, m.pt.= 235^{o}C, Anal. Calcd. for $C_{20}H_{26}CuN_2O_7$, (MW = 467.9 g/mol) %:C; 51.11, H; 5.58, N; 5.96, found C; 51.10, H; 5.59, N; 5.90.

The synthetic route to complexes **1** and **2** is represented in Fig. 2.

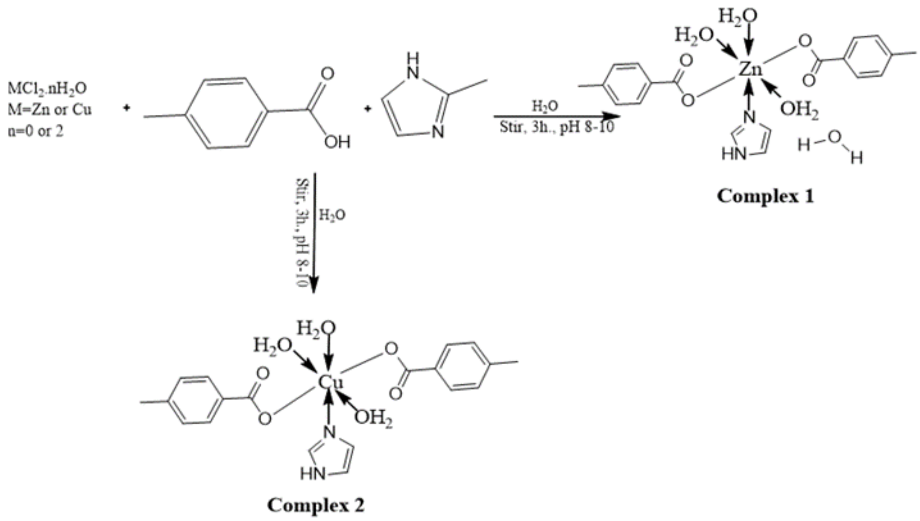

Figure 2. Synthetic Route for the Synthesis of Complex 1 and Complex 2

Antimicrobial Studies

The assessment of antimicrobial properties for both the ligands and the newly synthesized compounds was conducted in accordance with the procedure outlined by Obaleye et al. [15]. The sensitivity of bacterial isolates, including *P. aeruginosa*, *S. aureus* and *E. Coli* and strains of fungi viz: *A. niger*, *Candida* spp. and *A. flavus*, was investigated using the agar well diffusion method. The Muller-Hinton nutritional agar plates were carried out in duplicates per test organisms. Test organisms were made to equivalent 0.5 McFarland standards and inoculated in sterile petri dish. Sterile cork borer was used to make five 10 mm equivalent holes on the surface of the MHA agar. The test compounds (6 mg/mL) each was introduced into four of the holes while the control at the center hole contained DMSO. The bacterial and fungal strains were incubated for 24 h and 48 h at 37°C, respectively. The zone of inhibition's diameter was carefully assessed and recorded in millimeters (mm). All inhibition zones with a diameter of less than 10 mm are deemed inactive against a given strain.

Molecular Docking

The molecular interaction and binding affinity of the synthesized compounds were examined at a resolution of 3.34 using *Staphylococcus aureus* DNA gyrase (PDB ID: 2XCT) retrieved from the Protein Data Bank. According to the AutoDock Vina 4.2 protocol, the protein was processed by removing the water molecules and adding polar hydrogen and cofactors. The grid box was centered on vital amino acid residues surrounding the protein macromolecule's active sites (Tyr1025, Val1029, Arg1033, Val1177, Ile1175, Ala1034). AutoDock Vina was used to analyze the complexes with the target receptor.

3. Results and Discussion

Molar Conductivity

The molar conductivities of complexes **1** and **2** are presented in Table 1. The conductivity values, 15.35 for complex **1** and 14.57 for complex **2**, were less than 40 Scm^2mol^{-1}. This suggests that the complexes are non-electrolyte in DMSO solvent [16]. Moreover, the results above indicate that there are no counter ions outside the coordination sphere of the two complexes [17].

Table 1. Molar Conductivities of Synthesized Complexes

Complex	**Molar Conductivity** (Scm^2mol^{-1})
Complex 1	15.35
Complex 2	14.57

Infrared Spectra

The FTIR spectra of the ligands and complexes are presented in Fig. 3a-d, where some notable vibrational bands are observed.

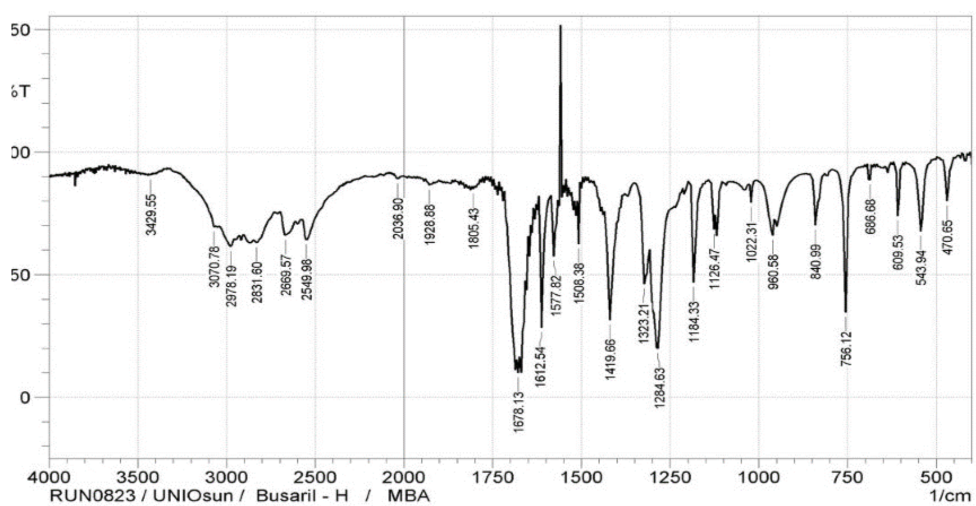

Figure 3a. FTIR Spectrum of 4MBA

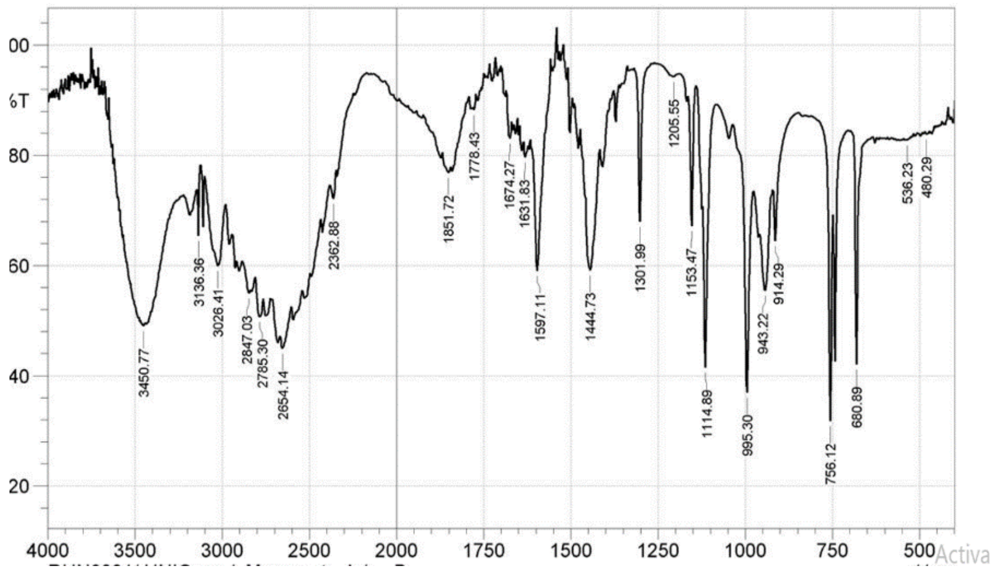

Figure 3b. FTIR Spectrum of 2MIm

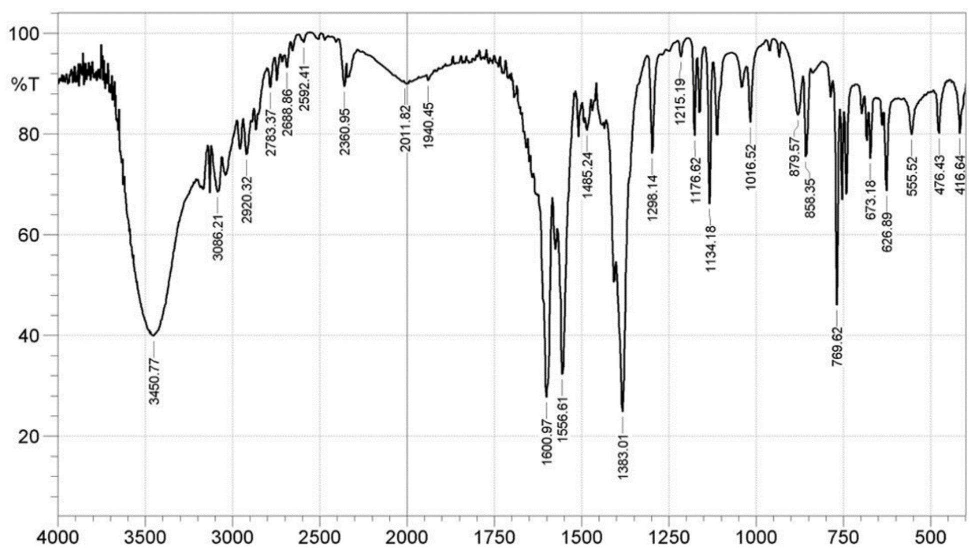

Figure 3c. FTIR Spectrum of Complex 1

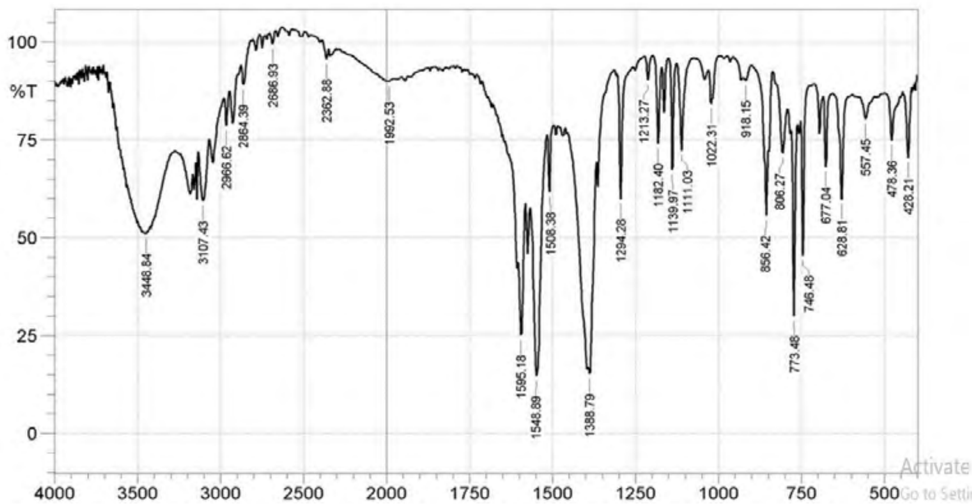

Figure 3d. FTIR Spectrum of Complex 2

At 1678 cm^{-1}, the carbonyl band of 4MBA ν(C=O) was observed, while at 1284cm^{-1}, an asymmetric aromatic stretching band ν(CO) was observed (Fig. 3a) [16,18]. The peaks at 1660cm-1 and 1383cm-1 for complex **1** (Fig. 3c); 1595cm-1 and 1388cm-1 for complex **2** (Fig. 3d) are attributed to $\nu_{asym(COO^-)}$ and $\nu_{sym(COO^-)}$, respectively. The difference Δv = [$\nu_{asym}(COO^-)$ - $\nu_{sym}(COO^-)$]; 217cm^{-1} for complex **1** and 207cm^{-1} for complex **2** reflects a monodentate mode of coordination of the carboxylate group. The sharp peaks at 1556cm^{-1} (Fig. 3c) and 1548cm^{-1} (Fig. 3d) in the complexes **1** and **2**, respectively, are attributed to aromatic C=C bond of the benzoic acid while the coordinated water molecules are found by the bands at 626cm^{-1} and 628 cm^{-1}, respectively, and these values agree with the literature reports [19]. In the spectrum of free 2MIm (Fig. 3b), there is no significant shift in the NH band (3450cm^{-1}) when compared with that of complex **1** (3450cm^{-1}) and complex **2** (3448cm^{-1}) to suggest coordination but indicates the involvement of 2MIm in coordination.

XRD Pattern

The powder XRD patterns of complexes **1** and **2** are shown in Fig. 4. The difference in their XRD pattern is an indication of their different structures. The Zn ion in complex **1** exists in cubic system matching JCPDS card number 00-412-2713 with space group P 21 3 having cell parameter a= 20.1619 Å. The Cu ion in complex **2** exists in orthorhombic system matching JCPDS card number 00-430-5279 with space group Pbcn. The cell parameters are a= 8.1953Å, b=7.5577Å, c= 13.4593Å. The X-ray diffraction (XRD) patterns of the newly synthesized Zn (II) and Cu (II) compounds exhibited distinct crystalline structures, as evidenced by the pronounced peaks in their XRD patterns.

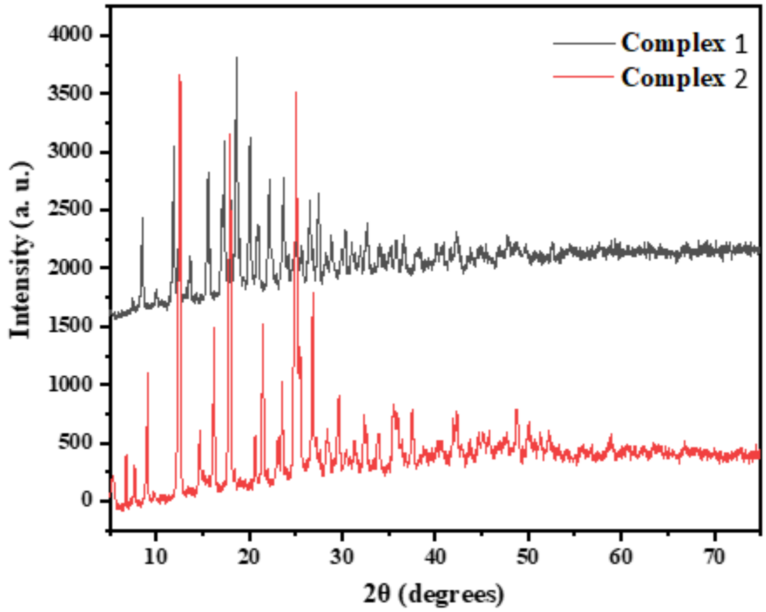

Figure 4. Powder XRD Patterns of Complex 1 and Complex 2

Mass Spectra

The mass spectra of the complexes are shown in Figures 5a and 5b.

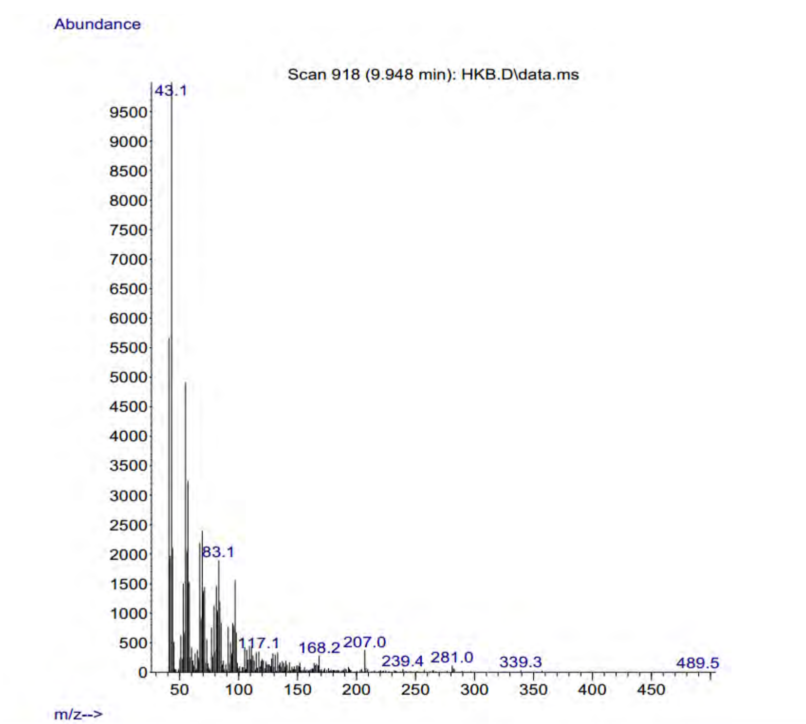

Figure 5a. Mass Spectrum of Complex 1

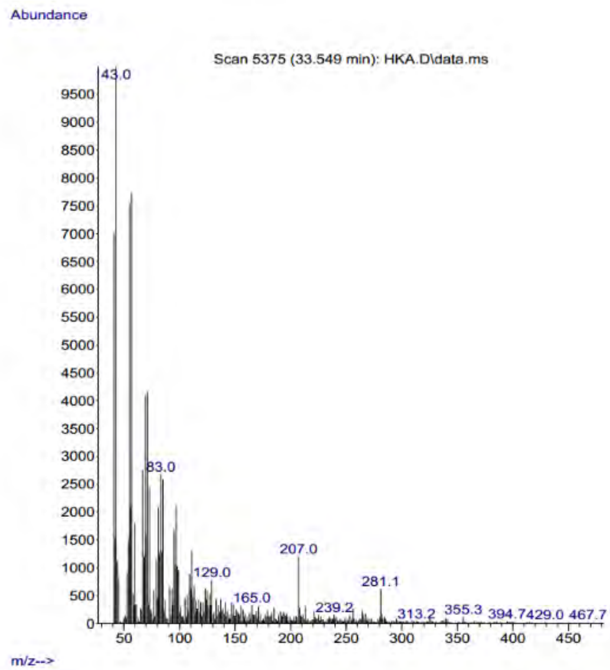

Figure 5b. Mass Spectrum of Complex 2

The observed molecular ion (M) peaks were used to confirm the proposed molecular weights of the complexes and hence determine the molecular formula. Complexes **1** and **2** show a molecular ion peak (m/z) at 489.5 and 467.7, respectively, as shown in their respective spectra. These peaks are consistent with the proposed molecular weights of the respective metal complexes as shown in Table 2. These findings agree with the hitherto studies of Damena et al. [20] and Uddin et al. [21].

Table 2. Mass Spectra Data of Complex 1 and 2

Complex	**Mol. wt.**	**Molecular ion peak** [M]	**Molecular formula**
Complex 1	489.8	489.5	$C_{20}H_{28}N_2O_8Zn$
Complex 2	467.9	467.7	$C_{20}H_{26}CuN_2O_7$

Antimicrobial Studies

The antifungal and antibacterial activities of complexes **1** and **2** were represented in Figures 6a and 6b. Complex **1** and **2** showed the better antibacterial potency against *S. aureus, E. coli* and *P. aeruginosa* than the ligands used in the study; with complex **2** showing the highest antibacterial activity (Figure 6a).

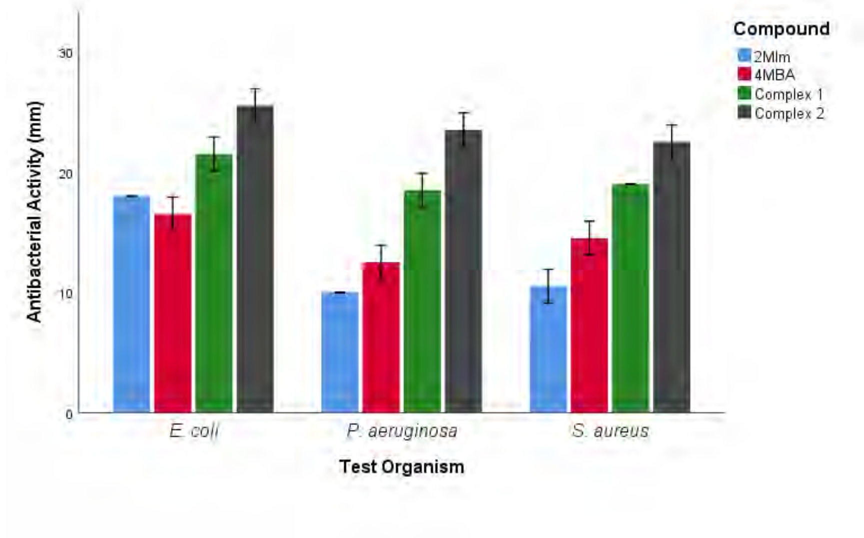

Figure 6a. Antibacterial Activity of the Ligands and the Metal Complexes

Also, amongst the compounds tested for antifungal activity, complex **2** was observed to be the most effective in inhibiting the growth of *A. flavus*, *A. niger* and *Candida* spp. Similar antifungal activities was observed for complex **1** and 4MBA ligand against *A. flavus* and complex **1** and 2Mlm against *Candida* spp. (Figure 6b).

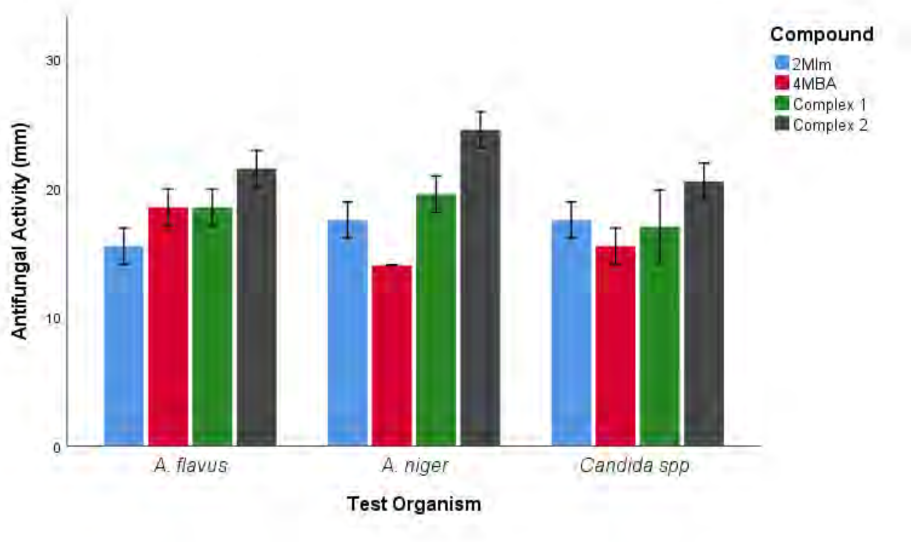

Figure 6b. Antifungal Activity of the Ligands and Metal Complexes

Against the tested organisms, complexes **1** and **2** showed differential antimicrobial activities compared to the free ligands. Notably, complexes **1** $[Zn(4MBA)_2(2MIm)(H_2O)_3].H_2O$ and **2** $[Cu(4MBA)_2(2MIm)(H_2O)_3]$ had higher antibacterial activity than 4MBA and 2MIm. In this present study, complex **2** displayed a high antibacterial activity when compared to the free ligands (4MBA and 2MIm) and complex **1**. This is consistent with report of Kaushal et al. [22] that reported the excellent antibacterial activity of copper complex against *S. aureus*. Similarly, Oladipo et al. [23] and Krishnegowda et al. [24] have described the excellent antibacterial activity of complex of copper against *P. aeruginosa*, *E. coli* and *S. aureus*. Also, complex **1** dis-played a remarkable antimicrobial property against gram-negative *E. coli* and gram-pos-itive *P. aeruginosa* and *S. aureus*. This is in line with reports of Ali et al. [25]; Boughou-gal et al. [26] and Basu Baul et al. [27] that described the antimicrobial potency of the zinc complex against multiple drug resistance pathogens. Overall, chelation raised the liposolubility of the complexes, which was boosted due to π electrons delocalization over the chelate ring of the complex, which increased the antibacterial activity of the synthesized metal complexes against the tested strains of organisms [12,28,29]

Molecular Docking Studies

The metal complexes were tested for their ability to inhibit *S. aureus* DNA gyrase. The complexes' orientation to the enzyme's active regions was determined by employing automated docking. Table 3 shows the binding energy for the interaction, while Figure 7 shows the complex with the best binding affinity to the active sites on the DNA gyrase.

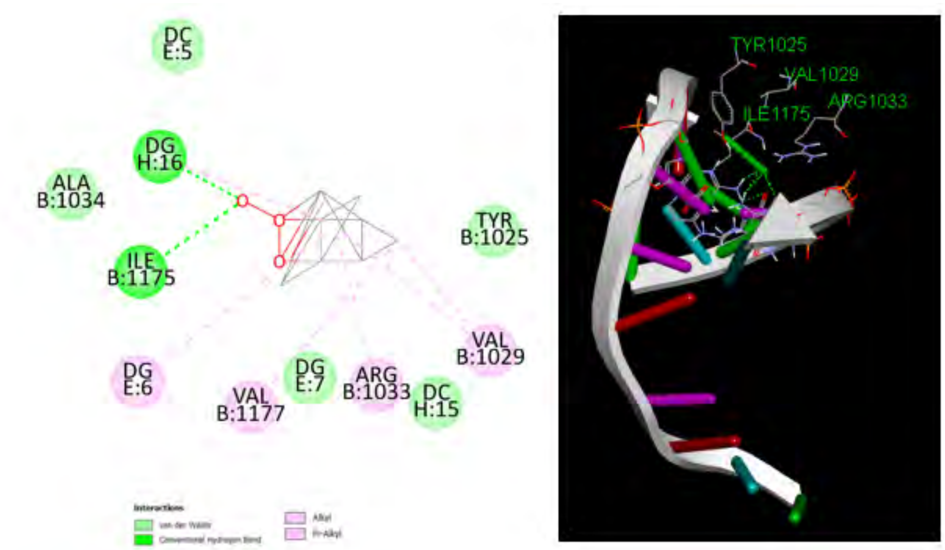

Figure 7. 2D and 3D Molecular Interaction of Complex 2 to DNA Gyrase

Table 3. Binding Energy of Metal Complexes to DNA Gyrase

Complex	**Binding energy** (kcal/mol)
Complex 1	-1.9
Complex 2	-8.6

4. Conclusion

The two complexes, **(1)** [Zn(4MBA)$_2$(2MIm)(H_2O)$_3$].H_2O and **(2)** [Cu(4MBA)$_2$(2MIm)(H_2O)$_3$], have been synthesized, characterized, and studied for antimicrobial activity. The FTIR spectra revealed that the 4-methylbenzoic acid ligand coordinated through the carbonyl oxygen atom of the carboxylate group in a monodentate mode in both complexes. In addition, the 2-methyl imidazole ligand coordinated in a monodentate mode through the imidazole nitrogen atom. The two complexes were proposed to exist in an octahedral coordinate system based on the comparison of the results from the elemental analysis, FTIR and mass spectra. Complex **1** was cubic and had the space group P 21 3, whereas complex **2** had the space group Pbcn and was orthorhombic. The two complexes had strong antibacterial action against the selected antimicrobial organisms; however, complex **2** displayed a better inhibitory tendency. This is in agreement with the results of the molecular simulation which showed that complex **2** had the higher binding energy against DNA gyrase and thus, the better antimicrobial potential. Therefore, complex **2** could then be considered as a preferred antimicrobial agent in the future.

5. Conflict of Interest

The authors declare no conflict of interest.

6. References

1. Evans A, Kavanagh KA. Evaluation of metal-based antimicrobial compounds for the treatment of bacterial pathogens. *J. Med. Microbiol.*, 2021, 70(5).
2. Fan X, Wang W. Quality of fresh and fresh-cut produce impacted by nonthermal physical technologies intended to enhance microbial safety. *Crit. Rev. Food Sci. Nutr.*, 2021, 62(2), 362-382.
3. Lin Y, Betts H, Keller S, Cariou K, Gasser G. Recent developments of metal-based compounds against fungal pathogens. *Chem. Soc. Rev.*, 2021, 50(18), 10346-10402.
4. Imre K, Herman V, Morar A. Scientific achievements in the study of the occurrence and antimicrobial susceptibility profile of major foodborne pathogenic bacteria in foods and food processing environments in Romania: Review of the last decade. *BioMed Res. Int.*, 2020, 2020.
5. Musa DA, Aremu KH, Adebayo ZA, Pellicano R, Smith SI. Molecular detection of main resistance genes by nested PCR in Salmonella spp. isolated from raw meat and stool samples in Niger State,

Nigeria. *Minerva Biotechnol.*, 2020, 32, 58-63.

6. Obaleye JA, Lawal M, Jadeja RN, Gupta VK, Nnabuike GG, Bamigboye MO, Roy H, Yusuff OK, Bhagariya P. Crystal structure, spectroscopic, DFT calculations and antimicrobial study of the Cu (II) complex bearing second-generation quinolone ofloxacin and 2, 2′-bipyridine. *Inorganica Chim. Acta*, 2021, 519, 120264.
7. Abu-Dief, AM, El-Metwaly NM, Alzahrani SO, Alkhatib F, Abualnaja MM, El-Dabea T, Ali MAEAA. Synthesis and characterization of Fe (III), Pd (II) and Cu (II)-thiazole complexes: DFT, pharmacophore modeling, *in-vitro* assay and DNA binding studies. *J. Mol. Liq.*, 2021, 326, 115277.
8. Adam MSS, Abu-Dief AM, Makhlouf MM, Shaaban S, Alzahrani SO, Alkhatib F, Masaret GS, Mohammed M.A, Alsehli M, El-Metway NM, Mohamad ADM. Tailoring, structural inspection of novel oxy and non-oxy metal-imine chelates for DNA interaction, pharmaceutical and molecular docking studies. *Polyhedron*, 2021, 201, 115167.
9. Alzahrani SO, Abu-Dief AM, Alkhamis K, Alkhatib F, El-Dabea T, Ali MAEAA, El-Metwaly NM. Synthesis and structural elucidation for new pyrano thiazole complexes: Biological screening and effects on DNA through *in-vitro* and *in-silico* approaches. *J. Mol. Liq.*, 2021, 332, 115844.
10. Jeyaseelan SC, Benial AMF. Quantum chemical, spectroscopic investigations, molecular docking and cytotoxic evaluation of 1-methyl-indole-3-carboxaldehyde. *Chem. Data Collect.*, 2021, 33, 100698.
11. Reshma R, Selwin Joseyphus R, Arish D, Reshmi Jaya RJ, Johnson J. Tridentate imidazole-based Schiff base metal complexes: Molecular docking, structural and biological studies. *J. Biomol. Struct. Dyn.*, 2021, 40(18), 8602-8614.
12. Ali B, Tahir S, Akhtar MN, Yameen M, Ashraf R, Hussain T, Ghaffar A, Abbass M, Iqbal, M. Cytotoxicity and antimicrobial activity of pivalic and benzoic acid-complexed Cu and Mn complexes. *Pol. J. Environ. Stud.*, 2017, 26(6).
13. Gonçalves IK, Oliveira WX, de Almeida FB, Marinho MV, Walace D, Silva-Caldeira PP. The versatile coordination chemistry of 1, 3-benzenedicarboxylate in the last 20 years: An investigation from the coordination modes to spectroscopic insights. *Polyhedron*, 2021, 198, 115068.
14. Chen X, An DL, Zhan XQ, Zhou ZH. 2-Methylimidazole copper iminodiacetates for the adsorption of oxygen and catalytic oxidation of cyclohexane. *Molecules,* 2020, 25(6), 1286.
15. Obaleye JA, Ajibola AA, Bernardus VB, Hosten EC, Ozarowski A. Synthesis, spectroscopic, structural and antimicrobial studies of a dimeric complex of copper (II) with trichloroacetic acid and metronidazole. *Inorganica Chim. Acta*, 2020, 503, 119404.
16. Zong GC, Ren N, Zhang JJ, Qi XX, Gao J. Lanthanide complexes with 3-bromine-4-methyl benzoic acid and 1, 10-phenanthroline. *J. Therm. Anal. Calorim.*, 2016, 123(1), 105-116.
17. Refat MS, El-Korashy SA, Hussien MA. Ligational, spectroscopic

(infrared and electronic) and thermal studies on the Mn (II), Co (II), Fe (II) and Cu (II) complexes with analgesic drugs. *Can. Chem. Trans*., 2014, 2, 24-35.

18. Nnabuike GG, Salunke-Gawali S, Patil AS, Butcher RJ, Lawal M, Bamigboye MO, Obaleye JA. Copper (II) and nickel (II) complexes of the non-steroidal anti-inflammatory drug indomethacin containing aromatic chelating N, N-donor ligand: Synthesis and structural studies. *J. Mol. Struct.*, 2021, 1224, 129069.
19. Bai EP, Vairam S. Co-ordination behaviour of hydrazine and isomers of acetoxy benzoic acids with transition metal ions. *Bull. Chem. Soc. Ethiop.*, 2021, 35(2), 337-350.
20. Damena T, Alem MB, Zeleke D, Desalegn T, Eswaramoorthy R, Demissie TB. Novel zinc (II) and copper (II) complexes of 2-((2-hydroxyethyl) amino) quinoline-3-carbaldehyde for antibacterial and antioxidant activities: A combined experimental, DFT, and docking studies. *ACS omega,* 2022, 7(30), 26336-26352.
21. Uddin MN, Siddique ZA, Akter J, Rahman MS, Shumi W, Nasiruddin M. Synthesis, molecular modeling, and biomedical applications of oxovanadium (IV) complexes of Schiff bases as a good SARS-CoV-2 inhibitor. *Inorg. Nano-Met. Chem.*, 2022, 52(6), 819-834.
22. Kaushal M, Lobana TS, Nim L, Bala R, Arora DS, Garcia-Santos I, Duff CE, Jasinski JP. Synthesis of 2-acetylpyridine-N-substituted thiosemicarbazonates of copper (II) with high antimicrobial activity against methicillin resistant *S. aureus*, *K. pneumoniae* 1 and *C. albicans*. *New J. Chem.*, 2019, 43, 11727-11742.
23. Oladipo SD, Omondi B, Mocktar C. Synthesis and structural studies of nickel (II)- and copper (II)- N, N-diarylformamidine dithiocarbamate complexes as antimicrobial and anti-oxidant agents. *Polyhedron*, 2019, 170, 712-722.
24. Krishnegowda HM, Karthik CS, Marichannegowda MH, Kumara K, Kudigana PJ, Lingappa M, Mallu P, Neratur LK. Synthesis and structural studies of 1-phenyl-1,3-butanedione copper (II) complexes as an excellent antimicrobial agent against methicillin-resistant *Staphylococcus aureus*. *Inorg. Chim. Acta*, 2019, 484, 227-236.
25. Ali HA, Omar SN, Darawsheh MD and Fares, H. Synthesis, characterization and antimicrobial activity of zinc (II) ibuprofen complexes with nitrogen-based ligands. *J. Coord. Chem.*, 2016, 69, 1110-1122.
26. Basu Baul T, Nongsiej K, Ka-Ot A, Joshi SR, León I, Höpfl H. Tweaking the affinity of aryl-substituted diazosalicylato- and pyridine ligands towards Zn (II) and its neighbours in the periodic system of the elements, Cu (II) and Cd (II), and their anti-microbial activity. *Appl. Organomet. Chem.*, 2019, 33, e4905.
27. Boughougal A, Cherchali FZ, Messai A, Attik N, Decoret D, Hologne M, Sanglar C, Pilet G, Tommasino JB and Luneau D. New model of metalloantibiotic: Synthesis, structure and biological activity of a zinc (II) mononuclear complex carrying two enrofloxacin and sulfadiazine antibiotics. *N. J. Chem.*, 2018, 42, 15346-15352.
28. Osowole AA, Wakil SM, Okediran EQ, Alao OK. Studies on some metal

(II) complexes of mixed ligands-benzoic and N, N’-dimethyldithiocarbamic acids. *Chem. J.*, 2016, 6, 27-31.

29. Liang J, Sun D, Yang Y, Li M, Li H, Chen L. Discovery of metal-based complexes as promising anti-microbial agents. *Eur. J. Med. Chem.*, 2021, 224, 113696.

The AIC Code of Ethics

Approved by the AIC Board of Directors, April 29, 1983

The profession of chemistry is increasingly important to the progress and the welfare of the community. The Chemist is frequently responsible for decisions affecting the lives and fortunes of others. To protect the public and maintain the honor of the profession, the American Institute of Chemists has established the following rules of conduct. It is the Duty of the Chemist:

1. To uphold the law; not to engage in illegal work nor cooperate with anyone so engaged;

2. To avoid associating or being identified with any enterprise of questionable character;

3. To be diligent in exposing and opposing such errors and frauds as the Chemist's special knowledge brings to light;

4. To sustain the institute and burdens of the community as a responsible citizen;

5. To work and act in a strict spirit of fairness to employers, clients, contractors, employees, and in a spirit of personal helpfulness and fraternity toward other members of the chemical profession;

6. To use only honorable means of competition for professional employment; to advertise only in a dignified and factual manner; to refrain from unfairly injuring, directly or indirectly, the professional reputation, prospects, or business of a fellow Chemist, or attempting to supplant a fellow chemist already selected for employment; to perform services for a client only at rates that fairly reflect costs of equipment, supplies, and overhead expenses as well as fair personal compensation;

7. To accept employment from more than one employer or client only when there is no conflict of interest; to accept commission or compensation in any form from more than one interested party only with the full knowledge and consent of all parties concerned;

8. To perform all professional work in a manner that merits full confidence and trust; to be conservative in estimates, reports, and testimony, especially if these are related to the promotion of a business enterprise or the protection of the public interest, and to state explicitly any known bias embodied therein; to advise client or employer of the probability of success before undertaking a project;

9. To review the professional work of other chemists, when requested, fairly and in confidence, whether they are:
    a. subordinates or employees
    b. authors of proposals for grants or contracts
    c. authors of technical papers, patents, or other publications
    d. involved in litigation;

10. To advance the profession by exchanging general information and experience with fellow Chemists and by contributing to the work of technical societies and to the technical press when such contribution does

not conflict with the interests of a client or employer; to announce inventions and scientific advances first in this way rather than through the public press; to ensure that credit for technical work is given to its actual authors;

11. To work for any client or employer under a clear agreement, preferable in writing, as to the ownership of data, plans, improvements, inventions, designs, or other intellectual property developed or discovered while so employed, understanding that in the absence of a written agreement:
    a. results based on information from the client or employer, not obtainable elsewhere, are the property of the client or employer
    b. results based on knowledge or information belonging to the Chemist, or publicly available, are the property of the Chemist, the client or employer being entitled to their use only in the case or project for which the Chemist was retained
    c. all work and results outside of the field for which the Chemist was retained or employed, and not using time or facilities belonging to a client or employer, are the property of the Chemist;

12. Special data or information provided by a client or employer, or created by the Chemist and belonging to the client or employer, must be treated as confidential, used only in general as a part of the Chemist's professional experience, and published only after release by the client or employer;

13. To report any infractions of these principles of professional conduct to the authorities responsible for enforcement of applicable laws or regulations, or to the Ethics Committee of The American Institute of Chemists, as appropriate.

The Chemist
Journal of the American Institute of Chemists

Manuscript Style Guide

The Chemist is the official online refereed journal of The American Institute of Chemists (AIC). We accept submissions from all fields of chemistry defined broadly (e.g., scientific, educational, socio-political). *The Chemist* will not consider any paper or part of a paper that has been published or is under consideration for publication anywhere else. The editorial office of *The Chemist* is located at: The American Institute of Chemists, Inc. 315 Chestnut Street Philadelphia, PA 19106-2702, Email: aicoffice@theaic.org.

Categories of Submissions

RESEARCH PAPERS

Research Papers (up to ~5000 words) that are original will only be accepted. Research Papers are peer-reviewed and include an abstract, an introduction, up to 5 figures or tables, sections with brief subheadings and a maximum of approximately 30 references.

REPORTS

Reports (up to ~3000 words) present new research results of broad interest to the chemistry community. Reports are peer- reviewed and include an abstract, an introductory paragraph, up to 3 figures or tables, and a maximum of approximately 15 references.

BRIEF REPORTS

Brief Reports (up to ~1500 words) are short papers that are peer-reviewed and present novel techniques or results of interest to the chemistry community.

REVIEW ARTICLES

Review Articles (up to ~6000 words) describe new or existing areas of interest to the chemistry community. Review Articles are peer-reviewed and include an abstract, an introduction that outlines the main point, brief subheadings for each section and up to 80 references.

LETTERS

Letters (up to ~500 words) discuss material published in The Chemist in the last 8 months or issues of general interest to the chemistry community.

BOOK REVIEWS

Book Reviews (up to ~ 500 words) will be accepted.

Manuscript Preparation

RESEARCH PAPERS, REPORTS, BRIEF REPORTS & REVIEW ARTICLES

- **The first page** should contain the title, authors and their respective institutions/affiliations and the corresponding author. The general area of chemistry the article represents should also be indicated, i.e. General Chemistry, Organic Chemistry, Physical Chemistry, Chemical Education, etc.

- **Titles** should be 55 characters or less for Research Papers, Reports, and Brief Reports. Review articles should have a title of up to 80 characters.

- **Abstracts** explain to the reader why the research was conducted and why it is important to the field. The abstract should be 100-150 words and convey the main point of the paper along with an outline of the results and conclusions.

- **Text** should start with a brief introduction highlighting the paper's significance and should be understood to readers of all chemistry disciplines. All symbols, abbreviations, and acronyms should be defined the first time they are used. All tables and figures should be cited in numerical order.

- **Units** must be used appropriately. Internationally accepted units of measurement should be used in conjunction with their numerical values. Abbreviate the units as shown: cal, kcal, µg, mg, g (or gm), %, ºC, nm, µm (not m), mm, cm, cm^3, m, in. (or write out inch), h (or hr), min, s (or sec), ml [write out liter(s)], kg. Wherever commonly used units are used their conversion factors must be shown at their first occurrence. Greek symbols are permitted as long as they show clearly in the soft copy.

- **References and notes** should be numbered in the order in which they are cited, starting with the text and then through the table and figure legends. Each reference should have a unique number and any references to unpublished data should be given a number in the text and referred to in the references. References should follow the standards presented in the AIC Reference Style Guidelines below.

REFERENCE STYLE GUIDELINES

References should be cited as numbers within square brackets [] at the appropriate place in the text. The reference numbers should be cited in the correct order throughout the text (including those in tables and figure captions, numbered according to where the table or figure is designated to appear). The references themselves are listed in numerical order at the end of the final printed text along with any Notes. Journal abbreviations should be consistent with those presented in Chemical Abstracts Service Source Index (CASSI) (http://www.cas.org) guide available at most academic libraries.

- **Names** and initials of all authors should always be given in the reference and must not be replaced by the phrase *et al*. This does not preclude one from referring to them by the first author, et al in the text.

- **Tables** should be in numerical order as they appear in the text and they should not duplicate the text. Tables should be completely understandable without reading the text. Every table should have a title. Table titles should be placed above the respective tables.

  Table 1. Bond Lengths (Å) of 2-aminophenol

- **Figure legends** should be in numerical order as they appear in the text. Legends should be limited to 250 words.

  Figure 1. PVC Melt Flow Characterized by Analytical Structural Method

- **Letters and Book Reviews** should be clearly indicated as such when being submitted. They are not peer-reviewed and are published as submitted. Legends should be placed after/under the respective figures.

- **Journals -** The general format for citations should be in the order: **author(s), journal, year, volume, page**. Page number ranges are preferred over single values, but either format is acceptable. Where page numbers are not yet known, articles may be cited by DOI (Digital Object Identifier). For example:

  Booth DE, Isenhour TL. *The Chemist*, 2000, 77(6), 7-14.

- **Books -** For example:

  Turner GK in *Chemiluminescence: Applications*, ed. Knox Van Dyke, CRC Press, Boca Raton, 1985, vol 1, ch. 3, pp 43-78.

- **Patents** should be indicated in the following form:

  McCapra F, Tutt D, Topping RM, UK Patent Number 1 461 877, 1973.

- **Reports and bulletins, etc. -** For example:

  Smith AB, Jones CD, *Environmental Impact Report for the US*, final report to the National Science Foundation on Grant AAA-999999, Any University, Philadelphia, PA, 2006.

- **Material presented at meetings -** For example:

  Smith AB. Presented at the Pittsburgh Conference, Atlantic City, NJ, March 1983, paper 101.

- **Theses -** For example:

  Jones AB, Ph.D. Thesis, Columbia University, 2004.

- For material presented at a meeting, congress or before a Society, etc., but not published, the following form should be used:

  Jones AB, presented in part at the 20th American Institute of Chemists National Meeting, Philadelphia, PA, June, 2004.

- For material accepted for publication, but not yet published, the following form should be used:

  Smith AB. *Anal. Chem.*, in press

- For material submitted for publication but not yet accepted the following form should be used:

  Jones AB, *Anal. Chem.* submitted for publication.

- For personal communications the following should be used:

  Smith AB, personal communication.

- If material is to be published but has not yet been submitted the following form should be used:

  Smith AB, unpublished work.

Reference to unpublished work should not be made without the permission of those by whom the work was performed.

Manuscript Selection

The submission and review process is completely electronic. Submitted papers are assigned by the Editors, when appropriate, to at least two external reviewers anonymously. Reviewers will have approximately 10 days to submit their comments. In selected situations the review process can be expedited. Selected papers will be edited for clarity, accuracy, or to shorten, if necessary. The Editor-in-Chief will have final say over the acceptance of submissions. Most papers are published in the next issue after acceptance. Proofs will be sent to the corresponding author for review and approval. Authors will be charged for excessive alterations at the discretion of the Editor-in-Chief.

Conditions of Acceptance

When a paper is accepted by *The Chemist* for publication, it is understood that:

- Any reasonable request for materials to verify the conclusions or experiments will be honored.

- Authors retain copyright but agree to allow *The Chemist* to exclusive license to publish the submission in print or online.
- Authors agree to disclose all affiliations, funding sources, and financial or management relationships that could be perceived as potential conflicts of interest or biases.
- The submission will remain a privileged document and will not be released to the public or press before publication.
- The authors certify that all information described in their submission is original research reported for the first time within the submission and that the data and conclusions reported are correct and ethically obtained.
- The Chemist, the referees, and the AIC bear no responsibility for accuracy or validity of the submission.

Authorship

By submitting a manuscript, the corresponding author accepts the responsibility that all authors have agreed to be listed and have seen and approved of all aspects of the manuscript including its submission to *The Chemist*.

Submissions

Authors are required to submit their manuscripts, book reviews and letters electronically. They can be submitted via email at aicoffice@theaic.org with "Submission for consideration in *The Chemist*" in the subject line. All submissions should be in Microsoft® Word format.

Copyright Assignment & Warranty Form for The Chemist

It is the policy of *The Chemist* to require all contributors to transfer the copyright for their contributions (hereafter referred to as the manuscript) to The American Institute of Chemists, Inc. (hereafter referred to as The AIC) the official publisher of *The Chemist*. By signing this agreement you assign to The AIC to consider publishing your manuscript the exclusive, royalty-free, irrevocable copyright in any medium internationally for the full term of the copyright. This agreement shall permit The AIC to publish, distribute, create derivative works, and otherwise use any materials accepted for publication in *The Chemist* internationally. A copy of the Copyright and Warranty Form for *The Chemist* will be sent to the author(s) whose manuscript is accepted for publication. The AIC will not publish any accepted manuscript in *The* Chemist without its author(s) fully complying with this requirement.

For further information or if you can any questions please contact the Publisher of *The Chemist* at (215) 873-8224 or via email at publications@theaic.org.

Website: http://www.theaic.org/ Email: aicoffice@theaic.org Phone: 215-873-8224

Announcements

INVITATION TO AUTHORS

Authors are invited to submit manuscripts for ***The Chemist,*** the official online refereed journal of The American Institute of Chemists (AIC). We accept submissions from all fields of chemistry defined broadly (e.g., scientific, educational, socio-political). *The Chemist* will not consider any paper or part of a paper that has been published or is under consideration for publication anywhere else.

Research Papers (up to ~5000 words) that are original will only be accepted. Research Papers are peer-reviewed and include an abstract, an introduction, up to 5 figures or tables, sections with brief subheadings and a maximum of approximately 30 references.

Reports (up to ~3000 words) present new research results of broad interest to the chemistry community. Reports are peer- reviewed and include an abstract, an introductory paragraph, up to 3 figures or tables, and a maximum of approximately 15 references.

Brief Reports (up to ~1500 words) are short papers that are peer-reviewed and present novel techniques or results of interest to the chemistry community.

Where to Send Manuscripts?

Please submit your manuscripts by email (aicoffice@theaic.org) to the attention of:

The Editor-in-Chief, The Chemist
The American Institute of Chemists, Inc.
315 Chestnut Street,
Philadelphia, PA 19106-2702
Email: aicoffice@theaic.org

Review Articles (up to ~6000 words) describe new or existing areas of interest to the chemistry community. Review Articles are peer-reviewed and include an abstract, an introduction that outlines the main point, brief subheadings for each section and up to 80 references.

Letters (up to ~500 words) discuss material published in *The Chemist* in the last 8 months or issues of general interest to the chemistry community.

Book Reviews (up to ~ 500 words) will be accepted.

American Institute of Chemists

www.TheAIC.org

From its earliest days in 1923 to the present, the American Institute of Chemists has fostered the advancement of the chemical profession in the United States.

The Institute has a corresponding dedication "to promote and protect the public welfare; to establish and maintain standards of practice for these professions; and to promote the professional experience through certification as to encourage competent and efficient service."

The AIC engages in a broad range of programs for professional enhancement through the prestigious Fellow membership category, awards program, certification programs, meetings, publications and public relations activities.

The American Institute of Chemists, Inc.
315 Chestnut Street, Philadelphia, PA 19106-2702.
Phone: (215) 873-8224 I Fax: (215) 629-5224 I E-mail: aicoffice@TheAIC.org